Chapter 6. Trends in IMPROVE Speciated Aerosol Concentrations

Trend analyses of aerosol concentrations are performed for a variety of purposes. Evaluating temporal changes in aerosol concentrations assists in determining whether emission mitigation strategies are effective in improving air quality. For example, the Regional Haze Rule, promulgated by the U.S. Environmental Protection Agency, addresses visibility impairment in Class I areas. The rule requires states and tribes to establish strategies to improve visibility in 156 national parks and wilderness areas by reducing emissions of visibility-impairing particulate matter (U.S. EPA, 1999). In addition, health effects standards, such as the National Ambient Air Quality Standards (NAAQS), require that states and tribes meet standards for criteria pollutants, including $PM_{2.5}$ and PM_{10} particulate matter (www.epa.gov/air/particlepollution/standards.html). Trend analyses provide information as to whether mitigation strategies are successful in meeting these types of goals.

On a global scale, trend analyses of global aerosol optical depth, a column-integrated light extinction coefficient, provide important information on "global dimming", a term used to describe the decrease of incoming solar radiation to the Earth's surface, due in part to changes in aerosol concentrations (Wild et al., 2005; Mishchenko and Geogdzhayev, 2007; Mishchenko et al., 2007). While trends in remote sensing products, such as aerosol optical depth or Ångstrom exponent, provide information related to the changes in the transmittance of the atmosphere, they do not inform as to the specific species responsible. Modeling studies have been used to investigate this particular issue by investigating effects of changing emissions, meteorology, and atmospheric processes that affect aerosol concentrations in the atmosphere (e.g., Streets et al., 2009). To this end, long-term trend analyses of speciated aerosol concentrations provide constraints for global models (e.g., Bahadur et al., 2009; Streets et al., 2009).

While long-term trend analyses of speciated aerosol concentrations are important, few have been performed because long-term speciated datasets are not widely available. However, trend analyses have been performed for precipitation chemistry data from the National Atmospheric Deposition Program (NADP) and have provided important results regarding changes in aerosol chemistry in wet deposition around the United States (e.g., Holland et al., 1995; Lynch et al., 1995; Walker et al., 2000; Nilles and Conley, 2001; Lehmann et al., 2007; Lloyd, 2010). Analyses of aerosol data from high latitude locations in the North American continent, such as Arctic sites in Canada and Alaska, have provided long-term trends in aerosol species such as sulfate and black carbon in an effort to understand Arctic haze (e.g., Polissar et al., 1999; Sirois and Barrie, 1999; Quinn et al., 2007; Gong et al., 2010; Hirdman et al., 2010). The IMPROVE network is an important source of data for trend analyses in the United States because of its duration (observations initiated in 1988), spatial distribution of sites, and consistent sampling methodology for all sites in the network. Previous trends studies were reviewed by Malm et al. (2002), who also demonstrated through trend analyses that IMPROVE sulfate concentrations were decreasing at most sites over a period of 10 years (1988–1999). More recently, Murphy et al. (2011) investigated trends in light absorbing carbon (LAC) and found that LAC concentrations were decreasing at most IMPROVE sites in the United States. In addition, a comprehensive trend analysis on IMPROVE reconstructed aerosol visibility (deciview) at national parks was reported in the most recent *Air Quality in National Parks 2009 Annual Performance and Progress Report* for the 1999–2008 time period (NPS, 2010).

The analyses of IMPROVE data presented in the previous chapters focused on spatial and seasonal patterns in aerosol species from 2005 through 2008 but did not investigate trends in aerosol concentrations over longer periods. In this chapter we present trend analyses over "short-term" (20 years, 2000–2008) and "long-term" (9 years, 1989–2008) time periods. We did not perform trend analyses with CSN data because trends are sensitive to changes in CSN sampling methodology (e.g., sampler and analytical methodology vary from site to site and over time) and because of CSN's shorter history (network established in 2000 with additional sites coming online over a period of several years).

Trends were computed for a total of eight parameters: annual mean, 10^{th}, 50^{th}, and 90^{th} percentiles, and four seasons (winter included December, January, February; spring included March, April, May; summer included June, July, August; fall included September, October, November). Fifty percent of yearly data was required for a given site to be included in the trend analysis. In addition, long-term and short-term trends were computed with the requirement that data for 70% of the years were complete for a trend analysis to be performed at a given site (i.e., 6 out of 9 years for short-term trends and 14 out of 20 years for long-term trends). A Theil regression was performed with the concentration data as the dependent variable and the year as the independent variable. An advantage to the Theil regression is that heavy influence by outliers on the regression results is avoided (Theil, 1950). Slopes for every possible combination of data at a given site were computed and the median slope ($\mu g\ m^{-3}\ yr^{-1}$) was computed from all possible slopes. Kendall tau statistics were used to determine the significance by using the difference in each combination of data points at a given site. A positive difference was assigned a + 1, a negative difference was assigned a - 1, and the sum of values was computed. The sum was used to determine the probability that the differences occurred by chance. We assumed that a trend was statistically significant at 5% ($p \leq 0.05$), meaning that there was a 95% chance that the slope was not due to random chance. We also present trends that were significant at 15% ($0.05 < p \leq 0.15$). We refer to "trend" as percent change per year (% yr^{-1}) and computed it by dividing the slope derived from the Theil regression by the median concentration value over the time period of the trend, multiplied by 100%. Reporting trend instead of slope reflects the relative change in concentration at a given site. However, trends can be quite large (>100%) when median concentrations are very low (e.g., 10^{th} percentile).

We present long-term trends for sulfate ion, total carbon (TC = organic carbon + light absorbing carbon), fine soil, fine mass (FM), coarse mass (CM), and PM_{10} concentrations. In addition to the species listed above, short-term trends were computed for nitrate ion concentrations. No trends were computed for sea salt because of issues with chloride measurements (White, 2008). In an effort to condense this discussion, not all of the trend results will be presented here but are available in Appendix F. Instead, we identify interesting trends for given species and parameters, as well as individual sites. Percent change per year for each site and species is presented on a map of the United States. Sites with positive trends with significance levels of 95% and greater ($p \leq 0.05$) correspond to solid red, upward-pointing triangles. Positive trends with significance levels of 85–95% ($0.05 < p \leq 0.15$) correspond to red, unfilled, upward-pointing triangles. A similar methodology was applied to sites with decreasing trends but in blue. The size of the triangle corresponds to the magnitude of the trend, with the same scale maintained for all species and parameters for comparison purposes. Sites with no significant trends ($p > 0.15$) but with complete data are represented as black triangles with size

scaled by the magnitude and orientation by the direction of the trend. We present both long- and short-term trends within the discussion of a given species.

Summaries of network-wide long-term and short-term trend information for all of the major components are provided in Tables 6.1 and 6.2, respectively. The first five columns of these tables provide a useful overview of particulate mass trends at IMPROVE sites that are described in greater detail in the sections that follow. For example, notice that the large majority of sites with statistically significant long-term trends (Table 6.1) have negative (i.e., improving) trends for all components, except for fine soil which has positive trends at half or more of the sites with significant trends. The situation is similar for the short-term trends (Table 6.2) at an expanded number of sites, except that coarse mass joins fine soil as having half or more positive trends, with all other components having generally decreasing trends at the large majority of sites. This seems to suggest that emissions controls applied in the United States over the last two decades have been successful in reducing particulate mass concentrations.

6.1 SULFATE ION TRENDS

Decreasing trends in sulfate ion concentrations were typical for most IMPROVE sites, regardless of the percentile, season, or time period. The 10^{th} percentile and winter periods were associated with some of the negative trends. A map of the 10^{th} percentile, long-term sulfate ion trends is shown in Figure 6.1.1. Decreasing trends occurred at sites in the southwestern United States (e.g., Gila Wilderness, New Mexico, GICL1, -5.6% yr^{-1}; Guadalupe Mountains, Texas, GUMO1, -3.6% yr^{-1}; Petrified Forest, Arizona, PEFO1,-3.7% yr^{-1}) and in the eastern United States (e.g., Acadia, Maine, ACAD1,
-4.0% yr^{-1}; Lye Brook, Vermont, LYBR1, -3.9% yr^{-1}; Dolly Sods, West Virginia, DOSO1, -4.2% yr^{-1}; Shenandoah, Virginia, SHEN1, -3.3% yr^{-1}; Washington, D.C., WASH1, -4.2% yr^{-1}). As shown in Figure 6.1.2, large decreasing trends occurred during winter months at sites in the southwestern United States, such as Canyonlands, Utah (CANY1, -5.7% yr^{-1}), Bryce Canyon, Utah (BRCA1, -4.6% yr^{-1}), Indian Gardens, Arizona (INGA1, -5.2% yr^{-1}), Petrified Forest, Arizona (PEFO1, -4.7% yr^{-1}), Tonto, Arizona (TONT1, -4.7% yr^{-1}), and the northwestern United States (e.g., Snoqualmie Pass, Washington, SNPA1, -5.0% yr^{-1}; Mount Rainier, Washington, MORA1, -5.0% yr^{-1}) and a few sites in the Northeast United States (Acadia, Maine, ACAD1, -4.4% yr^{-1}; Lye Brook, Vermont, LYBR1, -4.2% yr^{-1}). Recall from Chapter 4.1.1 that the lowest concentrations in regional mean ammonium sulfate (derived from sulfate ion concentrations) from 2005 through 2008 occurred during winter in the southwestern United States (Figure 4.1.5). The long-term trends suggested that the lowest sulfate ion concentration days in winter have been decreasing for several years at many sites. An example of decreasing long-term sulfate ion concentrations during winter is shown for Denali, Alaska (DENA1, -4.7% yr^{-1}), in Figure 6.1.3.

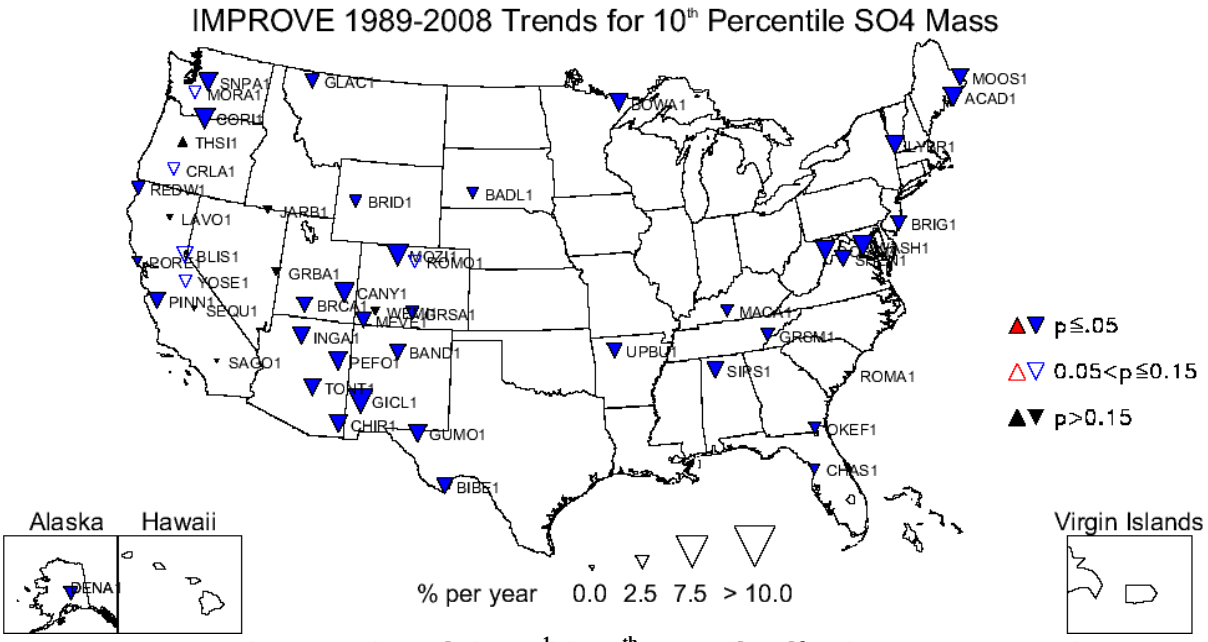

Figure 6.1.1. Long-term (1989–2008) trends (% yr^{-1}) in 10th percentile sulfate ion mass concentrations.

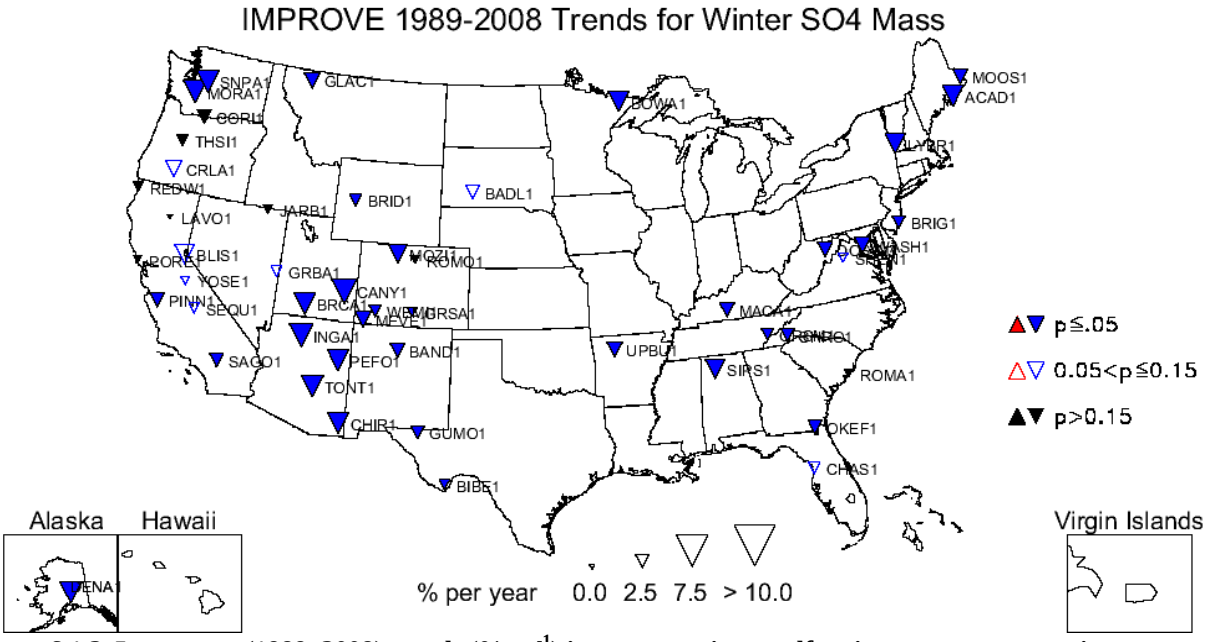

Figure 6.1.2. Long-term (1989–2008) trends (% yr^{-1}) in average winter sulfate ion mass concentrations.

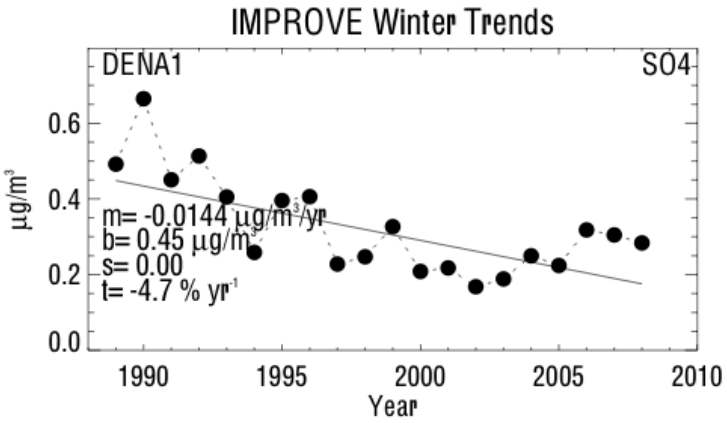

Figure 6.1.3. Average winter sulfate ion mass concentrations (μg m^{-3}) for Denali, Alaska (DENA1). Regression results, including Theil slope (m, μg m^{-3} yr^{-1}), intercept (b, μg m^{-3}), significance (s), and trend (t, % yr^{-1}) are included. The trend line is plotted as a solid line. The intercept corresponds to the initial year of data.

In contrast to the 10th percentile map, the 90th percentile map presented much lower trends in sulfate ion concentrations, especially in the southwestern United States (Figure 6.1.4). Positive long-term trends occurred at Big Bend, Texas (BIBE1), for the 90th percentile and spring season (1.5% yr^{-1} and 1.3% yr^{-1}, respectively) and at Lassen Volcanic NP, California (LAVO1), during summer (1.4% yr^{-1}). The increase in the 90th percentile sulfate ion concentrations at BIBE1 is shown in Figure 6.1.5; concentrations increased slowly but steadily since 1989. The sites listed above were the only IMPROVE locations that corresponded to positive trends for any long-term-trend parameter investigated. The largest negative long-term, 90th percentile trend occurred at Snoqualmie Pass, Washington (SNPA1), during summer (-6.3% yr^{-1}). Of the parameters investigated, approximately fifty sites typically met the completeness criteria for trend analyses and of these, 25–45 sites corresponded to significant trends ($p \leq 0.15$), depending on the parameter (see Table 6.1).

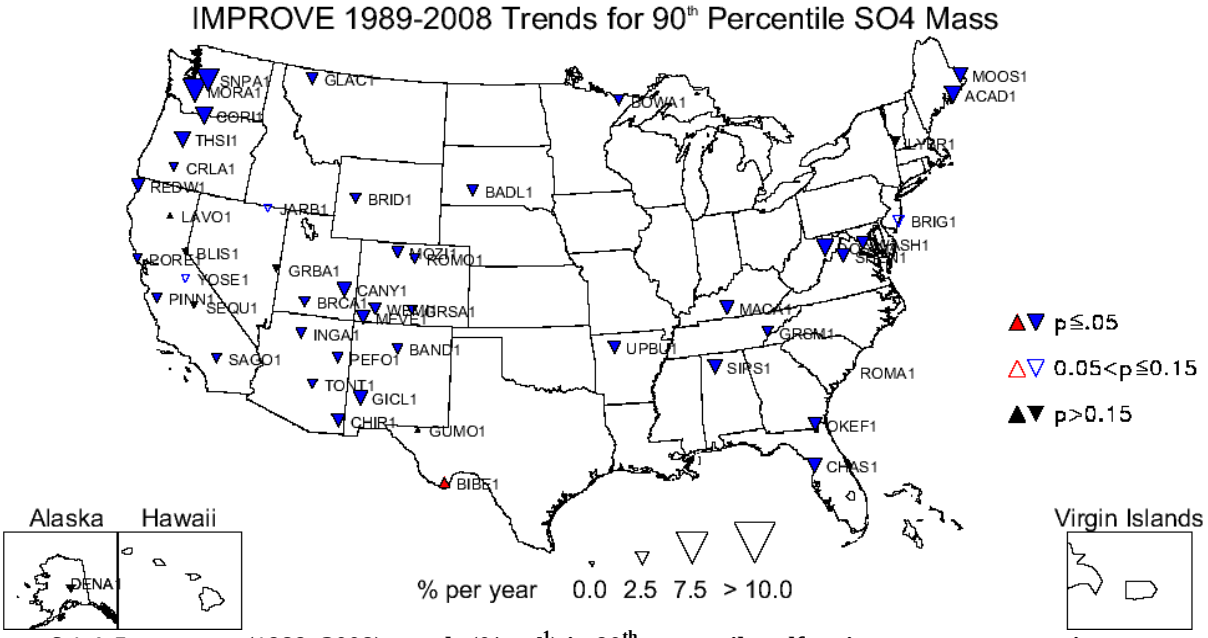

Figure 6.1.4. Long-term (1989–2008) trends (% yr^{-1}) in 90th percentile sulfate ion mass concentrations.

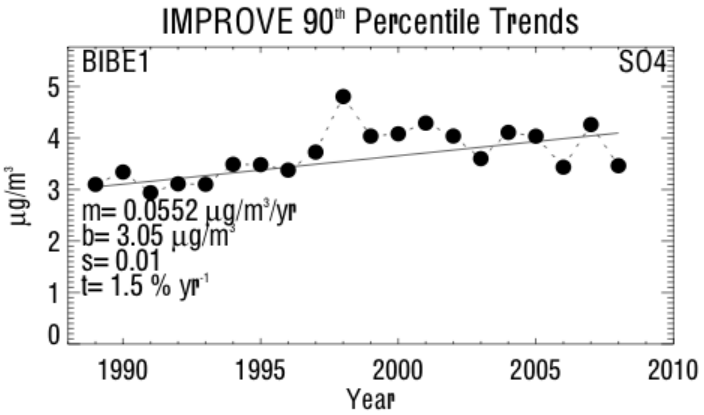

Figure 6.1.5. 90th percentile sulfate ion mass concentrations (μg m^{-3}) for Big Bend, Texas (BIBE1). Regression results, including Theil slope (m, μg m^{-3} yr^{-1}), intercept (b, μg m^{-3}), significance (s), and trend (t, % yr^{-1}) are included. The trend line is plotted as a solid line. The intercept corresponds to the initial year of data.

Table 6.1. Results from long-term (1989–2008) trend analyses for sulfate ion, total carbon (organic carbon + light absorbing carbon), fine soil, gravimetric fine mass, coarse mass, and PM_{10}. The minimum and maximum slope (μg m^{-3} yr^{-1}) and trend (% yr^{-1}) are provided, along with the site corresponding to the maximum and minimum.

Parameter	N_{tot}	N_{sig}	N_{neg}	N_{pos}	Slope (min.) (μg m^{-3} yr^{-1})	Site (min)	Slope (max.) (μg m^{-3} yr^{-1})	Site (max)	Trend (min.) (% yr^{-1})	Site (min)	Trend (max.) (% yr^{-1})	Site (max)
Sulfate Ion												
10th	49	41	41	0	-0.078	WASH1	-0.001	CRLA1	-5.6	GICL1	-1.4	PORE1
50th	49	43	43	0	-0.124	WASH1	-0.003	JARB1	-5.4	ACAD1	-1.1	JARB1
90th	49	41	40	1	-0.297	DOSO1	0.055	BIBE1	-5.2	MORA1	1.5	BIBE1
Mean	50	45	45	0	-0.140	DOSO1	-0.003	DENA1	-4.6	SNPA1	-0.9	DENA1
Winter	49	41	41	0	-0.114	WASH1	-0.002	YOSE1	-5.7	CANY1	-1.1	YOSE1
Spring	50	25	24	1	-0.119	WASH1	0.027	BIBE1	-4.5	ACAD1	1.3	BIBE1
Summer	51	39	37	2	-0.291	DOSO1	0.019	BIBE1	-6.3	SNPA1	1.4	LAVO1
Fall	50	36	36	0	-0.121	DOSO1	-0.003	DENA1	-4.6	ACAD1	-0.9	TONT1
Total Carbon												
10th	48	46	46	0	-0.046	WASH1	-0.003	BAND1	-14.6	THSI1	-0.7	BAND1
50th	48	45	45	0	-0.090	WASH1	-0.005	GRSA1	-5.0	MORA1	-0.8	GRSA1
90th	48	25	23	2	-0.172	WASH1	0.027	BRID1	-4.5	MORA1	1.6	BRID1
Mean	49	29	29	0	-0.103	WASH1	-0.009	CANY1, GUMO1	-4.7	MORA1	-1.0	PEFO1
Winter	49	44	44	0	-0.130	WASH1	-0.004	BRID1	-6.8	MORA1	-1.3	GRSM1
Spring	50	35	35	0	-0.094	WASH1	-0.009	CANY1	-4.6	MORA1	-1.3	TONT1
Summer	50	27	21	6	-0.064	GRGU1	0.045	BRID1	-3.9	REDW1	3.8	BRID1
Fall	50	30	29	1	-0.158	WASH1	0.030	CRLA1	-4.3	MORA1	3.2	CRLA1
Fine Soil												
10th	57	18	16	2	-0.003	MOZI1	0.006	TONT1	-5.0	DENA1	3.2	TONT1
50th	57	16	9	7	-0.035	VIIS1	0.025	DEVA1	-5.3	VIIS1	3.3	DEVA1
90th	57	18	4	14	-0.357	VIIS1	0.128	DEVA1	-4.3	VIIS1	6.9	CORI1
Mean	59	14	6	8	-0.081	VIIS1	0.060	DEVA1	-3.2	VIIS1	5.3	DEVA1
Winter	56	14	7	7	-0.006	BOWA1	0.025	CHIR1	-5.9	SNPA1	5.7	CHIR1
Spring	57	15	2	13	-0.013	SNPA1	0.085	DEVA1	-4.2	SNPA1	5.6	DEVA1
Summer	60	17	8	9	-0.181	VIIS1	0.103	CORI1	-4.3	CHAS1	12.4	CORI1
Fall	58	11	5	6	-0.112	VIIS1	0.041	DEVA1	-8.1	SAGO1	4.8	DEVA1
Gravimetric Fine Mass												
10th	57	49	49	0	-0.195	SIPS1	-0.013	CRLA1	-6.1	CRMO1	-0.9	CHAS1
50th	57	55	55	0	-0.376	WASH1	-0.027	MEVE1	-4.1	SNPA1	-0.6	BIBE1
90th	57	33	32	1	-0.698	DOSO1	0.202	SAWT1	-3.9	MORA1	3.3	SAWT1
Mean	59	47	45	2	-0.384	WASH1	0.071	SAWT1	-4.2	MORA1	2.4	SAWT1

Parameter	N_{tot}	N_{sig}	N_{neg}	N_{pos}	Slope (min.) ($\mu g\ m^{-3}\ yr^{-1}$)	Site (min)	Slope (max.) ($\mu g\ m^{-3}\ yr^{-1}$)	Site (max)	Trend (min.) (% yr^{-1})	Site (min)	Trend (max.) (% yr^{-1})	Site (max)
Winter	56	52	52	0	-0.395	WASH1	-0.027	BRID1	-6.5	MORA1	-1.0	EVER1
Spring	57	33	32	1	-0.334	SAGO1	0.125	DEVA1	-5.1	SNPA1	2.5	DEVA1
Summer	60	33	29	4	-0.584	DOSO1	0.242	SAWT1	-4.1	GRGU1	5.0	SULA1
Fall	58	36	35	1	-0.407	WASH1	0.111	SAWT1	-4.9	ACAD1	3.4	SAWT1
Coarse Mass												
10^{th}	50	42	42	0	-0.234	BRIG1	-0.023	ACAD1	-44.0	SNPA1	-2.2	BADL1
50^{th}	50	41	41	0	-0.377	BRIG1	-0.047	MEVE1	-12.7	SNPA1	-1.4	BADL1
90^{th}	50	34	34	0	-0.624	BRIG1	-0.121	BRCA1	-8.2	SNPA1	-1.6	YOSE1
Mean	50	40	40	0	-0.420	BRIG1	-0.055	MEVE1	-11.7	SNPA1	-1.4	GLAC1
Winter	48	42	42	0	-0.363	SEQU1	-0.062	JARB1	-18.7	SNPA1	-1.8	UPBU1
Spring	49	29	28	1	-0.242	REDW1	0.129	UPBU1	-7.7	MOOS1	1.7	UPBU1
Summer	51	31	29	2	-0.436	ROMA1	0.862	CORI1	-7.2	SNPA1	8.5	CORI1
Fall	51	37	37	0	-0.394	SAGO1	-0.049	BLIS1	-8.7	SNPA1	-1.1	PORE1
PM_{10}												
10th	50	50	50	0	-0.416	BRIG1	-0.046	THSI1	-9.9	MOZI1	-1.2	MACA1
50th	50	46	46	0	-0.569	BRIG1	-0.087	CHIR1	-8.0	SNPA1	-0.8	UPBU1
90th	50	26	26	0	-1.016	BRIG1	-0.126	BRID1	-4.6	SNPA1	-1.0	PORE1
Mean	50	44	44	0	-0.656	BRIG1	-0.058	MEVE1	-5.6	SNPA1	-0.9	UPBU1
Winter	49	46	46	0	-0.594	ROMA1	-0.118	ROMO1	-9.0	SNPA1	-1.7	TONT1
Spring	49	33	33	0	-0.511	SAGO1	-0.093	WEMI1	-4.9	MORA1	-1.2	GRSM1
Summer	51	29	28	1	-0.899	DOSO1	0.763	CORI1	-5.0	GRGU1	4.6	CORI1
Fall	51	39	39	0	-0.688	BRIG1	-0.075	CHIR1	-5.2	ACAD1	-0.9	CHIR1

N_{tot} refers to the total number of sites in the analysis
N_{sig} refers to the number of sites with significant trends ($p \leq 0.15$)
N_{pos} refers to the number of significant positive trends
N_{neg} refers to the number of significant negative trends

Examining shorter time periods (2000–2008) resulted in additional sites that met completeness criteria (usually > 150 sites, depending on the parameter, see Table 6.2); however, typically, 40–50% of the sites were significant. Negative 10th percentile trends at sites in the southwestern United States were relatively large (see Figure 6.1.6), as well as sites in the northwestern and eastern United States. Many of these same sites corresponded to significantly large negative trends during winter also, but fewer sites were significant for winter trends (Figure 6.1.7), compared to trends for 10th percentile. The largest negative short-term trend occurred at Martha's Vineyard, Massachusetts, in spring (MAVI1, -13.6% yr^{-1}), although El Dorado Springs, Missouri (ELDO1,
-13.2% yr^{-1}, 90th percentile), and Snoqualmie Pass, Washington (SNPA1, -13.1% yr^{-1} in summer), were similar. The spring sulfate ion concentrations at MAVI1 are shown in Figure 6.1.8. Concentrations have decreased from 2.8 µg m^{-3} to 1.9 µg m^{-3} in 9 years.

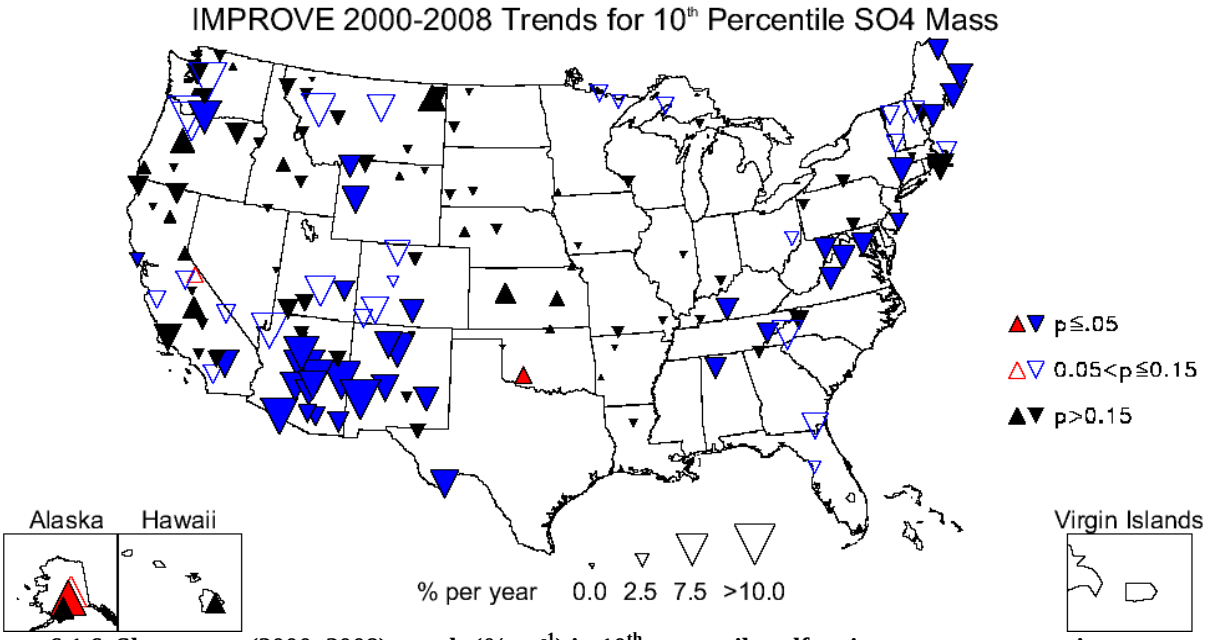

Figure 6.1.6. Short-term (2000–2008) trends (% yr^{-1}) in 10th percentile sulfate ion mass concentrations.

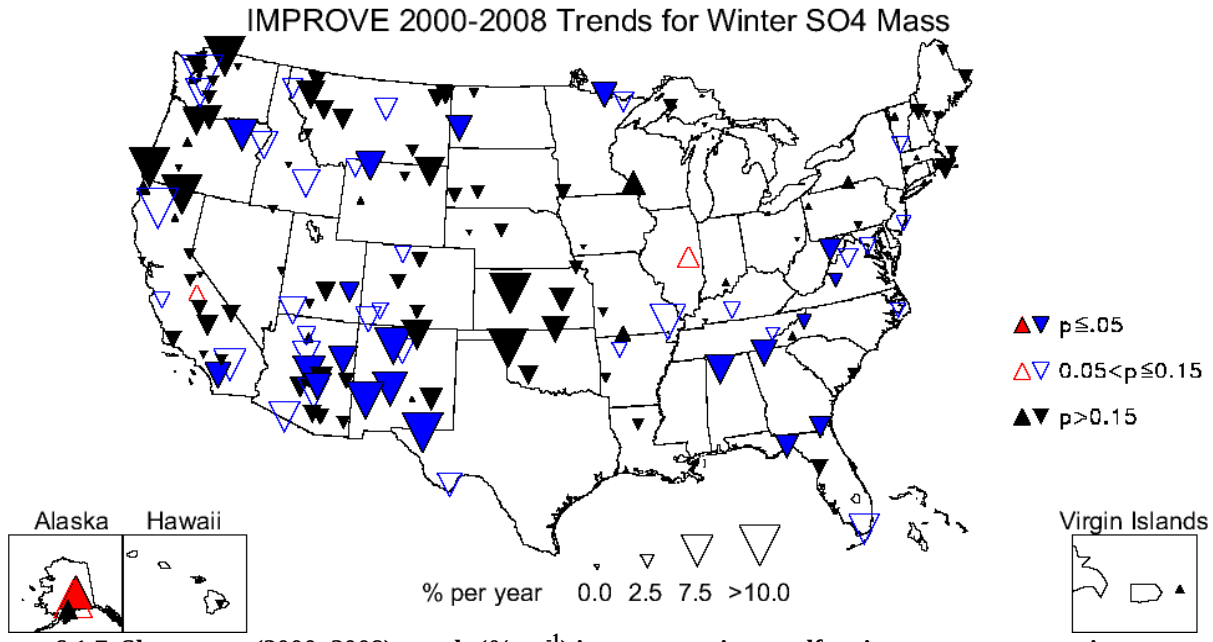

Figure 6.1.7. Short-term (2000–2008) trends (% yr^{-1}) in average winter sulfate ion mass concentrations.

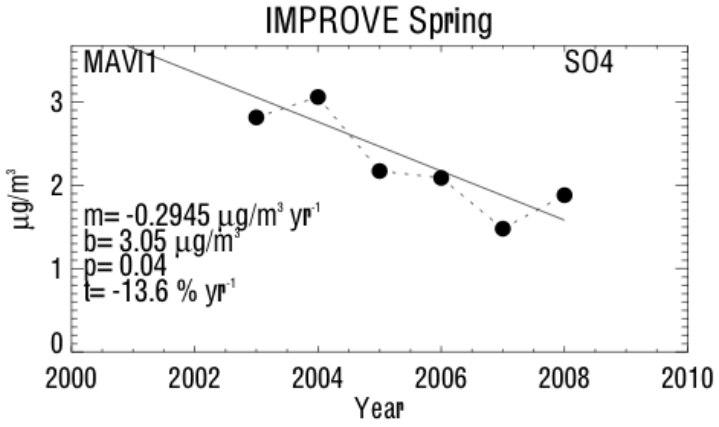

Figure 6.1.8. Average spring sulfate ion mass concentrations (µg m^{-3}) for Martha's Vineyard, Massachusetts (MAVI1). Regression results, including Theil slope (m, µg m^{-3} yr^{-1}), intercept (b, µg m^{-3}), significance (p), and trend (t, % yr^{-1}) are included. The trend line is plotted as a solid line. The intercept corresponds to the initial year of data.

Table 6.2. Results from short-term (2000–2008) trend analyses for sulfate ion, nitrate ion, total carbon (organic carbon + light absorbing carbon), fine soil, gravimetric fine mass, coarse mass, and PM_{10}. The minimum and maximum slope ($\mu g\ m^{-3}\ yr^{-1}$) and trend ($\%\ yr^{-1}$) are provided, along with the site corresponding to the maximum and minimum.

Parameter	N_{tot}	N_{sig}	N_{neg}	N_{pos}	Slope (min.) ($\mu g\ m^{-3}\ yr^{-1}$)	Site (min)	Slope (max.) ($\mu g\ m^{-3}\ yr^{-1}$)	Site (max)	Trend (min.) ($\%\ yr^{-1}$)	Site (min)	Trend (max.) ($\%\ yr^{-1}$)	Site (max)
Sulfate Ion												
10th	153	67	63	4	-0.078	WASH1	0.018	WIMO1	-11.7	GICL1	8.7	TRCR1
50th	153	75	67	8	-0.165	SHEN1	0.020	HOOV1	-8.8	COGO1	6.8	TRCR1
90th	153	61	58	3	-0.706	JARI1	0.817	HAVO1	-13.2	ELDO1	11.8	HAVO1
Mean	155	91	87	4	-0.260	JARI1	0.229	HAVO1	-9.3	MAVI1	10.7	HAVO1
Winter	153	55	51	4	-0.197	MING1	0.106	BOND1	-11.9	TRIN1	9.4	TRCR1
Spring	155	43	30	13	-0.295	MAVI1	0.481	HAVO1	-13.6	MAVI1	16.8	HAVO1
Summer	155	54	52	2	-0.464	MKGO1	0.134	HAVO1	-13.1	SNPA1	14.1	HAVO1
Fall	154	46	41	5	-0.204	WASH1	0.206	HAVO1	-11.2	ACAD1	10.2	HAVO1
Nitrate Ion												
10th	153	116	116	0	-0.022	WASH1	-0.001	DENA1	-18.8	SAGO1	-2.3	BOND1
50th	153	97	97	0	-0.146	SAGO1	-0.002	HAVO1	-15.0	TALL1	-1.4	SIKE1
90th	153	62	62	0	-0.314	SAFO1	-0.005	THSI1	-16.8	HECA1	-1.0	SAGU1
Mean	155	90	90	0	-0.140	SAGO1	-0.002	CABI1	-10.0	SAGA1	-1.3	CABI1
Winter	153	40	38	2	-0.251	ELDO1	0.012	JARB1	-25.5	TRIN1	11.9	JARB1
Spring	155	31	27	4	-0.149	SAGA1	0.039	MELA1	-12.9	CRES1	8.9	VIIS1
Summer	155	77	77	0	-0.126	SAGO1	-0.002	CABI1	-19.9	VILA1	-2.1	CHIR1
Fall	154	81	81	0	-0.177	SAGO1	-0.002	DENA1	-21.0	ZICA1	-2.9	KALM1
Total Carbon												
10th	153	95	95	0	-0.073	CHER1	-0.004	BALD1	-125.3	TUXE1	-1.3	QUVA1
50th	153	92	92	0	-0.129	STAR1	-0.008	THRO1,WEMI1	-25.2	HAVO1	-1.1	THRO1
90th	153	59	59	0	-0.456	PUSO1	-0.018	GUMO1	-15.4	GICL1	-1.1	JARI1
Mean	155	70	70	0	-0.172	PHOE1	-0.008	CANY1	-23.3	HAVO1	-1.5	CANY1
Winter	151	67	67	0	-0.289	PHOE1	-0.005	WHPE1	-21.7	STAR1	-1.6	WHPE1
Spring	154	59	58	1	-0.324	CHER1	0.136	COHU1	-25.6	HAVO1	6.0	COHU1
Summer	155	36	31	5	-0.225	MOMO1	0.209	DOME1	-23.0	SIME1	8.8	GAMO1
Fall	154	58	56	2	-0.324	MING1	0.182	SAWT1	-30.4	HAVO1	11.0	ZICA1
Fine Soil												
10th	153	26	19	7	-0.022	SAGU1	0.013	FOPE1 SWAN1	-13.5	MONT1	15.2	SWAN1
50th	153	38	22	16	-0.114	VIIS1	0.035	PEFO1	-22.1	VIIS1	7.3	FOPE1
90th	153	16	8	8	-0.261	BIBE1	0.282	CHER1	-10.1	BIBE1	8.5	CHER1
Mean	154	15	9	6	-0.144	SYCA1	0.084	CHER1	-10.5	COHI1	7.2	FOPE1

Parameter	N_{tot}	N_{sig}	N_{neg}	N_{pos}	Slope (min.) ($\mu g\ m^{-3}\ yr^{-1}$)	Site (min)	Slope (max.) ($\mu g\ m^{-3}\ yr^{-1}$)	Site (max)	Trend (min.) (% yr^{-1})	Site (min)	Trend (max.) (% yr^{-1})	Site (max)
Winter	152	12	10	2	-0.142	BIBE1	0.009	MKGO1	-20.8	BIBE1	2.7	MKGO1
Spring	154	15	8	7	-0.147	BIBE1	0.339	ZICA1	-13.5	CACO1	25.1	ZICA1
Summer	154	26	9	17	-0.079	COHI1	0.197	CHER1	-13.4	COHI1	14.3	INGA1
Fall	154	21	7	14	-0.070	THBA1	0.181	CHER1	-8.6	MEVE1	20.8	ZICA1
Gravimetric Fine Mass												
10th	153	47	42	5	-0.210	SIPS1	0.063	WIMO1	-12.2	STAR1	11.9	TRCR1
50th	153	60	57	3	-0.453	ELDO1	0.059	PEFO1	-7.2	STAR1	4.6	DENA1
90th	153	40	38	2	-0.887	GRSM1	1.438	HAVO1	-7.7	TUXE1	12.8	HAVO1
Mean	154	57	54	3	-0.457	QUCI1	0.296	HAVO1	-6.1	STAR1	7.3	HAVO1
Winter	152	47	43	4	-0.591	PHOE1	0.078	TRCR1	-14.6	STAR1	9.1	TRCR1
Spring	154	36	32	4	-1.049	TALL1	0.740	COHU1	-12.0	TALL1	12.0	HAVO1
Summer	154	39	37	2	-0.721	ADPI1	0.552	DOME1	-7.9	WHPE1	6.6	DOME1
Fall	154	44	33	11	-0.483	AREN1	0.386	ZICA1	-6.5	MOOS1	12.3	ZICA1
Coarse Mass												
10th	153	32	17	15	-0.246	VIIS1	0.173	QUCI1	-40.0	SNPA1	40.0	PASA1
50th	153	45	26	19	-0.730	VILA1	0.345	INGA1	-16.3	FLAT1	11.6	COHU1
90th	153	34	24	10	-1.374	GUMO1	0.809	DOME1	-8.8	MONT1	8.6	COHU1
Mean	154	35	23	12	-0.860	ELDO1	0.392	INGA1	-13.5	HOOV1	9.5	LYBR1
Winter	152	37	28	9	-0.831	BIBE1	0.310	THBA1	-18.2	HOOV1	12.7	SULA1
Spring	154	28	18	10	-0.662	WIMO1	0.933	CORI1	-16.4	MONT1	16.4	COHU1
Summer	154	44	17	27	-1.210	ELDO1	2.066	DOME1	-9.6	OLYM1	12.9	INGA1
Fall	154	25	13	12	-0.737	SAFO1	1.817	CHER1	-8.7	MONT1	12.9	SHRO1
PM_{10}												
10th	154	37	34	3	-0.707	CHER1	0.125	NEBR1	-15.1	STAR1	12.1	TRCR1
50th	154	50	48	2	-1.191	CHER1	0.424	INGA1	-9.9	STAR1	5.6	INGA1
90th	154	38	33	5	-1.566	SAFO1	1.630	HAVO1	-8.1	TUXE1	12.5	HAVO1
Mean	155	47	43	4	-1.140	ELDO1	0.429	DOME1	-6.8	MONT1	6.0	HAVO1
Winter	153	42	40	2	-1.656	VILA1	0.242	BOND1	-12.9	STAR1	1.7	BOND1
Spring	155	30	25	5	-1.361	VILA1	1.642	COHU1	-8.2	MONT1	12.3	COHU1
Summer	155	34	29	5	-1.802	ELDO1	2.701	DOME1	-7.1	ELDO1	13.4	INGA1
Fall	154	37	29	8	-0.733	SAFO1	2.177	CHER1	-6.0	GICL1	10.0	ZICA1

N_{tot} refers to the total number of sites in the analysis
N_{sig} refers to the number of sites with significant trends ($p \leq 0.15$)
N_{pos} refers to the number of significant positive trends
N_{neg} refers to the number of significant negative trends

A greater number of sites had positive short-term trends compared to positive long-term trends. In fact, some sites with decreasing long-term trends had positive short-term trends. For example, sulfate ion concentrations at the Denali, Alaska, site (DENA1) started increasing in later years. Notice the upward-trending sulfate concentrations for the most recent 10 years on the timeline for DENA1 in Figure 6.1.3, which was the period evaluated for the short-term trends analyses.

The 50th percentile and spring season corresponded to the highest number of significant positive short-term sulfate ion trends for all of the parameters investigated. Short-term sulfate trends during spring were very interesting (Figure 6.1.9). Many sites in the western United States corresponded to positive trends in the spring, the only season to exhibit such patterns. Recall that many western U.S. regions corresponded to maximum ammonium sulfate mean concentrations (2005–2008) during spring (Figure 4.5.1). The Hawaii Volcanoes HI site (HAVO1) corresponded to positive trends for the 50th, 90th, spring, summer, and fall seasons (10th percentile and winter trends were not significant). In fact, out of all significant short-term trends, the largest positive short-term trends in the United States occurred at HAVO1 for spring, summer, fall, and 90th percentile (16.8% yr^{-1}, 14.1% yr^{-1}, 10.2% yr^{-1}, and 11.8% yr^{-1}, respectively). The 90th percentile concentrations at HAVO1 are shown in Figure 6.1.10. High sulfate ion concentrations in 2008 were likely associated with volcanic activity. The maximum short-term sulfate ion trends for other percentiles and seasons were associated with the Trapper Creek site in Alaska (TRCR1, 8.7% yr^{-1}, 6.8% yr^{-1}, and 9.4% yr^{-1} for 10th percentile, 50th percentile, and winter, respectively).

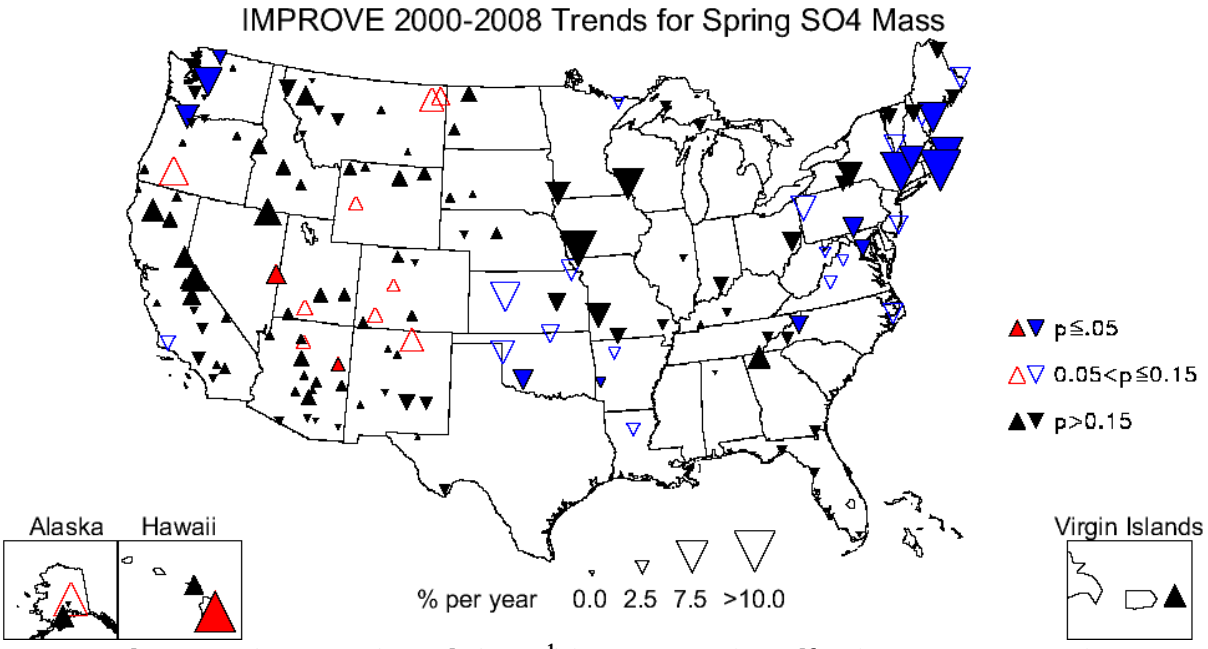

Figure 6.1.9. Short-term (2000–2008) trends (% yr^{-1}) in average spring sulfate ion mass concentrations.

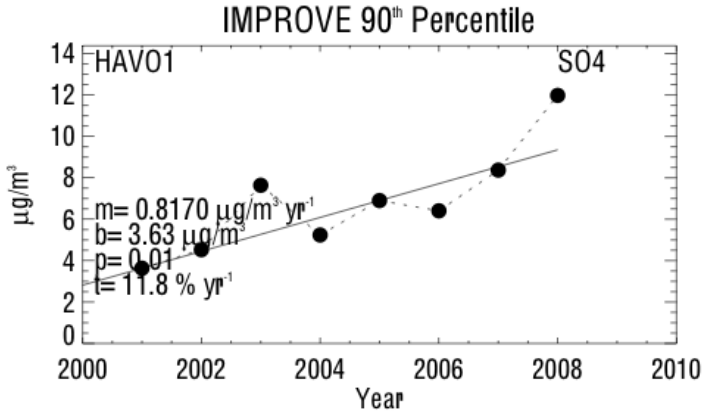

Figure 6.1.10. Average spring sulfate ion mass concentrations (µg m^{-3}) for Hawaii Volcanoes (HAVO1). Regression results, including Theil slope (m, µg m^{-3} yr^{-1}), intercept (b, µg m^{-3}), significance (p), and trend (t, % yr^{-1}) are included. The trend line is plotted as a solid line. The intercept corresponds to the initial year of data.

6.2 NITRATE ION TRENDS

During the late 1990s, IMPROVE nitrate ion concentrations at many sites fell below historical values during winter months. Investigations into a period from 1996 through 2000 revealed lower than usual concentrations during winter months and the cause remains unknown (McDade, 2007). Concentrations returned to normal levels after 2000, after which the data were deemed valid. Given these uncertainties, we computed short-term trends only for nitrate concentrations.

Approximately 155 sites met the completeness criteria for the nitrate ion short-term trend analysis, and only 31–116 of those (20–75%) were determined to be significant, depending on parameter. The 10th percentile had the highest number of significant sites, while the average spring concentrations had the lowest. The map corresponding to the 10th percentile trends is presented in Figure 6.2.1. Recall that the scale used to represent the magnitude of the trend was kept the same for all species. The 10th percentile nitrate ion trends at most sites were relatively large compared to the short-term sulfate ion trends and highly significant ($p \leq 0.05$) at most sites around the United States. No sites were associated with positive 10th percentile trends. The largest negative short-term nitrate ion trend for any percentile or season occurred at Trinity, California, in winter (TRIN1, -25.5% yr^{-1}). Winter nitrate ion concentrations at TRIN1 are shown in Figure 6.2.2. Concentrations decreased from 0.4 µg m^{-3} to 0.03 µg m^{-3} from 2000 to 2008. The individual site trends for the fall season, which corresponded to the season with the largest number of sites with significant trends, are shown in Figure 6.2.3. Large decreasing trends occurred for sites all around the United States during fall months, and no positive trends occurred at any site. Summer was the only other season that had no sites with positive trends.

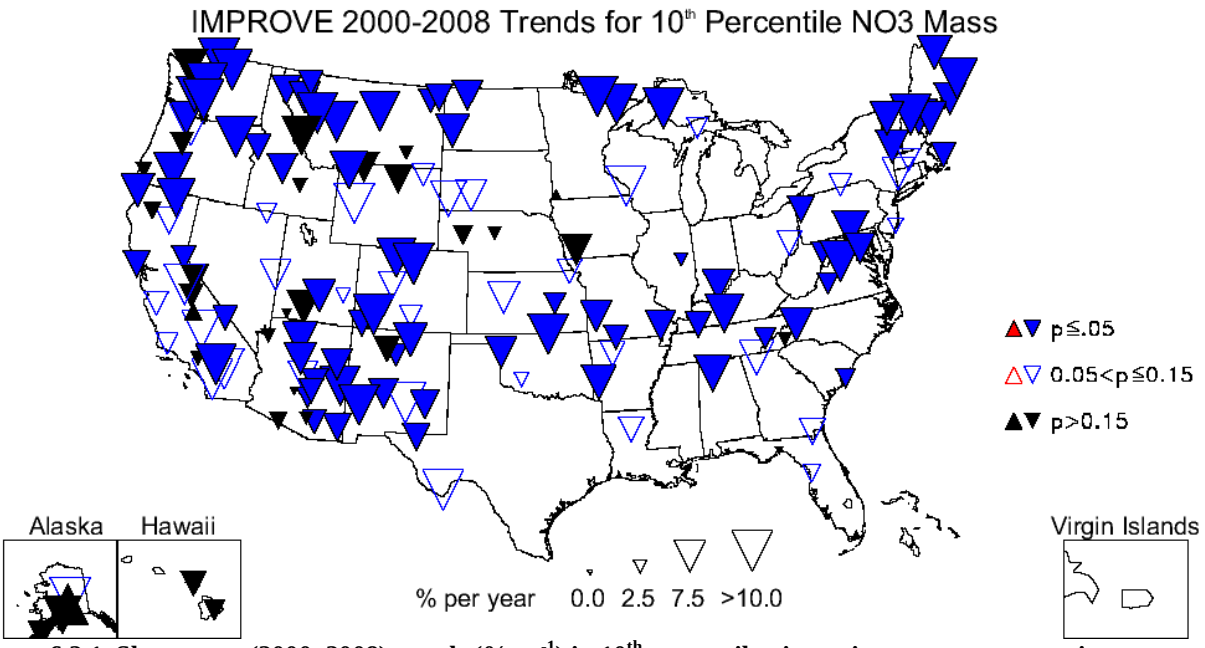

Figure 6.2.1. Short-term (2000–2008) trends (% yr^{-1}) in 10th percentile nitrate ion mass concentrations.

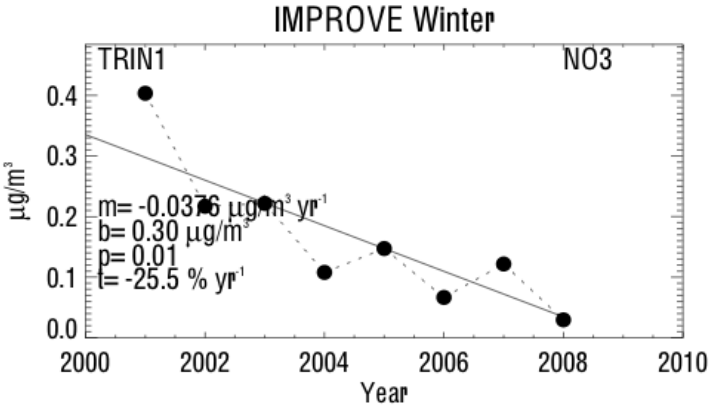

Figure 6.2.2. Average winter nitrate ion mass concentrations (µg m^{-3}) for Trinity, California (TRIN1). Regression results, including Theil slope (m, µg m^{-3} yr^{-1}), intercept (b, µg m^{-3}), significance (p), and trend (t, % yr^{-1}) are included. The trend line is plotted as a solid line. The intercept corresponds to the initial year of data.

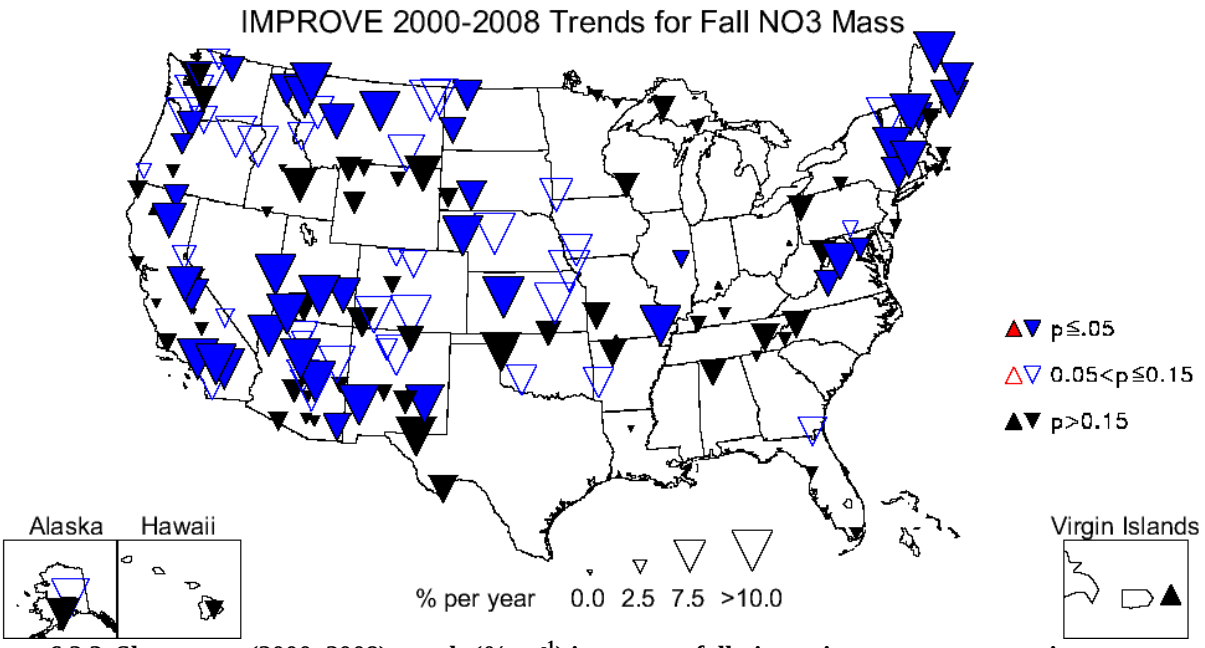

Figure 6.2.3. Short-term (2000–2008) trends (% yr^{-1}) in average fall nitrate ion mass concentrations.

The map for the 50th percentile, short-term nitrate ion trends is shown in Figure 6.2.4. As was the case with the trends for the 10th percentile and fall season, the magnitude of 50th percentile trends was fairly consistent for most sites across the United States, although several sites in the Mountain West corresponded to less significant ($p \leq 0.15$) negative trends. The map for spring nitrate ion trends at individual sites is shown in Figure 6.2.5. Only 20% of the sites with complete data corresponded to significant trends for spring. Positive trends in spring occurred at the Virgin Islands site (VIIS1, 8.9% yr^{-1}), Medicine Lake, Montana (MELA1, 6.0% yr^{-1}), Fort Peck, Montana (FOPE1, 6.6% yr^{-1}), and Denali, Alaska (DENA1, 6.2% yr^{-1}). Recall from Figure 4.2.1 that both the Virgin Islands and Alaska regions corresponded to maximum monthly mean ammonium nitrate concentrations during spring months. Positive trends also occurred for winter months, such as at Great Basin, Nevada (GRBA1, 3.8% yr^{-1}), and Jarbidge, Nevada (JARB1, 11.9%), which had the largest positive trend of any site for any percentile or season. The timeline of mean winter concentrations at JARB1 is shown in Figure 6.2.6 and demonstrates variable concentrations from year to year.

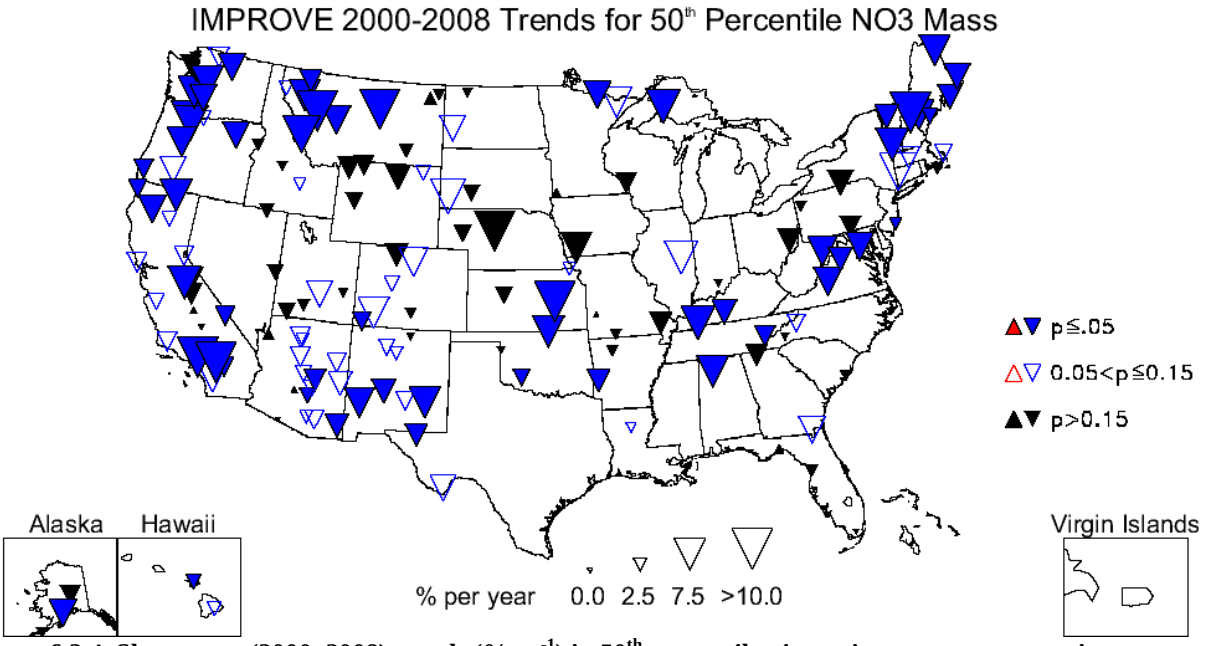

Figure 6.2.4. Short-term (2000–2008) trends (% yr^{-1}) in 50th percentile nitrate ion mass concentrations.

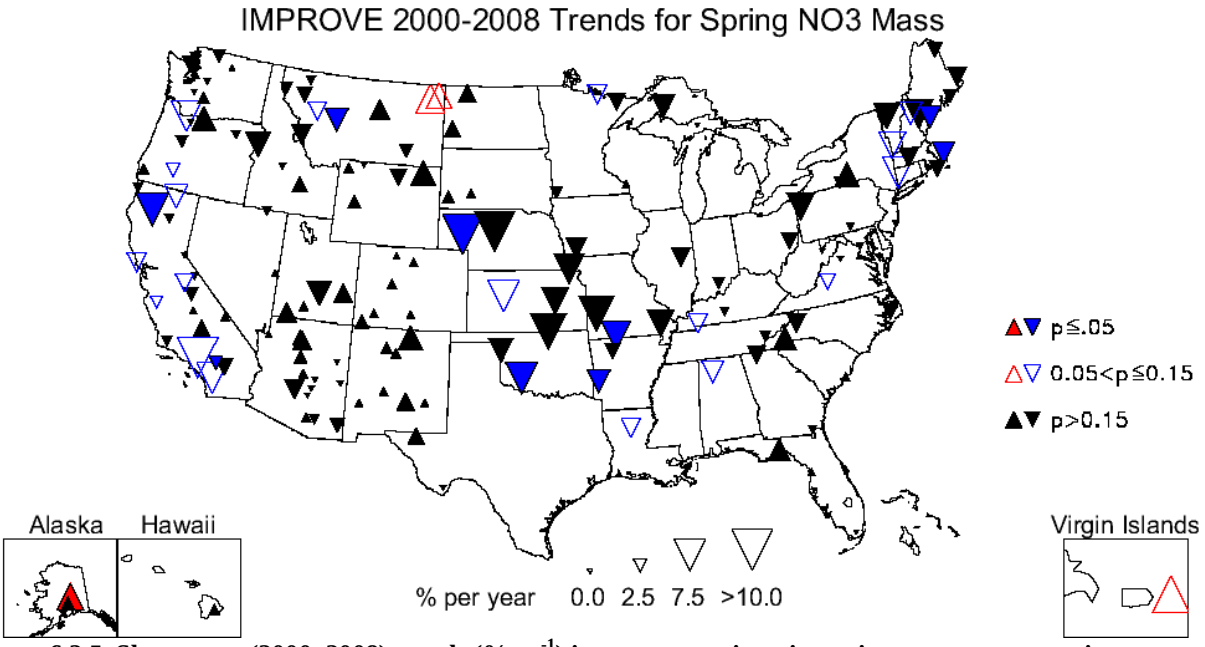

Figure 6.2.5. Short-term (2000–2008) trends (% yr^{-1}) in average spring nitrate ion mass concentrations.

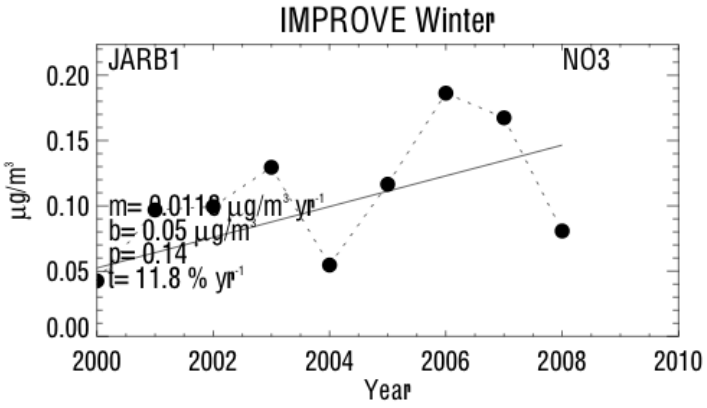

Figure 6.2.6. Average winter nitrate ion mass concentrations (µg m^{-3}) for Jarbidge NV (JARB1). Regression results, including Theil slope (m, µg m^{-3} yr^{-1}), intercept (b, µg m^{-3}), significance (p), and trend (t, % yr^{-1}) are included. The trend line is plotted as a solid line. The intercept corresponds to the initial year of data.

6.3 TOTAL CARBON TRENDS

We computed trends on total carbon, rather than on OC and LAC individually, because changes in analytical methods due to hardware upgrades on 1 January 2005 resulted in changes in the split between OC and LAC that introduced uncertainty to trend analyses (Chow et al., 2007; White, 2007). Higher LAC/TC ratios were reported after the change in analytical methods, but no changes in total carbon were detected (see Chapter 1.3.1.1).

Evaluating long-term trends in TC typically resulted in roughly 50 sites with complete data; 25–46 of these sites were associated with significant trends depending on the parameter (see Table 6.1). The 10^{th} percentile, long-term trends corresponded to the highest number of significant trends (46) for any parameter. A map of the 10^{th} percentile, TC long-term trends is shown in Figure 6.3.1. Sites with larger negative trends were located along the western coast. The least negative 10^{th} percentile trend occurred at Redwood, California (REDW1, -3.9% yr^{-1}), and the largest negative 10^{th} percentile trend occurred at Three Sisters, Oregon (THSI1, -14.6% yr^{-1}). The timeline of the 10^{th} percentile TC concentrations at the THSI1 site is presented in Figure 6.3.2 and shows a large decrease in low TC concentrations since the mid-1990s. No positive trends were associated with any site for 10^{th} percentile concentrations. The winter season was also associated with large, decreasing, long-term trends and corresponded to sites in the western United States (Figure 6.3.3). The largest negative trend during winter occurred at the Mount Rainier, Washington, site (MORA1, -6.8% yr^{-1}), and the least negative trend occurred at Great Smoky Mountains, Tennessee (GRSM1, -1.3% yr^{-1}). It is possible that the low TC concentrations associated with the 10^{th} percentile occurred mainly in winter; recall that in the western United States both OC and LAC minimum monthly mean concentrations (2005–2008) occurred during winter months for many regions (see Figure 4.3.1 and Figure 4.4.1, respectively). Concentrations on these already low concentration days in winter appear to be decreasing. For example, see the timeline of winter concentrations for the MORA1 site (Figure 6.3.4). Winter concentrations decreased from 2.3 µg m^{-3} to 0.7 µg m^{-3} from 1989 to 2008.

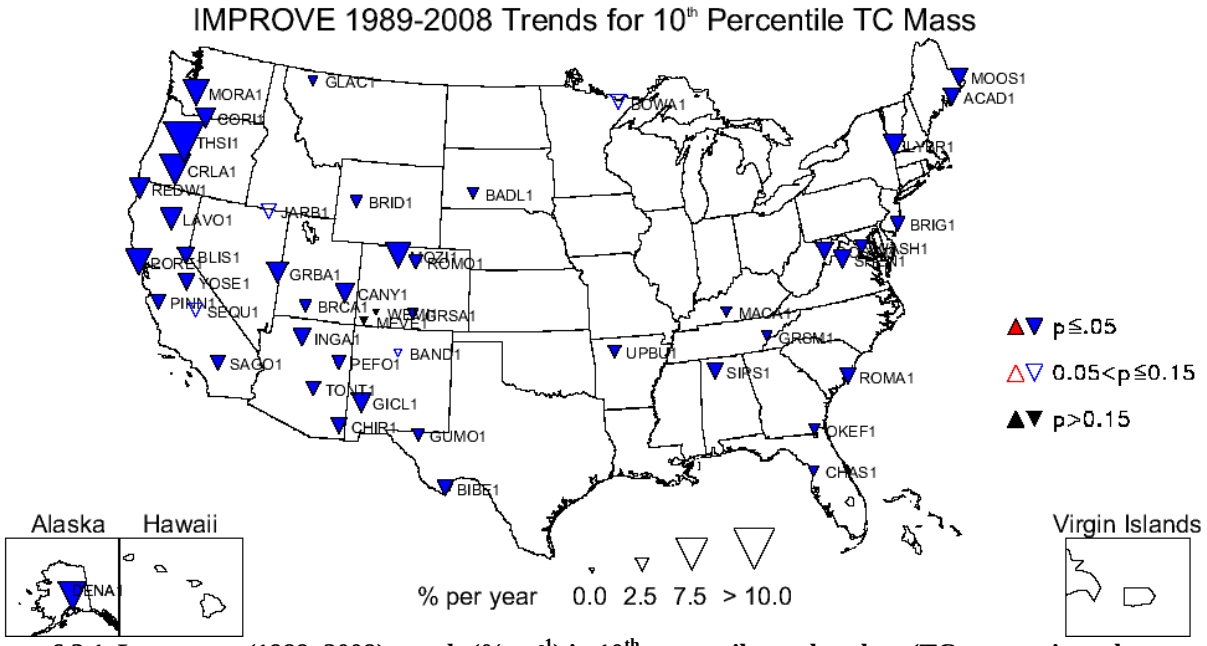

Figure 6.3.1. Long-term (1989–2008) trends (% yr^{-1}) in 10th percentile total carbon (TC = organic carbon + light absorbing carbon) mass concentrations.

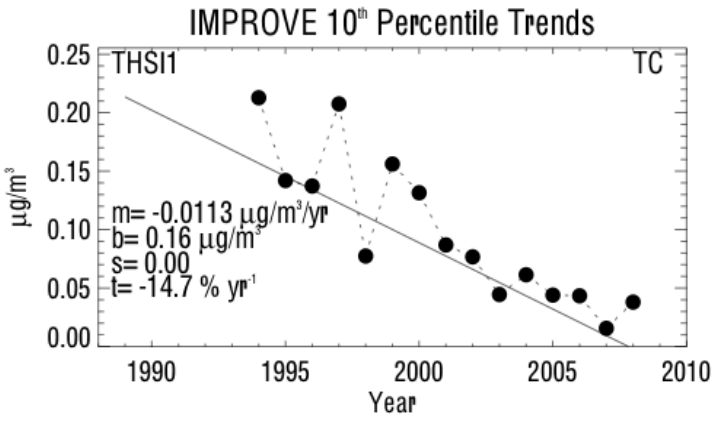

Figure 6.3.2. 10th percentile total carbon (TC = organic carbon + light absorbing carbon) mass concentrations (µg m^{-3}) for Three Sisters, Oregon (THSI1). Regression results, including Theil slope (m, µg m^{-3} yr^{-1}), intercept (b, µg m^{-3}), significance (s), and trend (t, % yr^{-1}) are included. The trend line is plotted as a solid line. The intercept corresponds to the initial year of data.

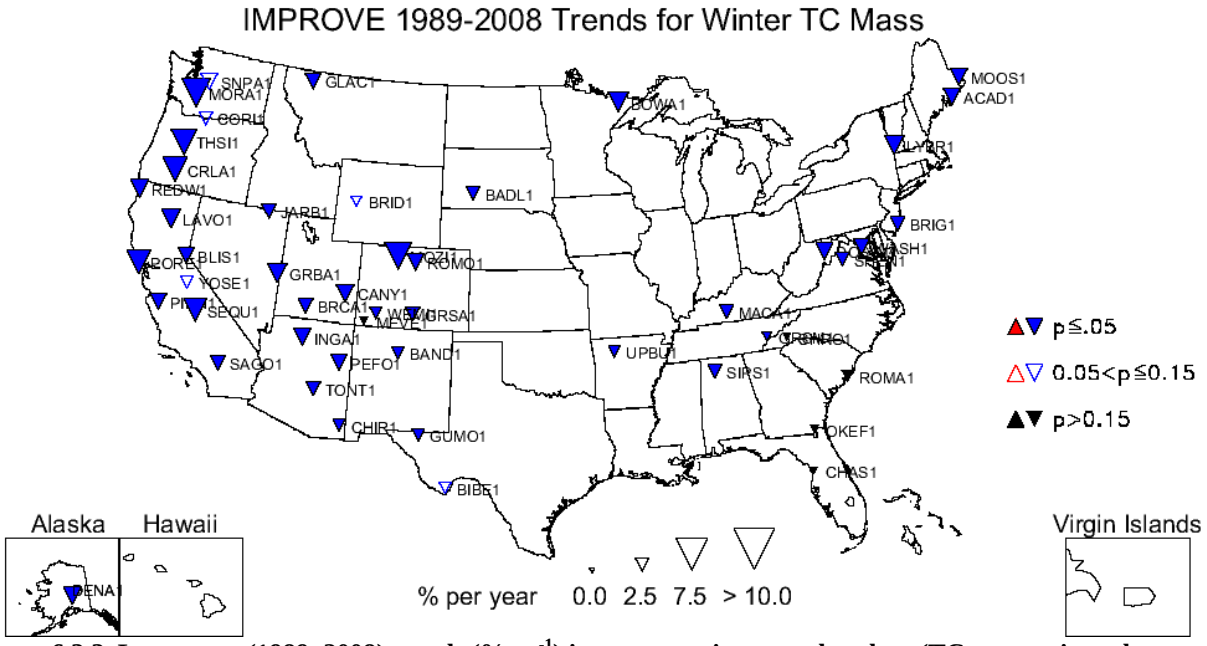

Figure 6.3.3. Long-term (1989–2008) trends (% yr^{-1}) in average winter total carbon (TC = organic carbon + light absorbing carbon) mass concentrations.

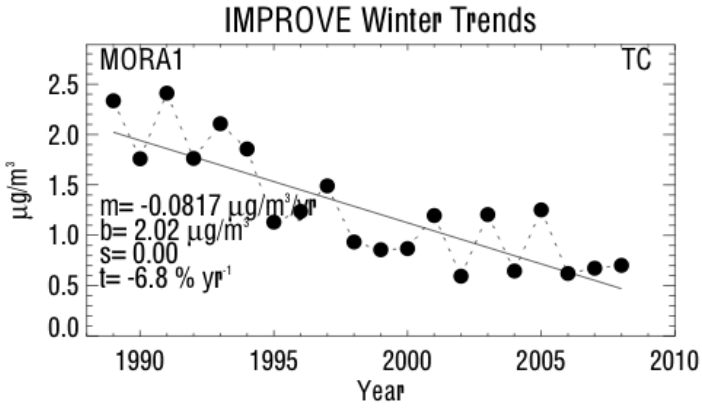

Figure 6.3.4. Average winter total carbon (TC = organic carbon + light absorbing carbon) mass concentrations (µg m^{-3}) for Mount Rainier, Washington (MORA1). Regression results, including Theil slope (m, µg m^{-3} yr^{-1}), intercept (b, µg m^{-3}), significance (s), and trend (t, % yr^{-1}) are included. The trend line is plotted as a solid line. The intercept corresponds to the initial year of data.

The individual site trends for the 90th percentile concentration were less negative or insignificant, especially at sites along the western coast, compared to the 10th percentile trends (compare Figure 6.3.5 to Figure 6.3.1). Sites with positive 90th percentile, long-term TC trends corresponded to Bridger, Wyoming (BRID1, 1.7% yr^{-1}), and Bryce Canyon, Utah (BRCA1, 1.2% yr^{-1}). The BRID1 timeline of 90th percentile concentration is shown in Figure 6.3.6. The variability in the increasing TC concentration may be related to sporadic emissions from biomass burning. Of the 10th, 50th, and 90th percentiles, positive trends occurred only for the 90th percentile (see Table 6.1).

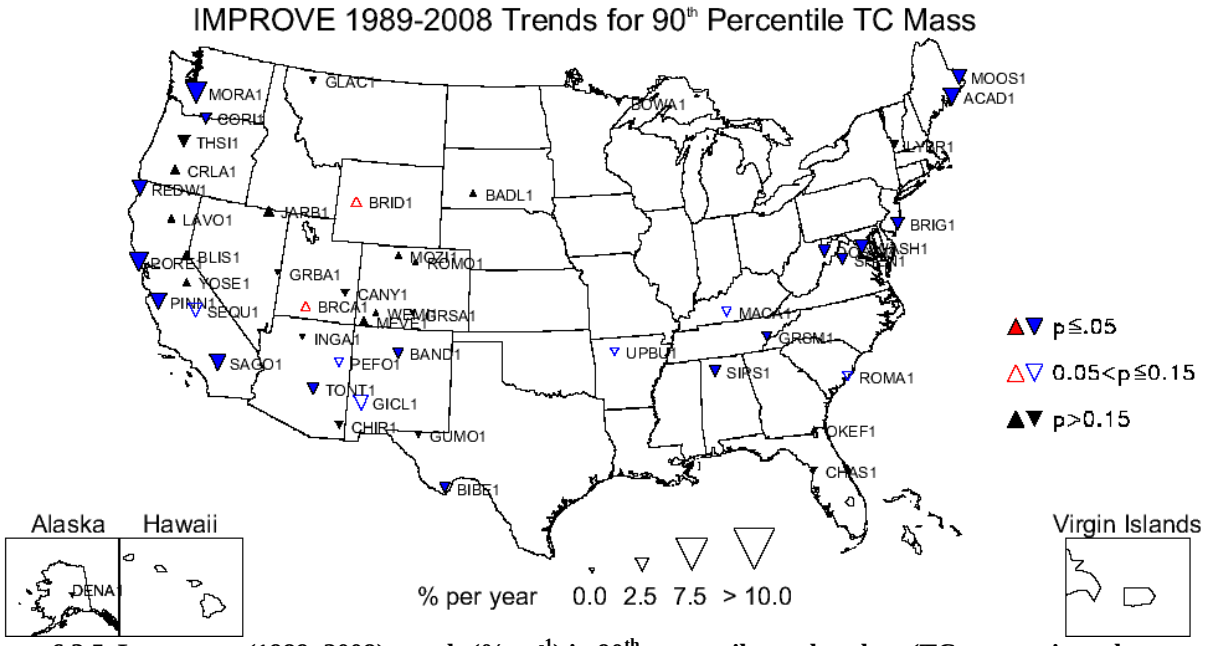

Figure 6.3.5. Long-term (1989–2008) trends (% yr^{-1}) in 90th percentile total carbon (TC = organic carbon + light absorbing carbon) mass concentrations.

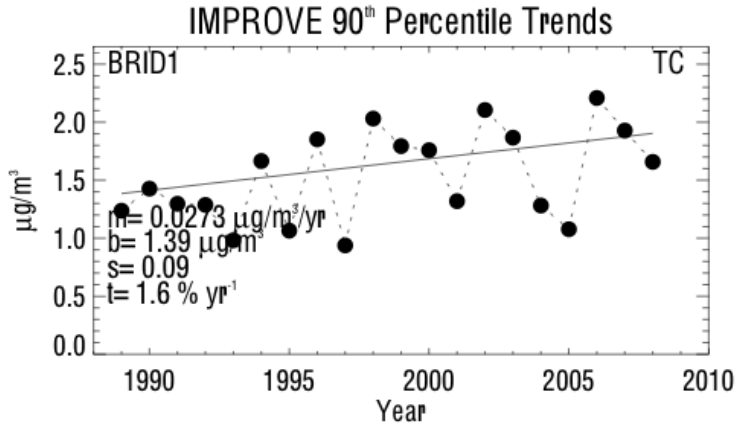

Figure 6.3.6. 90th percentile total carbon (TC = organic carbon + light absorbing carbon) mass concentrations (µg m^{-3}) for Bridger, Wyoming (BRID1). Regression results, including Theil slope (m, µg m^{-3} yr^{-1}), intercept (b, µg m^{-3}), significance (s), and trend (t, % yr^{-1}) are included. The trend line is plotted as a solid line. The intercept corresponds to the initial year of data.

Long-term, summer TC trends were associated with the largest number of sites (six) with positive trends of all the parameters investigated, although many sites corresponded to insignificant trends. In general, magnitudes of summer trends were fairly consistent (and low) around the United States (see Figure 6.3.7). The largest negative summer, long-term trend occurred at Redwood, California (REDW1, -3.9% yr^{-1}), and the largest positive summer trend occurred at Bridger, Wyoming (BRID1, 3.8% yr^{-1}). The other five sites associated with positive trends were Bliss, California (BLIS1, 2.3% yr^{-1}), Great Basin, Nevada (GRBA1, 2.1% yr^{-1}), Bryce Canyon, Utah (BRCA1, 2.4% yr^{-1}), Rocky Mountain National Park, Colorado (ROMO1, 1.04% yr^{-1}), and Great Sand Dunes, Colorado (GRSA1, 1.3% yr^{-1}). The timeline of summer TC

concentrations for BRID1 is shown in Figure 6.3.8. The variable summer concentrations were similar to the 90th percentile TC concentration shown in Figure 6.3.6, and suggested contributions from biomass burning emissions. Recall from Chapters 4.3 and 4.4 that most regions in the western United States corresponded to summer maxima in both OC and LAC (Figures 4.3.1 and 4.4.1, respectively). Unlike the strongly decreasing TC 10th percentile concentrations that likely occurred during winter days, the highest concentrations that were likely associated with summer months were decreasing to a much lower degree and in some cases actually increasing.

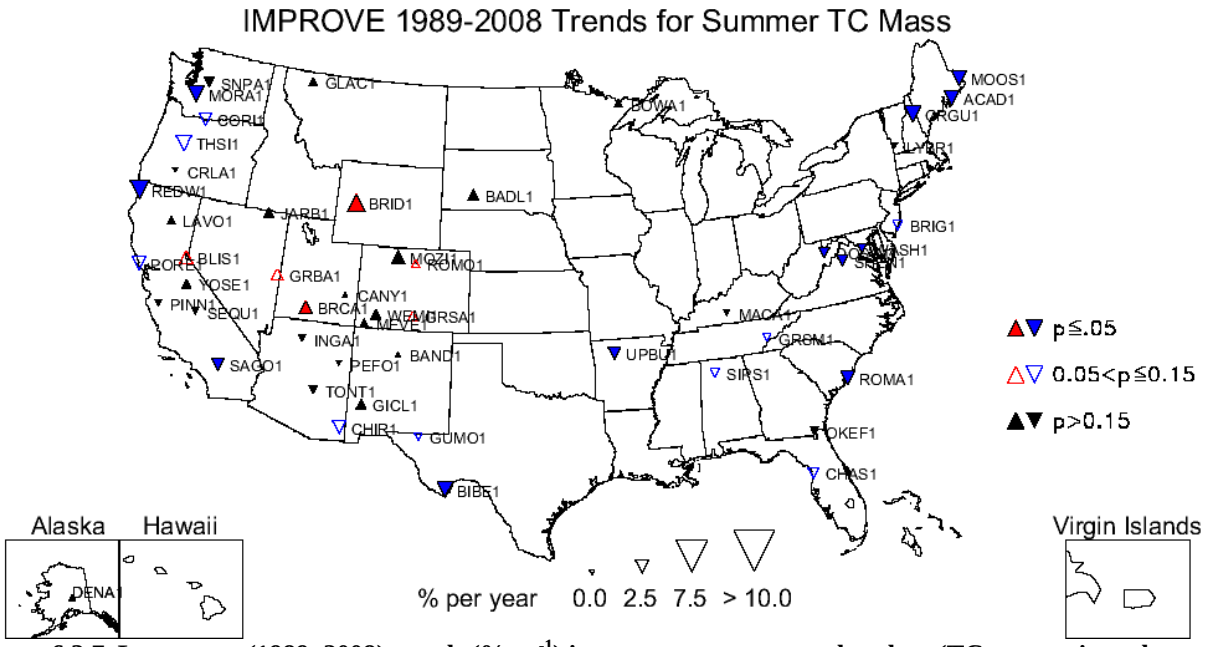

Figure 6.3.7. Long-term (1989–2008) trends (% yr^{-1}) in average summer total carbon (TC = organic carbon + light absorbing carbon) mass concentrations.

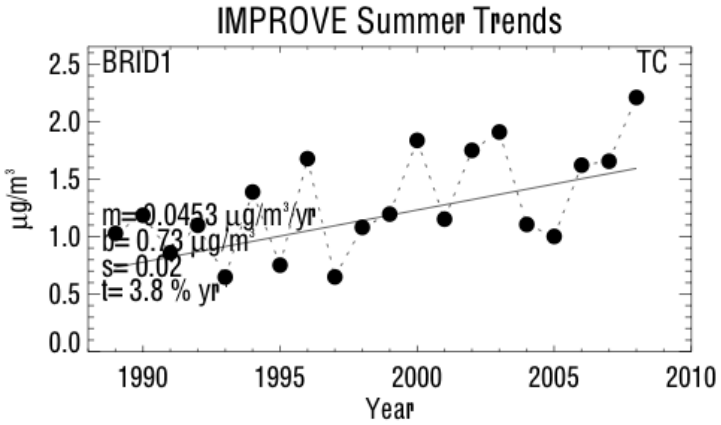

Figure 6.3.8. Average summer total carbon (TC = organic carbon + light absorbing carbon) mass concentrations (µg m^{-3}) for Bridger, Wyoming (BRID1). Regression results, including Theil slope (m, µg m^{-3} yr^{-1}), intercept (b, µg m^{-3}), significance (s), and trend (t, % yr^{-1}) are included. The trend line is plotted as a solid line. The intercept corresponds to the initial year of data.

Short-term trend analyses were performed on a much larger number of sites compared to the long-term trend analyses (150–155 sites, depending on parameter); roughly 20–60% of the sites were determined to be significant. The later time period allowed for more sites with complete data to be included in the analyses. The 10th percentile trends corresponded to the largest number of significant trends for the parameters investigated (see Table 6.2). The short-term, 10th percentile trends in TC for individual sites are shown in Figure 6.3.9. Short-term trends were much larger for many sites around the United States compared to long-term trends. Trends generally were less negative at sites in the eastern compared to the western United States. One of the largest negative 10th percentile trends occurred at Three Sisters, Oregon (THSI1, -22.9% yr^{-1}). The timeline for the 10th percentile TC concentration at THSI1 is shown in Figure 6.3.10 and demonstrates the downward trend of already low TC concentrations. The least negative 10th percentile trend occurred at Queen Valley, Arizona (QUVA1, -1.3% yr^{-1}). There were no sites associated with positive short-term trends for any of the percentiles. The large negative trends in winter for individual sites are presented in Figure 6.3.11. Although there were fewer sites with significant trends compared to the 10th percentile trends, the magnitudes were comparable. No positive short-term winter trends were associated with any site. The largest decreasing winter trend was associated with the Starkey, Oregon, site (STAR1, -21.7% yr^{-1}). The smallest decreasing trend in winter concentrations occurred at the Wheeler Peak, New Mexico, site (WHPE1, -1.6% yr^{-1}).

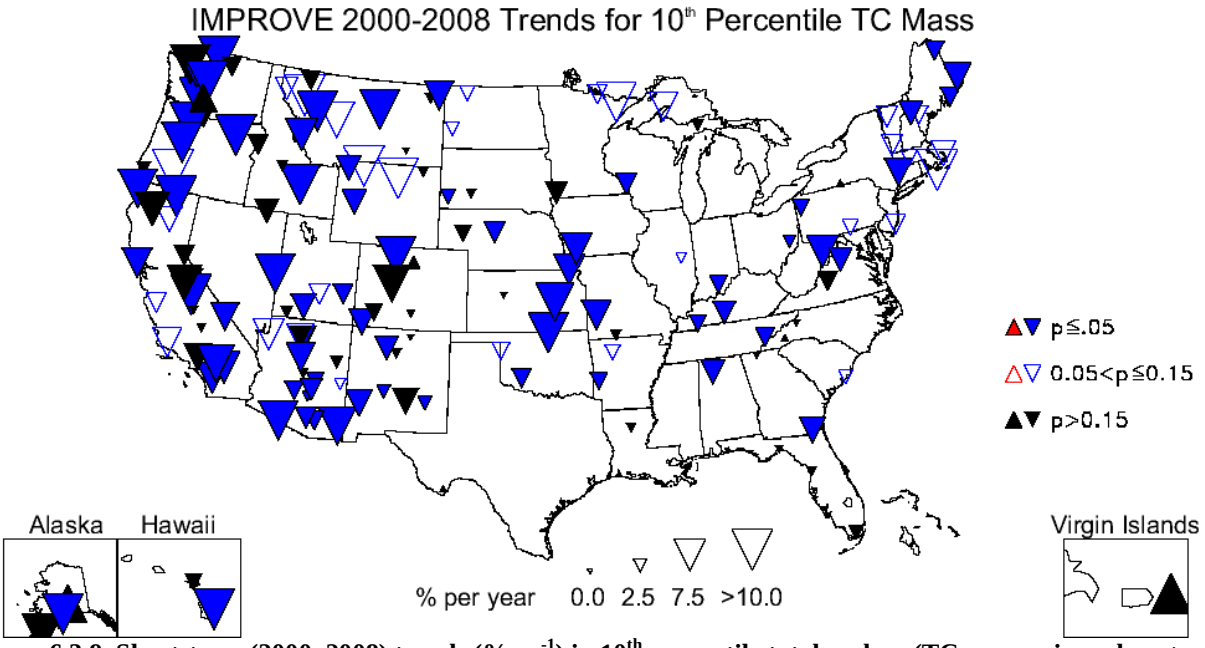

Figure 6.3.9. Short-term (2000–2008) trends (% yr^{-1}) in 10th percentile total carbon (TC = organic carbon + light absorbing carbon) mass concentrations.

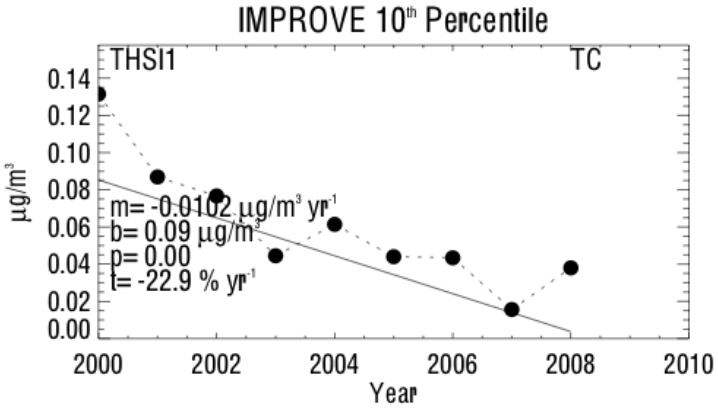

Figure 6.3.10. 10th percentile total carbon (TC = organic carbon + light absorbing carbon) mass concentrations (µg m^{-3}) for Three Sisters, Oregon (THSI1). Regression results, including Theil slope (m, µg m^{-3} yr^{-1}), intercept (b, µg m^{-3}), significance (p), and trend (t, % yr^{-1}) are included. The trend line is plotted as a solid line. The intercept corresponds to the initial year of data.

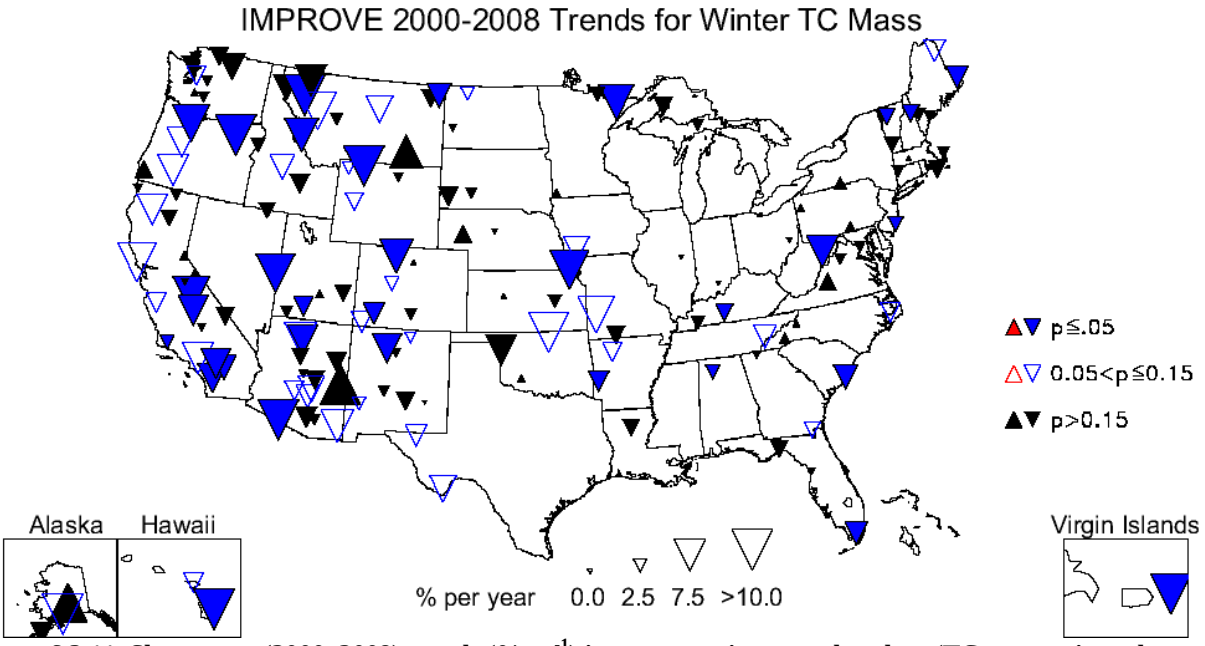

Figure 6.3.11. Short-term (2000–2008) trends (% yr^{-1}) in average winter total carbon (TC = organic carbon + light absorbing carbon) mass concentrations.

Although the number of sites with significant trends corresponding to the 10th and 50th percentiles was similar (95 versus 92, respectively), the 50th percentile trends were generally less negative. A map of 50th percentile trends is shown in Figure 6.3.12. Trends corresponding to sites in the eastern United States generally were less negative than trends for western sites. The largest decreasing 50th percentile, short-term trend occurred at Hawaii Volcanoes (HAVO1, -25.16% yr^{-1}), and the least negative 50th percentile trend occurred at James River Face Wilderness, Virginia (JARI1, -1.07% yr^{-1}). A timeline showing the decrease in 50th percentile TC concentrations at HAVO1 is presented in Figure 6.3.13. A precipitous drop in the 50th percentile TC concentrations occurred around 2003, after which concentrations decreased slowly. Results for short-term summer trends included five sites with positive trends (Figure 6.3.14). The sites at

Gates of the Mountains, Montana (GAMO1, 8.8% yr^{-1}), Dome Lands Wilderness, California (DOME1, 8.1% yr^{-1}), Hells Canyon, Oregon (HECA1, 5.4% yr^{-1}), Craters of the Moon, Idaho (CRMO1, 3.6% yr^{-1}), and Shenandoah, Virginia (SHEN1, 3.2% yr^{-1}), all corresponded to positive trends in summer concentrations. The trend line of summer concentration at GAMO1 is shown in Figure 6.3.15. High concentrations in 2003 and 2007 were most likely related to wildfire emissions. The trend line plotted alongside the data demonstrated that these outliers were not heavily weighted in the regression. Positive short-term TC trends also occurred during other seasons. In spring, a positive trend was associated with Cohutta, Georgia (COHU1, 6.0% yr^{-1}), and in fall the sites of Sawtooth, Idaho (SAWT1, 10.9% yr^{-1}), and Zion Canyon, Utah (ZICA1, 11.0% yr^{-1}), were associated with positive trends.

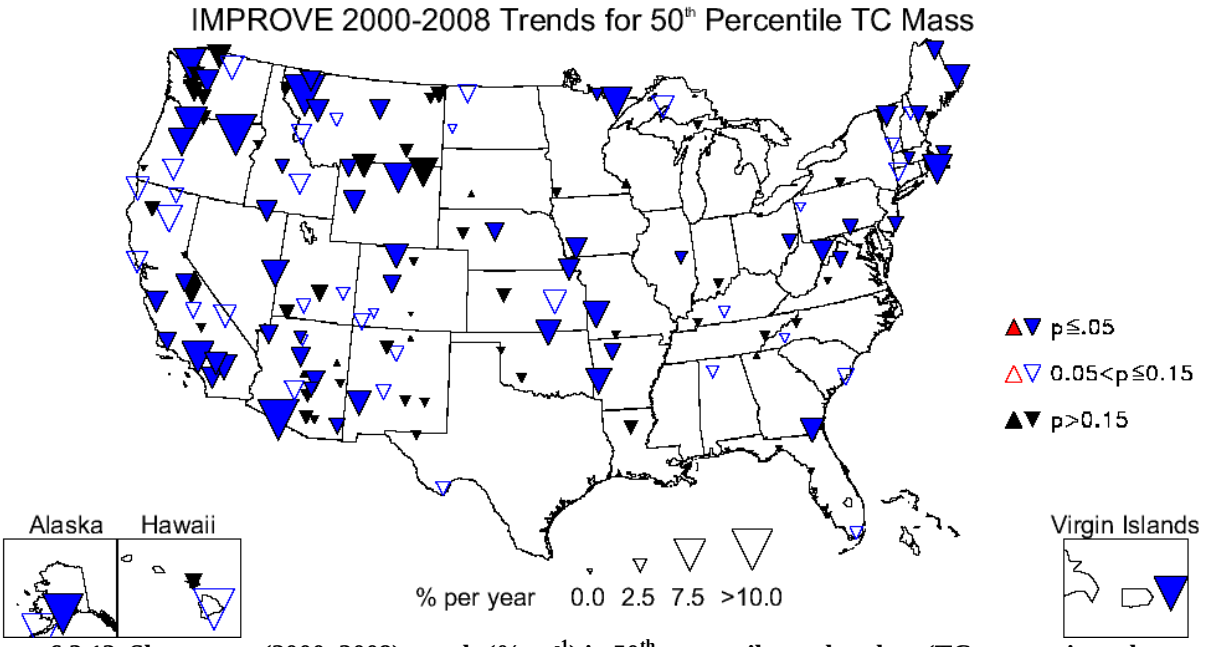

Figure 6.3.12. Short-term (2000–2008) trends (% yr^{-1}) in 50th percentile total carbon (TC = organic carbon + light absorbing carbon) mass concentrations.

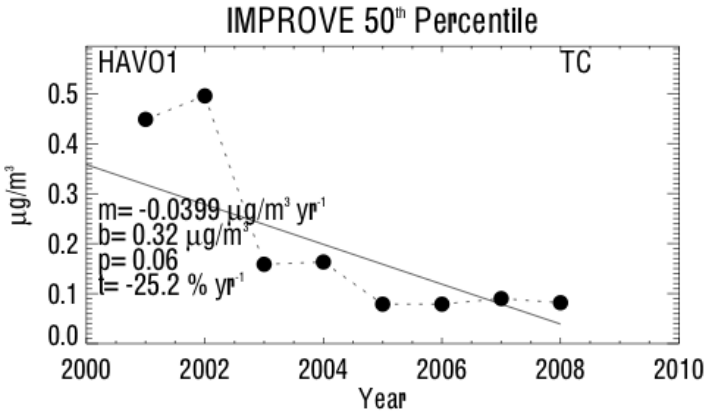

Figure 6.3.13. 50th percentile total carbon (TC = organic carbon + light absorbing carbon) mass concentrations (µg m^{-3}) for Hawaii Volcanoes (HAVO1). Regression results, including Theil slope (m, µg m^{-3} yr^{-1}), intercept (b, µg m^{-3}), significance (p), and trend (t, % yr^{-1}) are included. The trend line is plotted as a solid line. The intercept corresponds to the initial year of data.

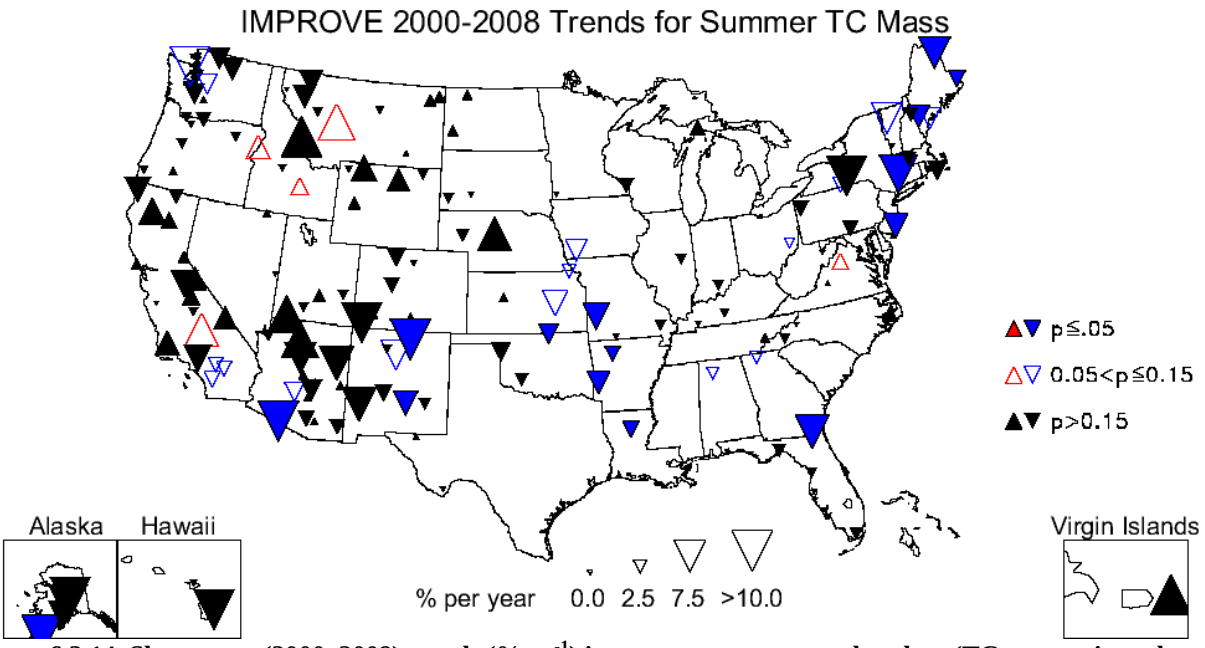

Figure 6.3.14. Short-term (2000–2008) trends (% yr^{-1}) in average summer total carbon (TC = organic carbon + light absorbing carbon) mass concentrations.

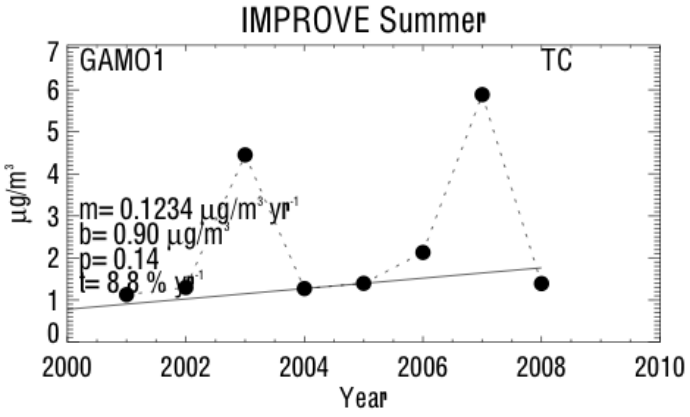

Figure 6.3.15. Average summer total carbon (TC = organic carbon + light absorbing carbon) mass concentrations (µg m^{-3}) for Gates of the Mountains, Montana (GAMO1). Regression results, including Theil slope (m, µg m^{-3} yr^{-1}), intercept (b, µg m^{-3}), significance (p), and trend (t, % yr^{-1}) are included. The trend line is plotted as a solid line. The intercept corresponds to the initial year of data.

6.4 $PM_{2.5}$ SOIL TRENDS

Recall from Chapter 2.1 that $PM_{2.5}$ soil mass concentrations were determined by combining the oxides of elemental mass concentrations of Al, Si, Ca, Fe, and Ti (see Table 2.1). The analytical methods used to determine these species have evolved over time and included PIXE (proton induced X-ray emission) and XRF (X-ray fluorescence) techniques. The transitions from PIXE to XFR methods, the change in XRF anodes from Mo to Cu, as well as different calibration procedures affect the data by changing minimum detection limits (see Chapters 1.3.1.2-1.3.1.5). No corrections to the elemental data were performed to account for changes in analytical methods as part of this trend analysis. These results should be interpreted with some

caution as the trends are sensitive to variability in analytical methods. Changes in analytical methods may not equally affect data for each soil species; therefore the integrated soil concentration may be less susceptible to possible variability introduced by the analytical methods, although this has not been specifically demonstrated. A thorough trend analysis that removed variability in the data due to analytical changes was beyond the scope of this report.

Trends in soil concentrations were quite different than trend results for the previous species and included a much higher number of sites with significant positive trends for all parameters. However, the number of sites with significant long-term soil trends was generally lower. Only 11–18 sites were significant (out of ~57), depending on the parameter. The map of sites for the 10^{th} percentile trends demonstrated the low number of sites and fairly low magnitude trends (Figure 6.4.1). Most of the sites with significant trends were in the western and the northeastern United States. The largest decreasing 10^{th} percentile trend occurred at the Denali, Alaska, site (DENA1, -5.0% yr^{-1}). A decrease in the very low 10^{th} percentile soil concentrations at DENA1 is shown in Figure 6.4.2. Only two sites corresponded to positive 10^{th} percentile trends: Tonto, Arizona (TONT1, 3.16% yr^{-1}), and Everglades, Florida (EVER1, 1.17% yr^{-1}). Long-term trends in average winter soil concentrations are shown for individual sites in Figure 6.4.3. Only 14 sites corresponded to statistically significant trends, and half of them were positive. The largest negative winter trend occurred at Snoqualmie Pass, Washington (SNPA1, -5.9% yr^{-1}), and the largest positive trend occurred at Chiricahua, Arizona (CHIR1, 5.7% yr^{-1}). Two sites in the southeastern United States with increasing winter trends (Okefenokee, Georgia, OKEF1, and Everglades, Florida, EVER1) were actually associated with minimum mean soil concentrations in winter (for 2005–2008, see Figure 4.5.1), suggesting that the lowest soil concentrations at these sites has increased over the last 20 years. Long-term soil trends at OKEF1 and EVER1 were negative during summer, when soil concentrations were typically highest and long-range transport of dust is a well-known phenomenon. An example of decreasing soil concentrations in summer is shown for the Virgin Islands site (VIIS1, -3.6yr^{-1}) in Figure 6.4.4. Soil concentrations are typically highest in summer at VIIS but are decreasing.

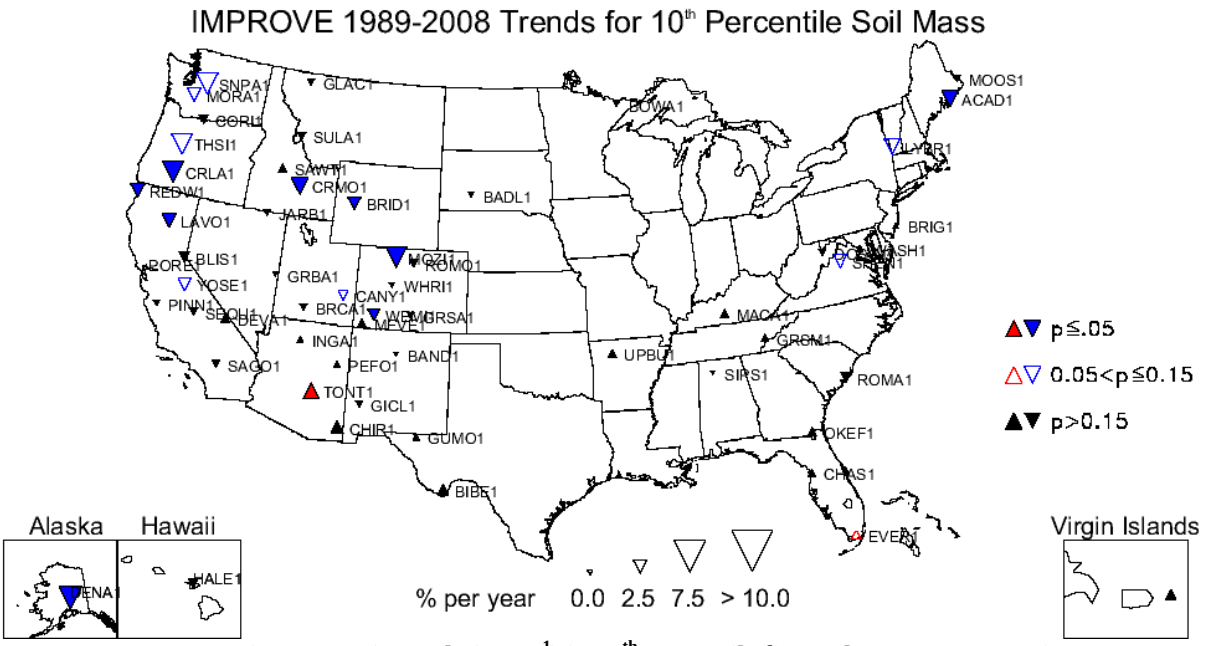

Figure 6.4.1. Long-term (1989–2008) trends (% yr^{-1}) in 10th percentile fine soil mass concentrations.

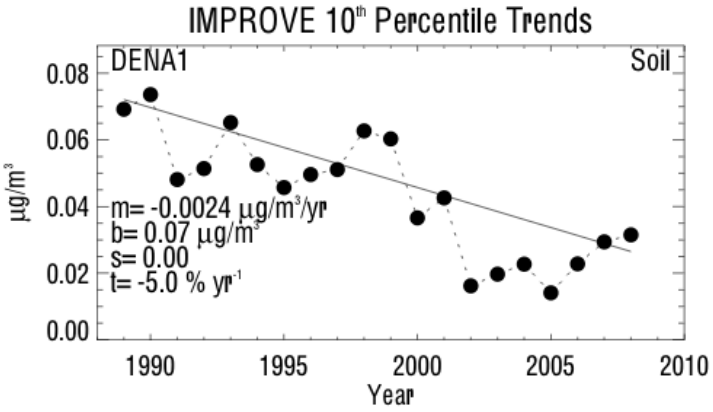

Figure 6.4.2. 10th percentile fine soil mass concentrations (µg m^{-3}) for Denali, Alaska (DENA1). Regression results, including Theil slope (m, µg m^{-3} yr^{-1}), intercept (b, µg m^{-3}), significance (s), and trend (t, % yr^{-1}) are included. The intercept corresponds to the initial year of data.

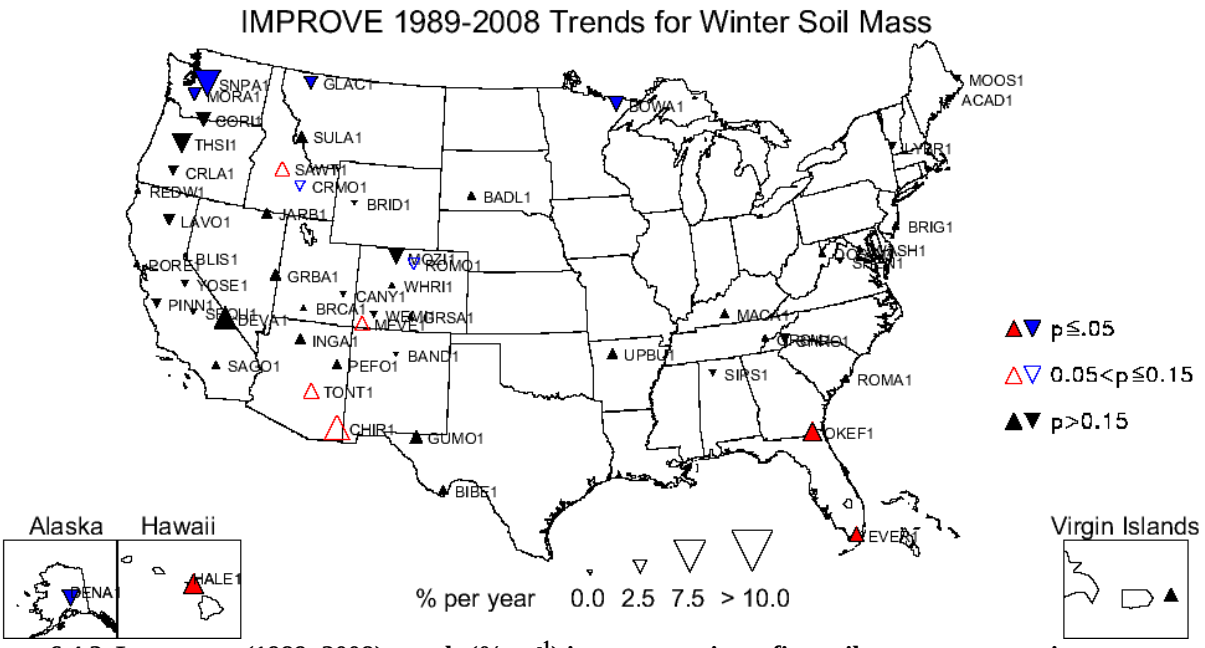

Figure 6.4.3. Long-term (1989–2008) trends (% yr^{-1}) in average winter fine soil mass concentrations.

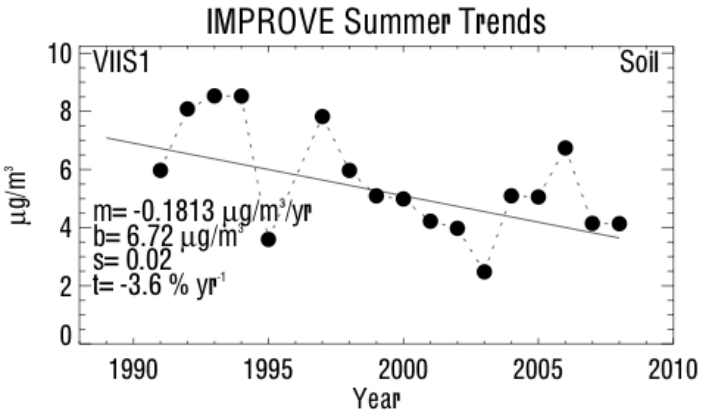

Figure 6.4.4. Average summer fine soil mass concentrations (µg m^{-3}) for Virgin Islands (VIIS1). Regression results, including Theil slope (m, µg m^{-3} yr^{-1}), intercept (b, µg m^{-3}), significance (s), and trend (t, % yr^{-1}) are included. The trend line is plotted as a solid line. The intercept corresponds to the initial year of data.

The 10th and 90th percentile trends corresponded to the highest number of sites with significant long-term soil trends of all the parameters investigated. Most of the 18 sites with statistically significant 90th percentile trends were in the western United States, and most were associated with positive trends (see Figure 6.4.5). Only four sites were associated with negative 90th percentile trends (Snoqualmie Pass, Washington, SNPA1, -2.4% yr^{-1}; San Gorgonio, California, SAGO1, -2.7% yr^{-1}; Virgin Islands, VIIS1, -4.3% yr^{-1}, and Denali, Alaska, DENA1, -2.9% yr^{-1}). The largest positive trend corresponded to the Columbia River Gorge, Washington, site (CORI1, 6.9% yr^{-1}). The timeline of 90th percentile soil concentrations at CORI1 shows variable but increasing soil concentrations (Figure 6.4.6). Contrasted to this timeline is the decreasing 90th percentile soil concentrations at Denali (DENA1, see Figure 6.4.7). With the exception of the concentration in 1990, the soil concentrations at DENA1 have been fairly steady

and slowly decreasing, unlike the variability seen in the much larger magnitude concentrations measured at the CORI1 site. Spring trends were associated with the second highest number of sites with positive trends. Individual trends for spring concentrations are presented in Figure 6.4.8. The largest spring trend occurred at Death Valley, California (DEVA1, 5.6% yr^{-1}), and most negative trend occurred at SNPA1 (-4.2% yr^{-1}). Of the 15 sites with statistically significant trends, only two were negative and corresponded to SNPA1 and DENA1 (-2.3% yr^{-1}). For many regions in the western United States, the 2005–2008 monthly mean maximum soil concentrations were associated with spring months (recall Figure 4.5.1). Trend results suggested that the highest soil concentrations are increasing, such as shown by the timeline of spring soil concentrations at DEVA1 (Figure 6.4.9). Spring concentrations increased from 1.2 μg m^{-3} to 3.2 μg m^{-3} from 1994 to 2008.

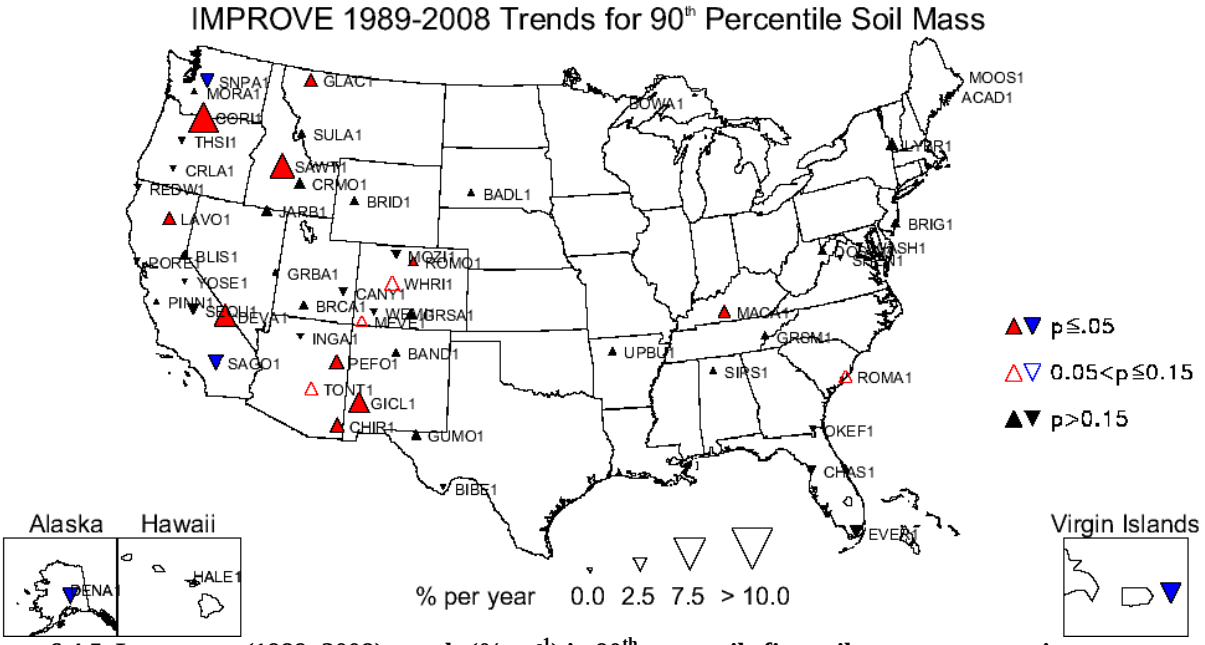

Figure 6.4.5. Long-term (1989–2008) trends (% yr^{-1}) in 90th percentile fine soil mass concentrations.

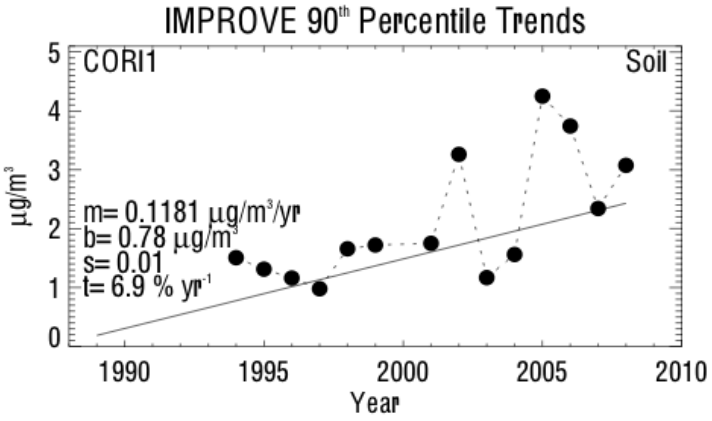

Figure 6.4.6. 90th percentile fine soil mass concentrations (μg m^{-3}) for Columbia River Gorge, Washington (CORI1). Regression results, including Theil slope (m, μg m^{-3} yr^{-1}), intercept (b, μg m^{-3}), significance (s), and trend (t, % yr^{-1}) are included. The intercept corresponds to the initial year of data.

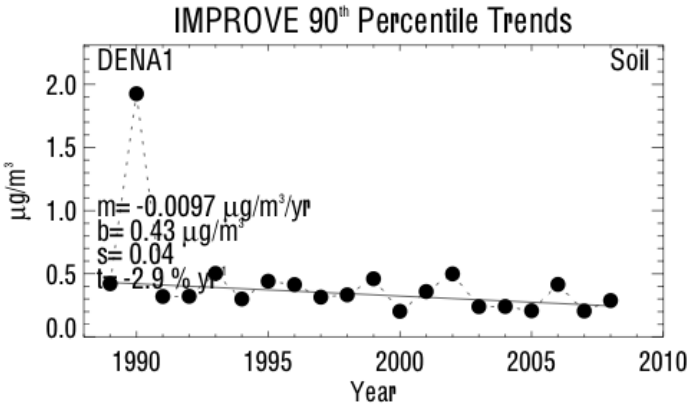

Figure 6.4.7. 90th percentile fine soil mass concentrations (µg m^{-3}) for Denali, Alaska (DENA1). Regression results, including Theil slope (m, µg m^{-3} yr^{-1}), intercept (b, µg m^{-3}), significance (s), and trend (t, % yr^{-1}) are included. The trend line is plotted as a solid line. The intercept corresponds to the initial year of data.

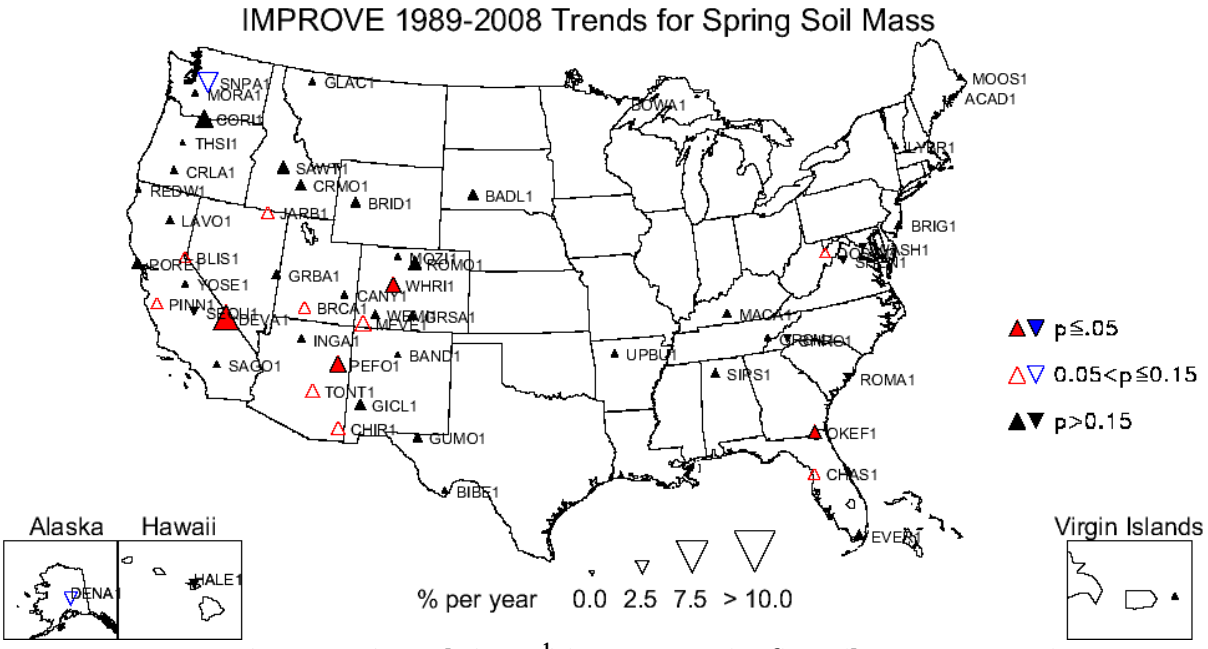

Figure 6.4.8. Long-term (1989–2008) trends (% yr^{-1}) in average spring fine soil mass concentrations.

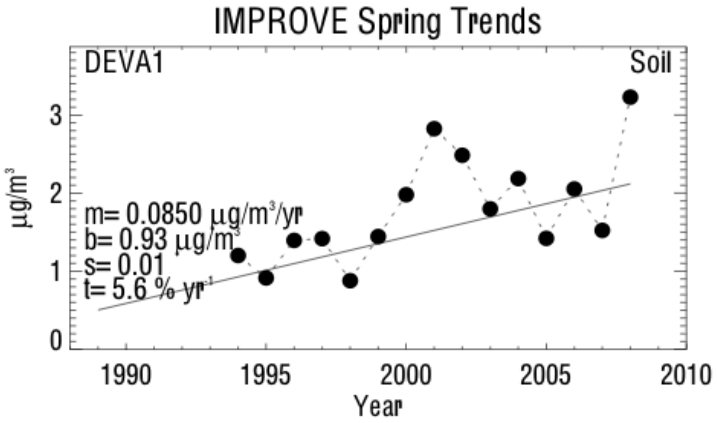

Figure 6.4.9. Average spring fine soil mass concentrations (µg m^{-3}) for Death Valley, California (DEVA1). Regression results, including Theil slope (m, µg m^{-3} yr^{-1}), intercept (b, µg m^{-3}), significance (s), and trend (t, % yr^{-1}) are included. The trend line is plotted as a solid line. The intercept corresponds to the initial year of data.

A much smaller percentage of sites corresponded to significant short-term soil trends compared to long-term soil trends (see Table 6.2). Both the 10^{th} and 50^{th} percentile, short-term soil trends corresponded to the highest number of sites with significant decreasing trends for all the parameters. Maps of 10^{th} and 50^{th} percentile trends are shown in Figures 6.4.10 and 6.4.11, respectively. Many sites in the western United States had negative (or insignificant) 10^{th} percentile trends compared to positive 50^{th} percentile trends in similar areas. In contrast, sites in the eastern United States had similar positive trends (but different magnitudes) for the 10^{th} and 50^{th} percentile concentrations. The largest positive 10^{th} and 50^{th} percentile, short-term soil trends corresponded to the Swanquarter, North Carolina (SWAN1, 15.2% yr^{-1}), and Fort Peck, Montana (FOPE1, 7.3% yr^{-1}), sites, respectively. The largest negative 10^{th} and 50^{th} percentile, short-term soil trends occurred at Monture, Montana (MONT1, -13.5% yr^{-1}), and the Virgin Islands (VIIS1, -22.10% yr^{-1}), respectively. Only 12 sites corresponded to statistically significant winter short-term soil trends (Figure 6.4.12). Two of these sites had positive trends (M.K. Goddard, Pennsylvania, MKGO1, 2.7% yr^{-1} and Brigantine, New Jersey, BRIG1, 1.8% yr^{-1}). The largest negative short-term, winter trend occurred at Big Bend, Texas (BIBE1, -20.8% yr^{-1}). The winter soil concentrations at BIBE1 have decreased significantly since 2000. The timeline of winter soil concentrations at BIBE1 is shown in Figure 6.4.13.

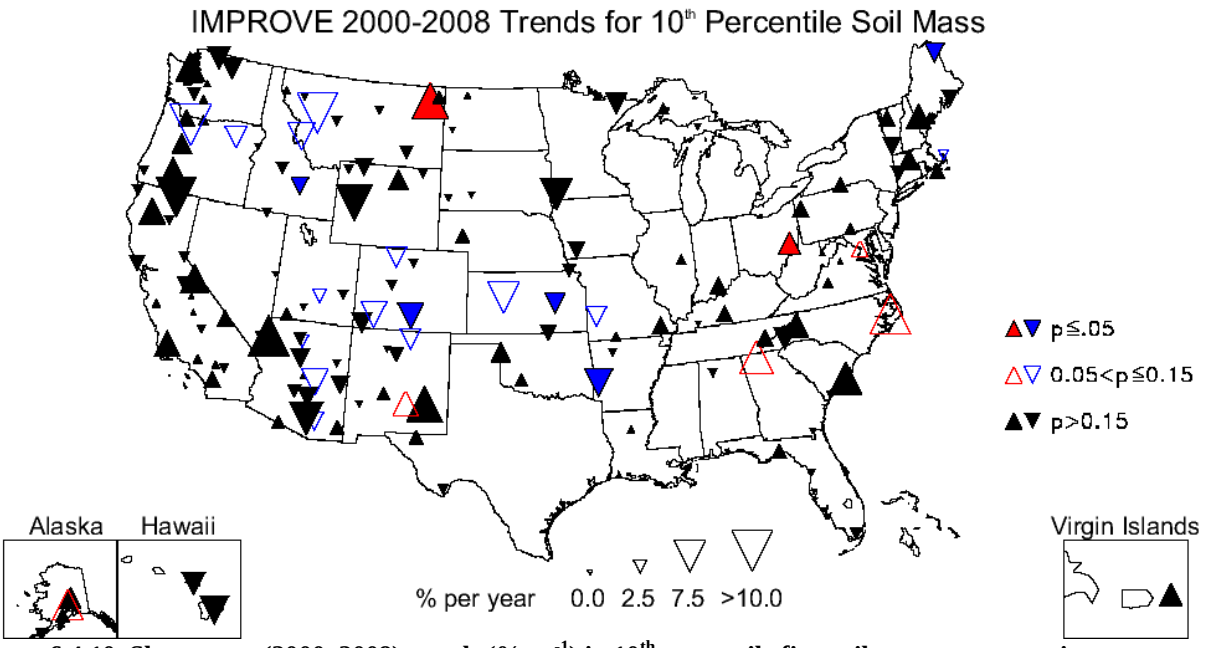

Figure 6.4.10. Short-term (2000–2008) trends (% yr^{-1}) in 10th percentile fine soil mass concentrations.

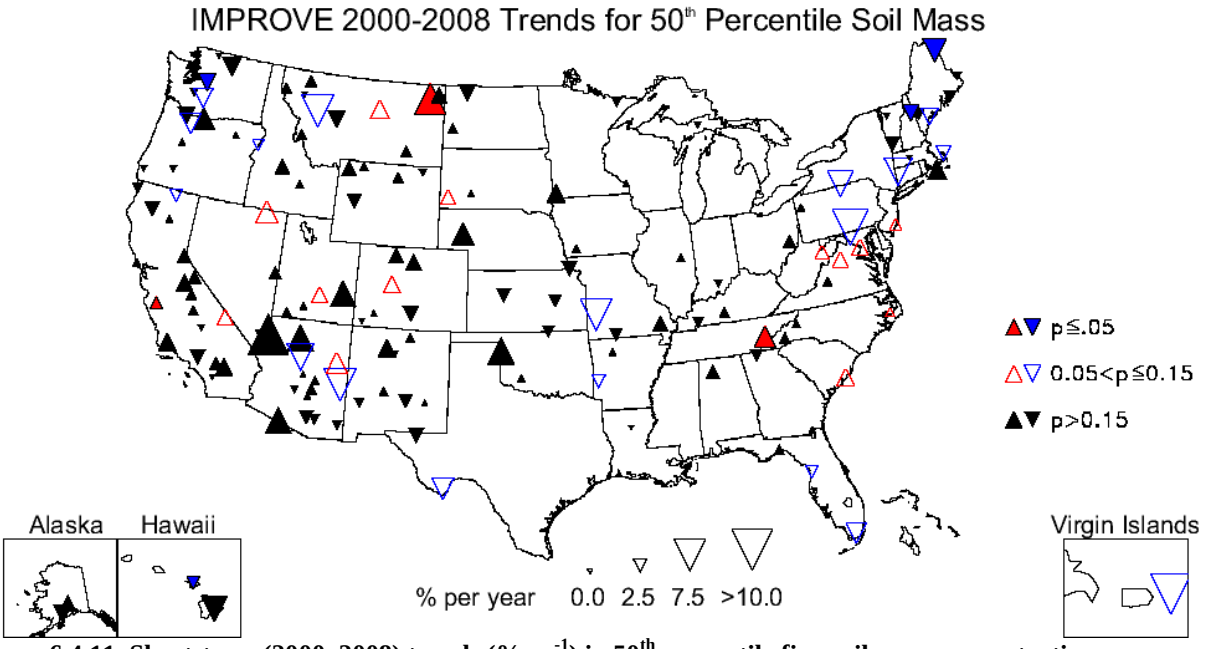

Figure 6.4.11. Short-term (2000–2008) trends (% yr^{-1}) in 50th percentile fine soil mass concentrations.

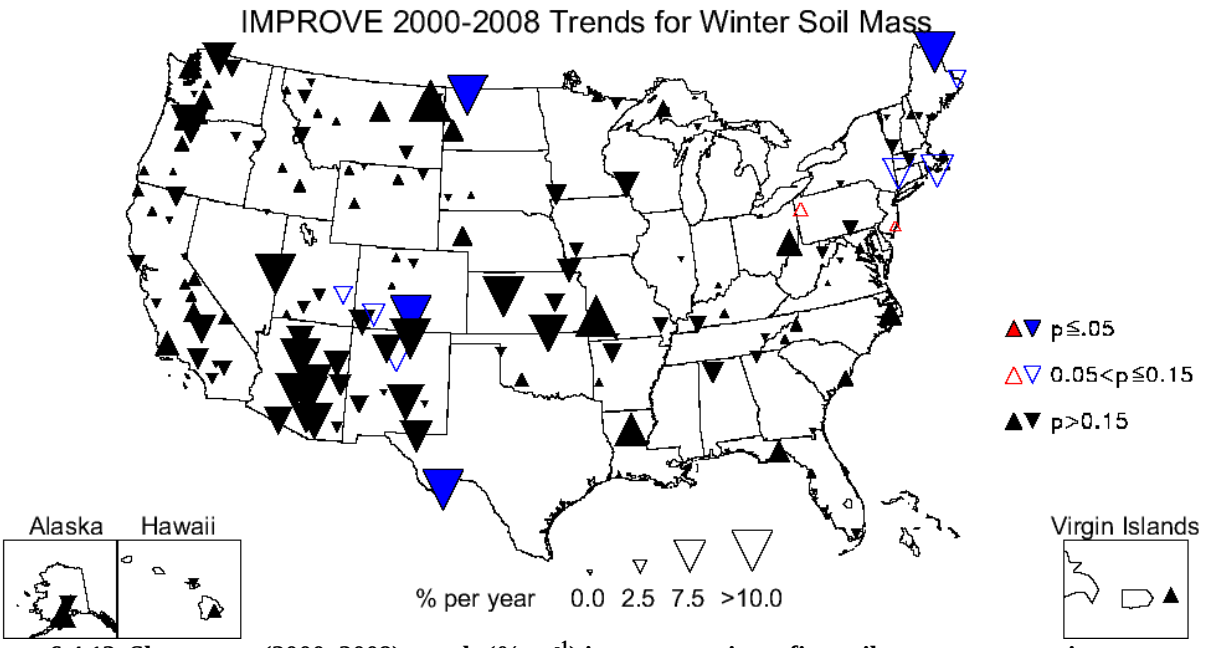

Figure 6.4.12. Short-term (2000–2008) trends (% yr^{-1}) in average winter fine soil mass concentrations.

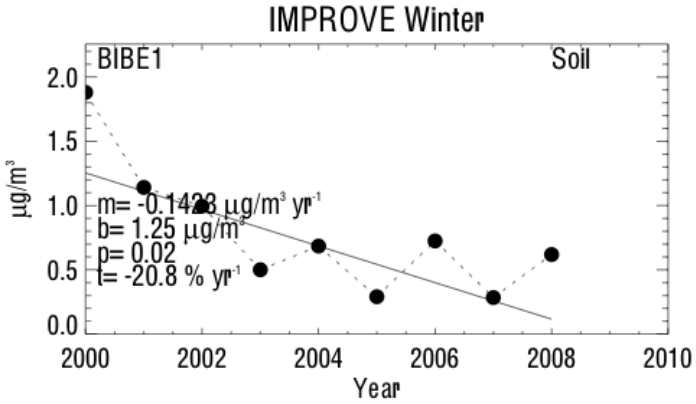

Figure 6.4.13. Average winter fine soil mass concentrations (µg m^{-3}) for Big Bend, Texas (BIBE1). Regression results, including Theil slope (m, µg m^{-3} yr^{-1}), intercept (b, µg m^{-3}), significance (p), and trend (t, % yr^{-1}) are included. The trend line is plotted as a solid line. The intercept corresponds to the initial year of data.

Of the sites with significant short-term trends, 50% or more were positive for the 90th percentile and summer and fall seasons. Several sites in the western United States corresponded to positive 90th percentile trends (Figure 6.4.14), while many sites in the northeastern United States were associated with negative trends. The map showing short-term fall soil trends is presented in Figure 6.4.15. Many sites at central latitudes were associated with positive trends. The largest positive fall trend was associated with Zion Canyon, Utah (ZICA1, 20.8% yr^{-1}). The timeline for fall soil concentrations at ZICA1 is shown in Figure 6.4.16 and demonstrates that soil concentrations increased steadily until 2007, when the concentrations dropped. In contrast, the largest decreasing trend occurred at Mesa Verde, Colorado (MEVE1, -8.6% yr^{-1}). An example of the mean fall soil concentrations at MEVE1 is given in Figure 6.4.17. While the fall soil concentrations at ZICA1 and MEVE1 were similar in magnitude, they displayed very different temporal patterns.

As was stated at the beginning of this section, trends in soil concentrations should be interpreted with some caution, and the trend analyses suggested that only a very few sites were associated with statistically significant trends (11–18 sites for long-term and 12–38 sites for short-term trends, depending on parameter). However, trend results at these sites suggested interesting patterns that should be investigated in further detail.

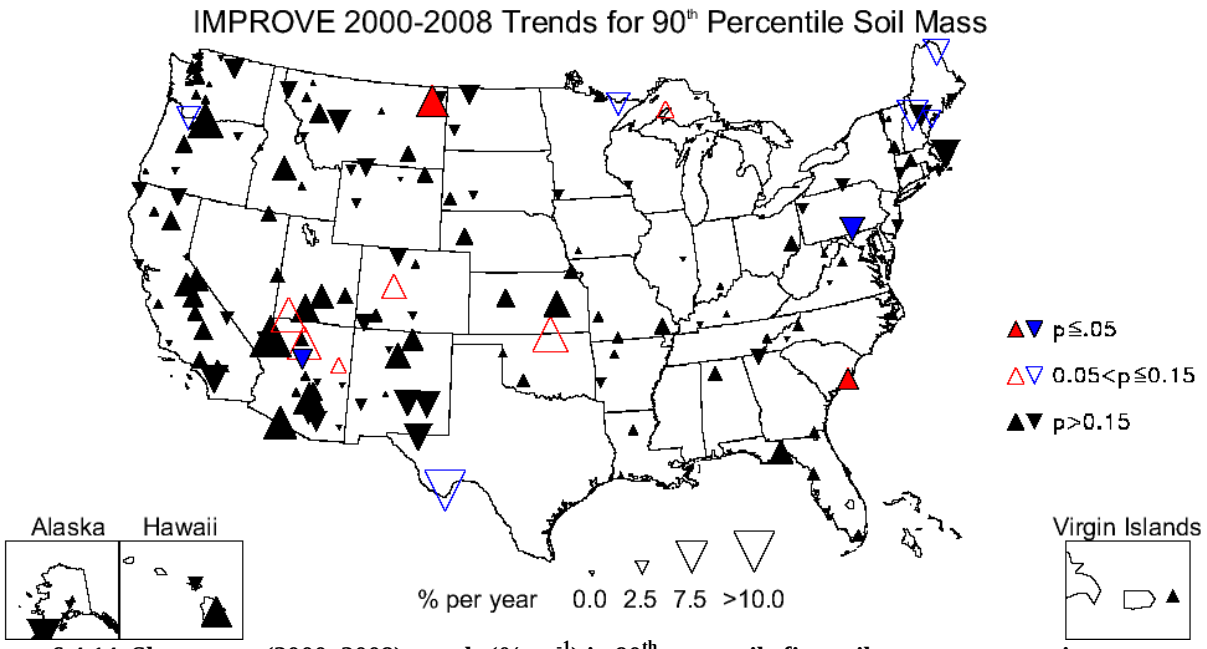

Figure 6.4.14. Short-term (2000–2008) trends (% yr^{-1}) in 90th percentile fine soil mass concentrations.

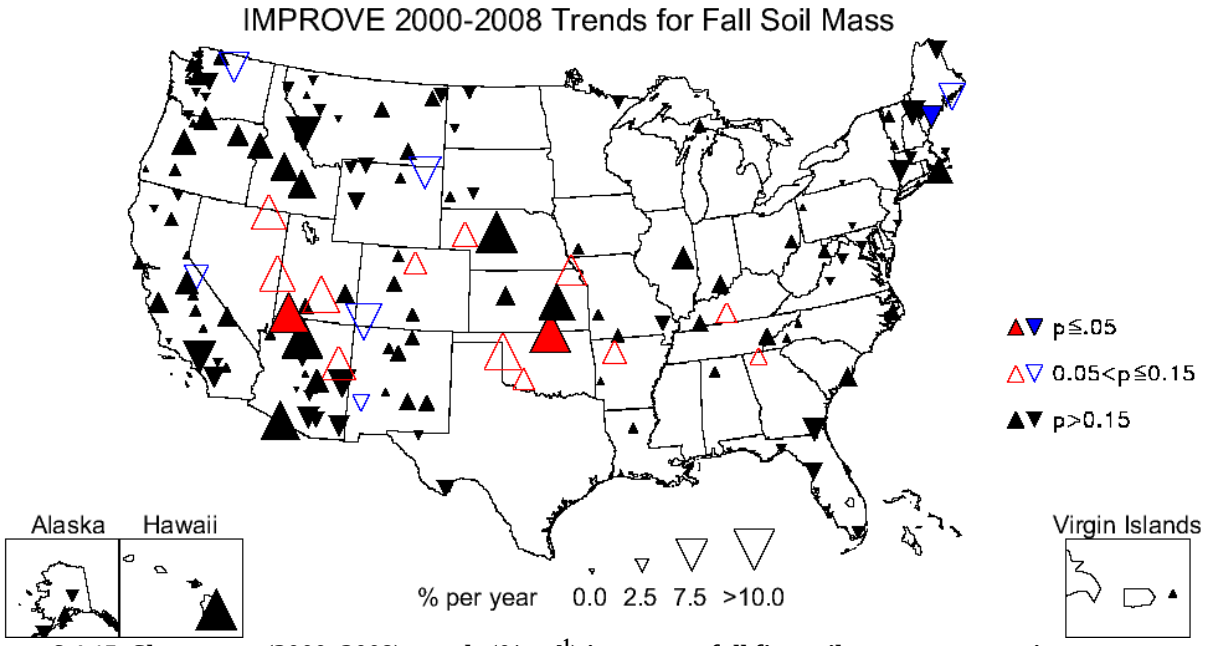

Figure 6.4.15. Short-term (2000–2008) trends (% yr^{-1}) in average fall fine soil mass concentrations.

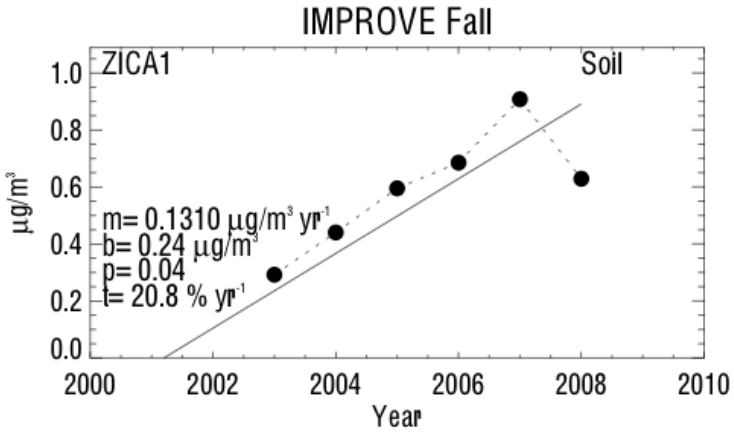

Figure 6.4.16. Average fall fine soil mass concentrations (µg m^{-3}) for Zion Canyon, Utah (ZICA1). Regression results, including Theil slope (m, µg m^{-3} yr^{-1}), intercept (b, µg m^{-3}), significance (p), and trend (t, % yr^{-1}) are included. The trend line is plotted as a solid line. The intercept corresponds to the initial year of data.

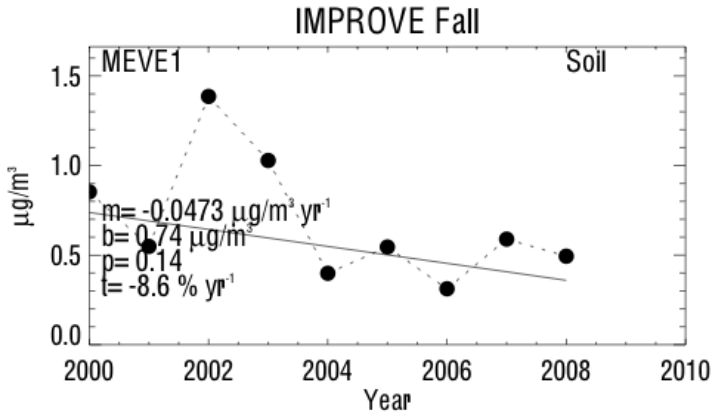

Figure 6.4.17. Fall fine soil mass concentrations (µg m^{-3}) for Mesa Verde, Colorado (MEVE1). Regression results, including Theil slope (m, µg m^{-3} yr^{-1}), intercept (b, µg m^{-3}), significance (p), and trend (t, % yr^{-1}) are included. The trend line is plotted as a solid line. The intercept corresponds to the initial year of data.

6.5 GRAVIMETRIC $PM_{2.5}$ FINE MASS TRENDS

Given the previous discussions, we might have some expectation of the trends in $PM_{2.5}$ fine mass (FM) since it is composed of the species presented in previous sections. However, inferring FM trends based on the trends of other species is complicated because of the difference in the behavior and seasonality of a specific species in relation to each other. In addition, the significance level of trends at a given site differs for each species and for FM trends, complicating comparisons of trends at a specific location. Due to sampling artifacts like those discussed in Chapter 8, FM does not equal the simple sum of all species. We did not discuss all of the species that compose fine mass, nor do we attempt to comment on the behavior of missing mass, both of which could impact the behavior of FM. However, when possible, we comment on an FM trend based on the behavior of trends of other species, including comparisons of timelines of data.

The number of sites with statistically significant long-term FM trends ranged from 33 (spring, summer, 90th percentile) to 49 (10th percentile), depending on parameter. The 10th percentile and winter long-term FM trend results were associated with a large number of sites with significantly decreasing trends. Trends for the 10th percentile for individual sites are shown in Figure 6.5.1. The magnitudes of trends were fairly similar across the United States, although sites in the southeastern United States had less-negative trends, similar to the sulfate ion and total carbon 10th percentile maps (Figures 6.1.1 and 6.3.1, respectively). No sites were associated with positive 10th percentile trends. The largest negative 10th percentile trend occurred at Craters of the Moon, Idaho (CRMO1, -6.1% yr^{-1}), and the least negative trend occurred at Chassahowitzka, Florida (CHAS1, -1.0% yr^{-1}). A timeline of 10th percentile FM concentrations at CRMO1 is shown in Figure 6.5.2. Concentrations decreased steadily until 2004, after which they flattened. Winter trends were larger in magnitude (more negative) at most sites compared to 10th percentile trends, and no sites were associated with positive trends (Figure 6.5.3). Recall that fine mass monthly mean concentrations (2005–2008) were at a minimum during winter months for many regions in the United States (Figure 4.7.1). The negative winter trends suggested that the days with the lowest FM concentrations were getting cleaner. The largest long-term, negative winter trend occurred at Mount Rainier, Washington (MORA1, -6.5% yr^{-1}), as did the largest negative winter trend in total carbon (see Section 6.3). The least-negative winter trend occurred at Everglades, Florida (EVER1, -1.0% yr^{-1}).

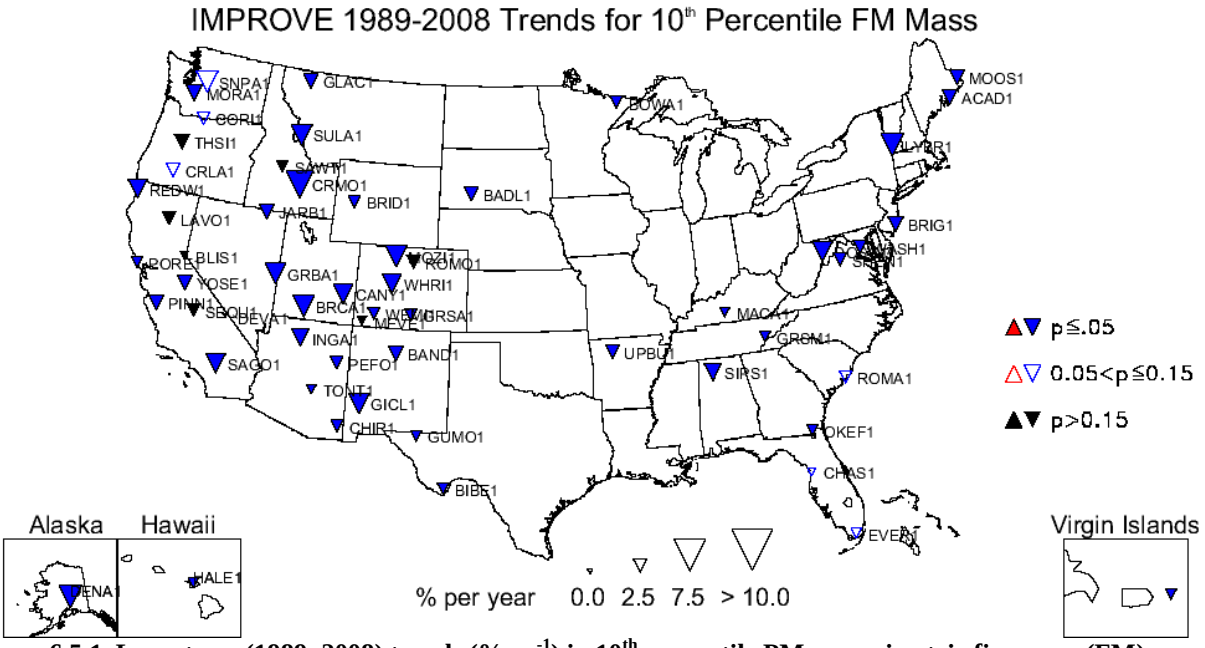

Figure 6.5.1. Long-term (1989–2008) trends (% yr^{-1}) in 10th percentile $PM_{2.5}$ gravimetric fine mass (FM) concentrations.

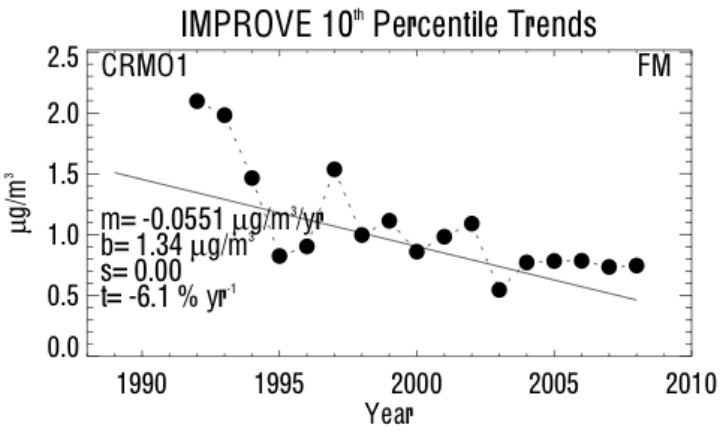

Figure 6.5.2. 10th percentile $PM_{2.5}$ gravimetric fine mass (FM) concentrations (µg m^{-3}) for Craters of the Moon, Idaho (CRMO1). Regression results, including Theil slope (m, µg m^{-3} yr^{-1}), intercept (b, µg m^{-3}), significance (s), and trend (t, % yr^{-1}) are included. The trend line is plotted as a solid line. The intercept corresponds to the initial year of data.

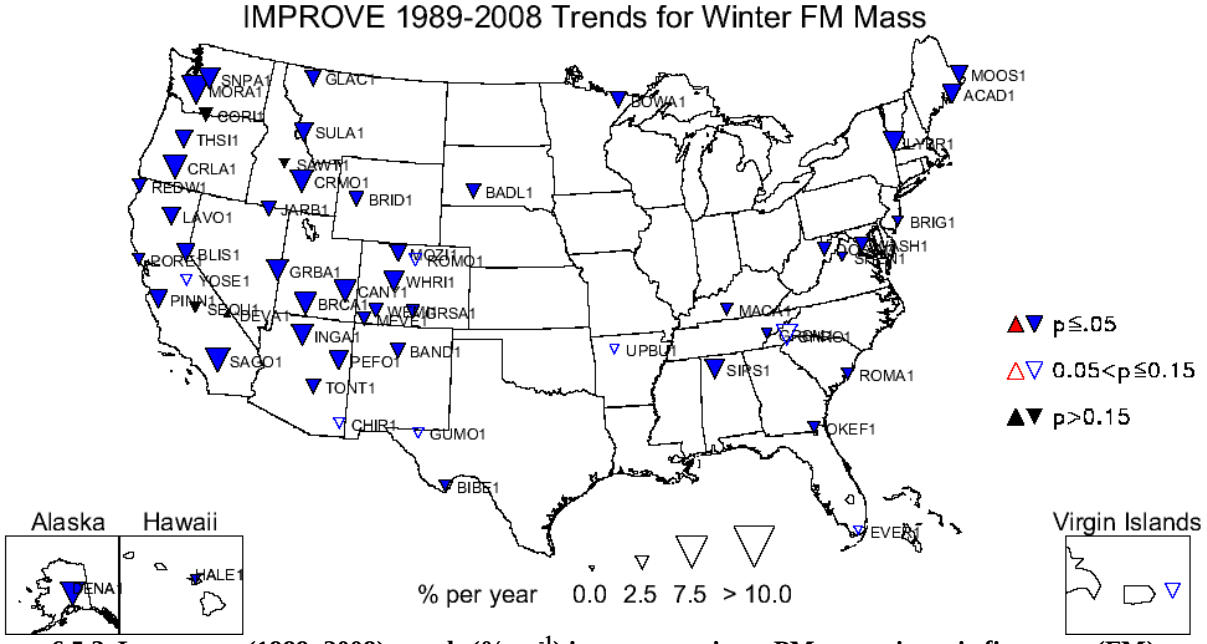

Figure 6.5.3. Long-term (1989–2008) trends (% yr^{-1}) in average winter $PM_{2.5}$ gravimetric fine mass (FM) concentrations.

Although there were fewer sites with significant 90th percentile, long-term FM trends compared to the 10th percentile trends (see Table 6.1), only 25 (out of 48) sites were associated with statistically significant trends in the 90th percentile FM concentrations. In general, the magnitude of long-term, 90th percentile, FM trends at many sites was less negative than the 10th percentile trends (See Figure 6.5.4). Several sites in the southwestern United States that were associated with significant 10th percentile trends did not have significant 90th percentile trends. The largest negative 90th percentile, long-term FM trend occurred at Mount Rainier, Washington (MORA1, -3.9% yr^{-1}), and the only positive 90th percentile trend occurred at Sawtooth, Idaho (SAWT1, 3.3% yr^{-1}). An example of increasing 90th percentile FM concentrations at SAWT1 is

shown in Figure 6.5.5. The high concentration in 2007 was most likely associated with biomass burning emissions as summer fine mass and total carbon concentrations were also high then. SAWT1 was one of the four sites with positive trends during summer (Sula Peak, Montana, SULA1, 5.0% yr^{-1}; Sawtooth, Idaho, SAWT1, 4.8% yr^{-1}; Death Valley, California, DEVA1, 1.3% yr^{-1}; and Bridger, Wyoming, BRID1, 1.10% yr^{-1}) (se Figure 6.5.6). The largest negative FM summer trend occurred at Great Gulf, New Hampshire (GRGU1, -4.10% yr^{-1}). Fine mass trends in the summer in the eastern United States were decreasing at most sites. Many western U.S. sites were associated with either low negative summer trends or trends that were statistically insignificant. Recall that most regions in the United States were associated with maximum FM monthly mean concentrations in the summer months (see Figure 4.7.1), probably due to total carbon concentrations; trend results suggested that these summer FM concentrations appeared to be decreasing less over time compared to other seasons.

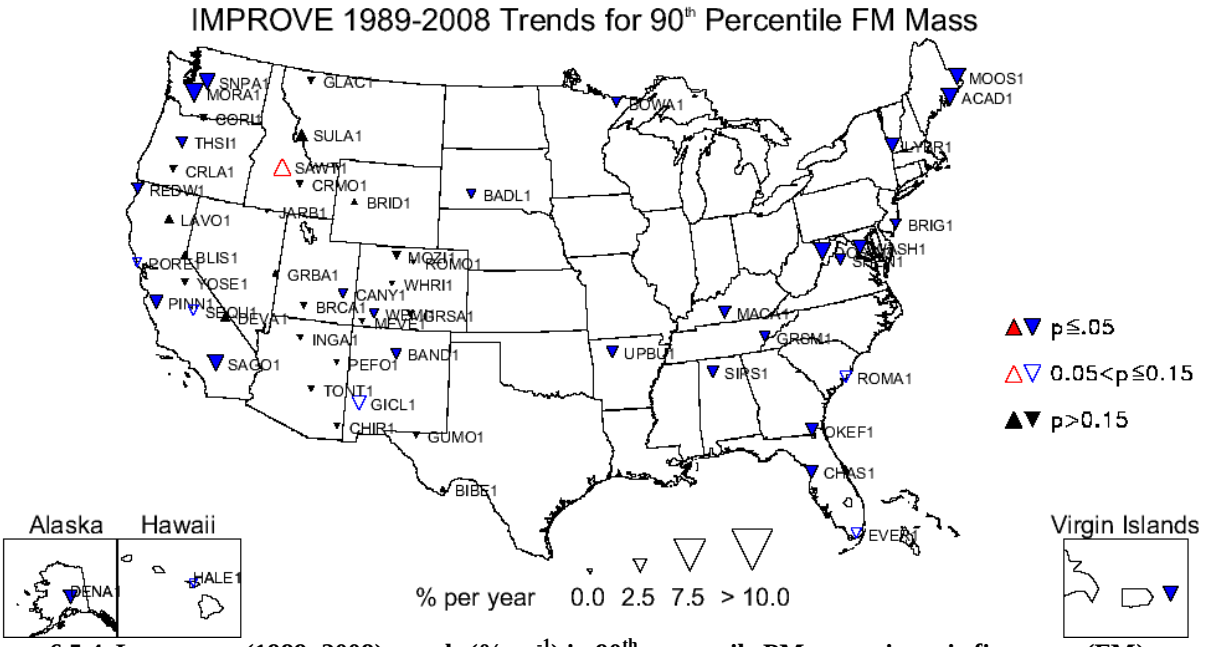

Figure 6.5.4. Long-term (1989–2008) trends (% yr^{-1}) in 90th percentile $PM_{2.5}$ gravimetric fine mass (FM) concentrations.

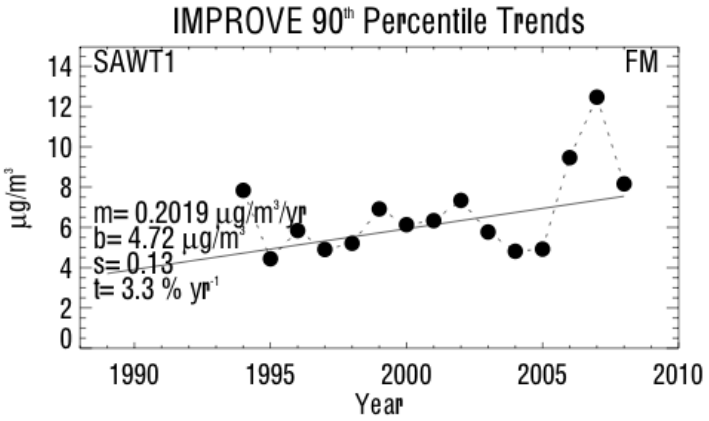

Figure 6.5.5. 90th percentile $PM_{2.5}$ gravimetric fine mass (FM) concentrations (µg m^{-3}) for Sawtooth, Idaho (SAWT1). Regression results, including Theil slope (m, µg m^{-3} yr^{-1}), intercept (b, µg m^{-3}), significance (s), and trend (t, % yr^{-1}) are included. The trend line is plotted as a solid line. The intercept corresponds to the initial year of data.

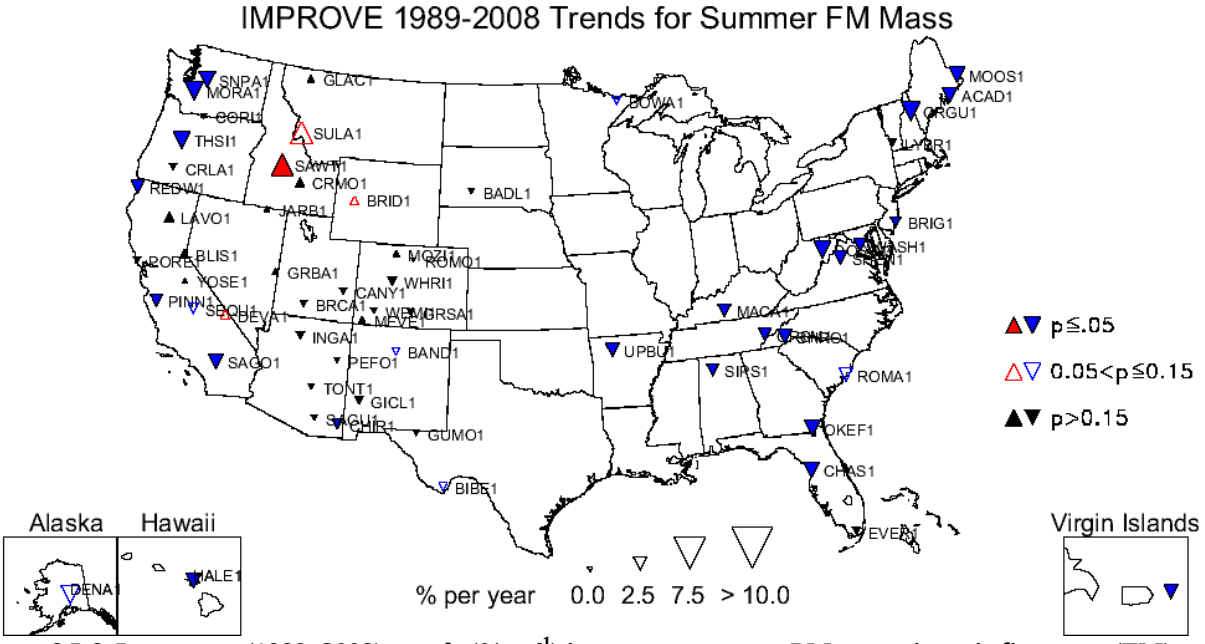

Figure 6.5.6. Long-term (1989–2008) trends (% yr^{-1}) in average summer $PM_{2.5}$ gravimetric fine mass (FM) concentrations.

The number of sites with statistically significant short-term FM trends ranged from 36 in spring to 60 for 50th percentile concentrations (out of ~153, see Table 6.2). Only two sites corresponded to positive short-term FM trends for both the summer season and the 90th percentile (the lowest for all parameters). A map of the 90th percentile, short-term trends is shown in Figure 6.5.7. The largest negative 90th percentile trend was associated with Tuxedni, Alaska (TUXE1, -7.7%), and the largest positive trend occurred at Hawaii Volcanoes (HAVO1, 12.8%). A timeline of the 90th percentile FM concentrations at HAVO1 is shown in Figure 6.5.8. High concentrations in 2008 were mostly likely associated with volcanic eruptions, as the 90th percentile concentrations of sulfate ion displayed similar behavior (Figure 6.1.10). The other

positive trend in the 90th percentile FM concentrations corresponded to Capitol Reef, Utah (CAPI1, 2.0% yr^{-1}).

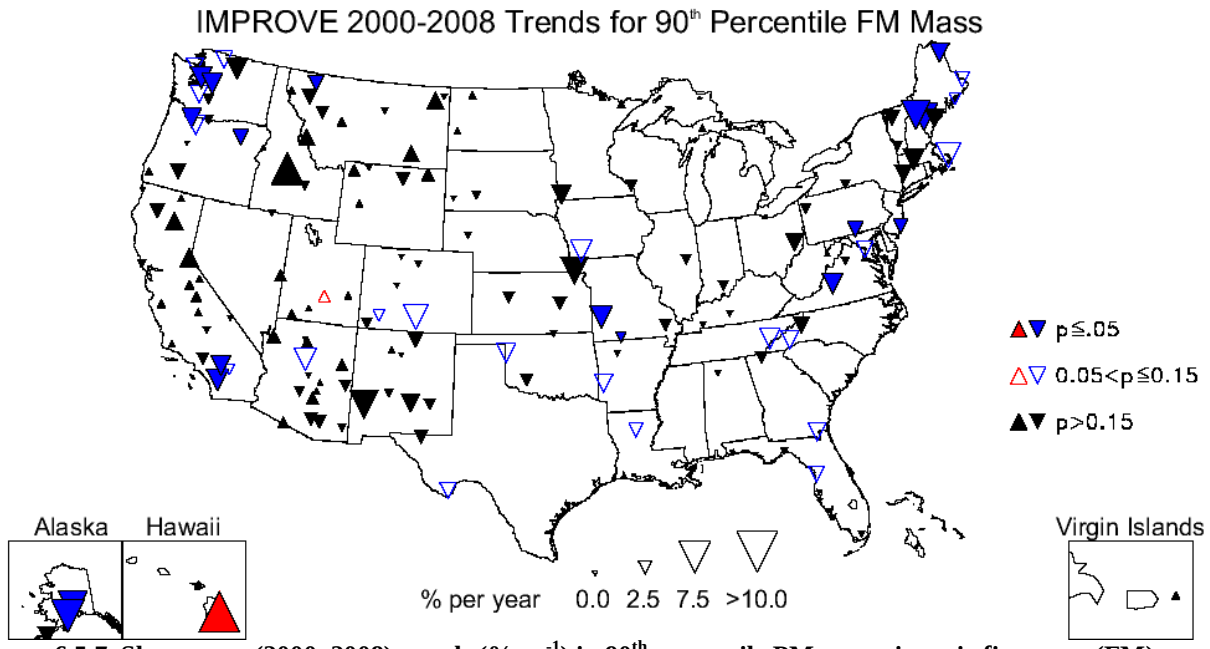

Figure 6.5.7. Short-term (2000–2008) trends (% yr^{-1}) in 90th percentile $PM_{2.5}$ gravimetric fine mass (FM) concentrations.

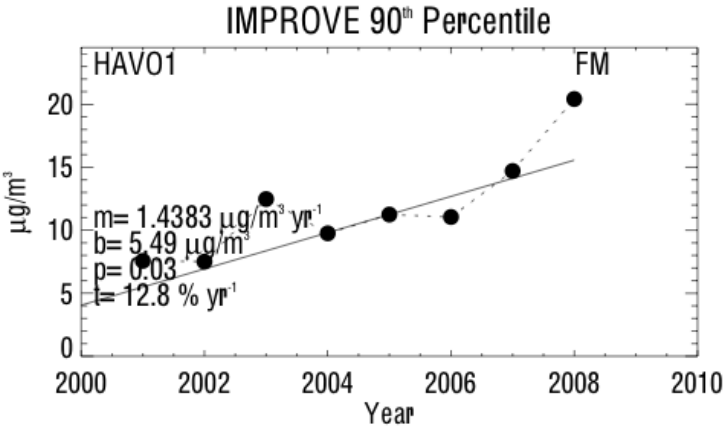

Figure 6.5.8. 90th percentile $PM_{2.5}$ gravimetric fine mass (FM) concentrations (µg m^{-3}) for Hawaii Volcanoes (HAVO1). Regression results, including Theil slope (m, µg m^{-3} yr^{-1}), intercept (b, µg m^{-3}), significance (p), and trend (t, % yr^{-1}) are included. The trend line is plotted as a solid line. The intercept corresponds to the initial year of data.

Many western U.S. sites were associated with relatively large negative short-term winter FM trends (Figure 6.5.9). The largest negative winter trend occurred at Starkey, Oregon (STAR1, -14.6% yr^{-1}), similar to total carbon. Sites in southern California were also associated with relatively large negative trends. The timeline showing steadily decreasing FM winter concentrations at STAR1 is shown in Figure 6.5.10. Winter concentrations dropped from 6.3 µg m^{-3} to 1.3 µg m^{-3} from 2001 to 2008. Four sites corresponded to positive, short-term, winter FM

trends, with the largest at Trapper Creek, Alaska (TRCR1, 9.1% yr^{-1}). An example of the increasing FM winter concentration at TRCR1 is shown in Figure 6.5.11. Notice the lowest concentrations at this site compared to the STAR1 site. The highest winter FM concentration at TRCR1 was comparable to the lowest winter FM concentration at STAR1.

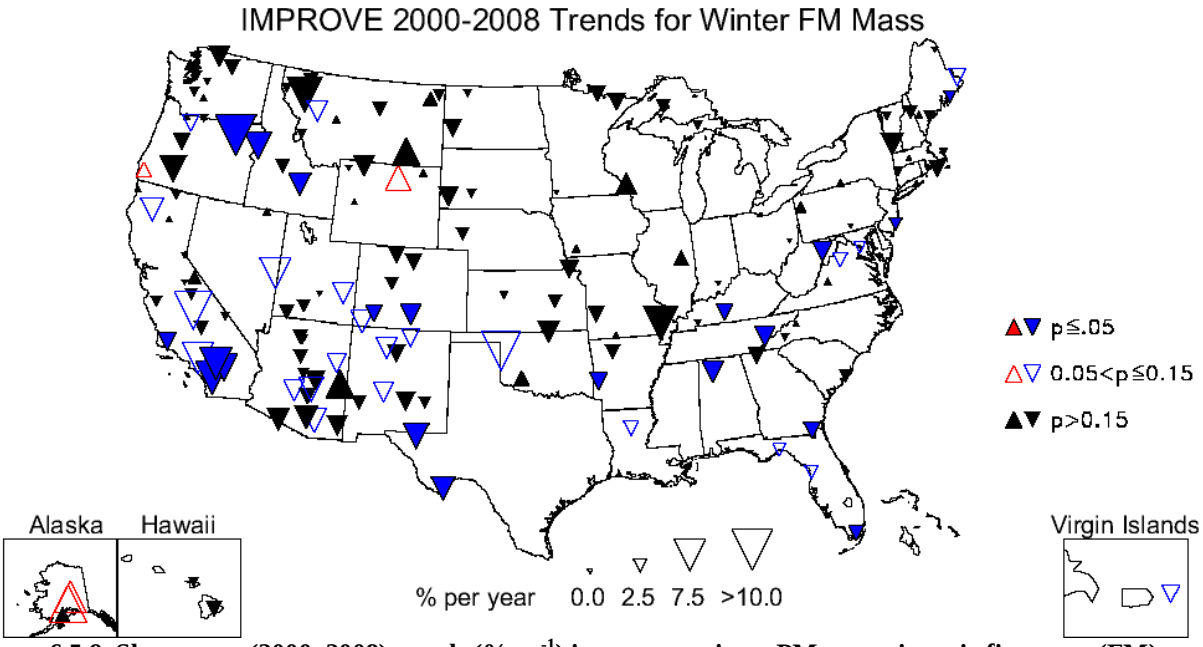

Figure 6.5.9. Short-term (2000–2008) trends (% yr^{-1}) in average winter $PM_{2.5}$ gravimetric fine mass (FM) concentrations.

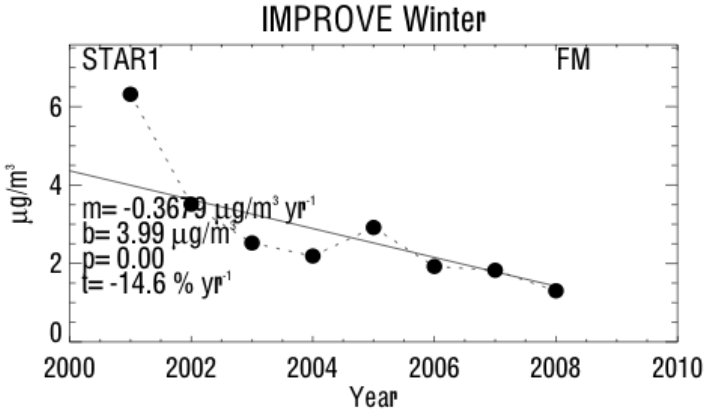

Figure 6.5.10. Average winter $PM_{2.5}$ gravimetric fine mass (FM) concentrations (µg m^{-3}) for Starkey, Oregon (STAR1). Regression results, including Theil slope (m, µg m^{-3} yr^{-1}), intercept (b, µg m^{-3}), significance (p), and trend (t, % yr^{-1}) are included. The trend line is plotted as a solid line. The intercept corresponds to the initial year of data.

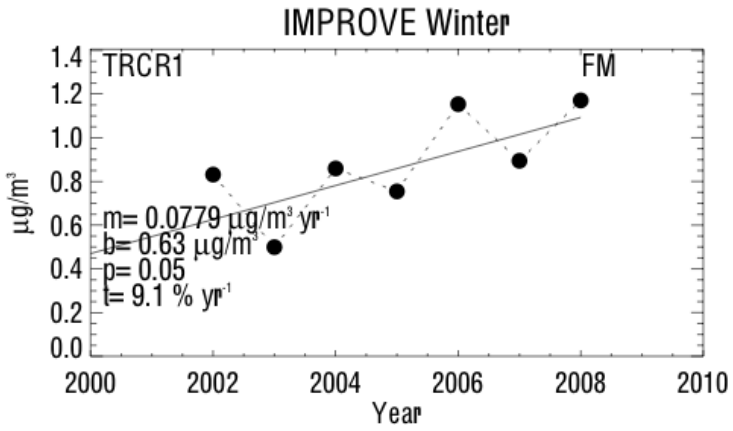

Figure 6.5.11. Average winter $PM_{2.5}$ gravimetric fine mass (FM) concentrations (µg m^{-3}) for Trapper Creek, Alaska (TRCR1). Regression results, including Theil slope (m, µg m^{-3} yr^{-1}), intercept (b, µg m^{-3}), significance (p), and trend (t, % yr^{-1}) are included. The trend line is plotted as a solid line. The intercept corresponds to the initial year of data.

The largest number of sites with significant positive short-term trends corresponded to the fall season. A map of the fall FM trends is shown in Figure 6.5.12. Most of the sites with positive, short-term fall trends were located in the western United States and in Alaska and Hawaii. No eastern U.S. sites were associated with positive fall trends. The largest positive fall trend occurred at Zion Canyon, Utah (ZICA1, 12.3% yr^{-1}), and the largest decreasing fall trend occurred at Moosehorn, Maine (MOOS1, -6.5% yr^{-1}). A timeline showing the steady increase in fall FM concentrations at ZICA1 is shown in Figure 6.5.13. The fine soil trend in fall at ZICA1 was also positive (see Figure 6.4.16 and discussion in Section 6.4). The only species to be associated with positive, short-term, fall trends in the western United States were sulfate (in Alaska, Hawaii, and Arizona), soil (several western U.S. sites), and total carbon at a couple of western sites; therefore the fall positive trends in FM in the western United States were most likely driven by different species, depending on the site.

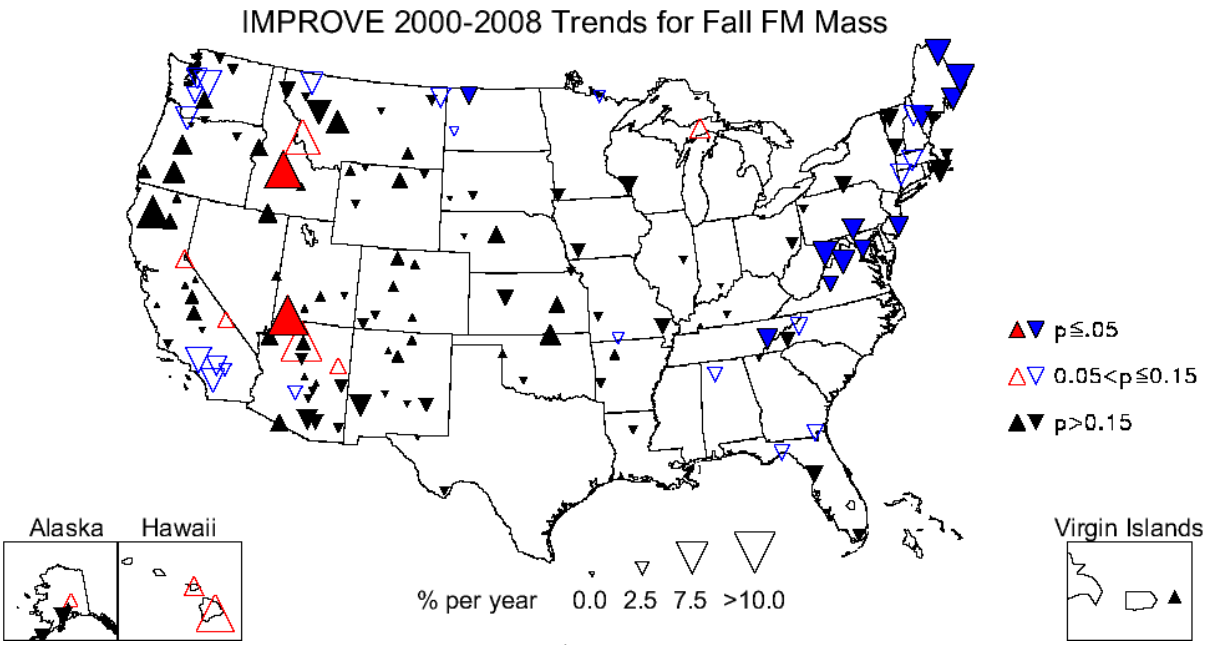

Figure 6.5.12. Short-term (2000–2008) trends (% yr^{-1}) in average fall $PM_{2.5}$ gravimetric fine mass (FM) concentrations.

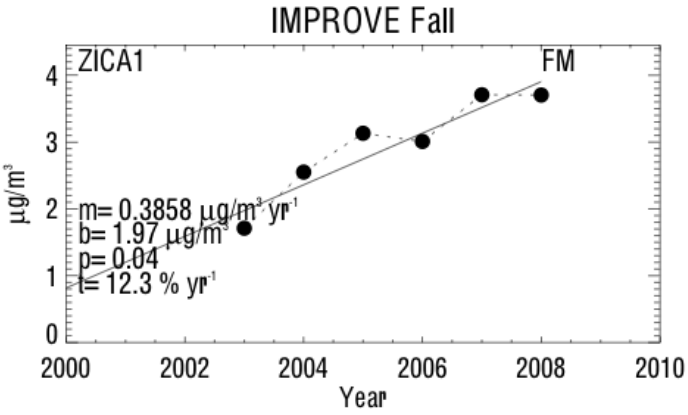

Figure 6.5.13. Average fall $PM_{2.5}$ gravimetric fine mass (FM) concentrations (µg m^{-3}) for Zion Canyon, Utah (ZICA1). Regression results, including Theil slope (m, µg m^{-3} yr^{-1}), intercept (b, µg m^{-3}), significance (p), and trend (t, % yr^{-1}) are included. The trend line is plotted as a solid line. The intercept corresponds to the initial year of data.

6.6 COARSE MASS TRENDS

The 10th percentile and winter, long-term CM trends were generally the most negative of the parameters. The map in Figure 6.6.1 shows sites with largely negative long-term CM trends, especially in the western United States, including Denali, Alaska (DENA1). A timeline of 10th percentile CM concentrations at Mount Zirkel, Colorado (MOZI1), provides an example of a site with one of the largest negative 10th percentile trends (-20.5% yr^{-1}, Figure 6.6.2). The CM 10th percentile concentration was near 1.4 µg m^{-3} in 1995 and decreased to 0.17 µg m^{-3} in 2008. The least negative 10th percentile, long-term trend occurred at Badlands, South Dakota (BADL1, -2.2% yr^{-1}).

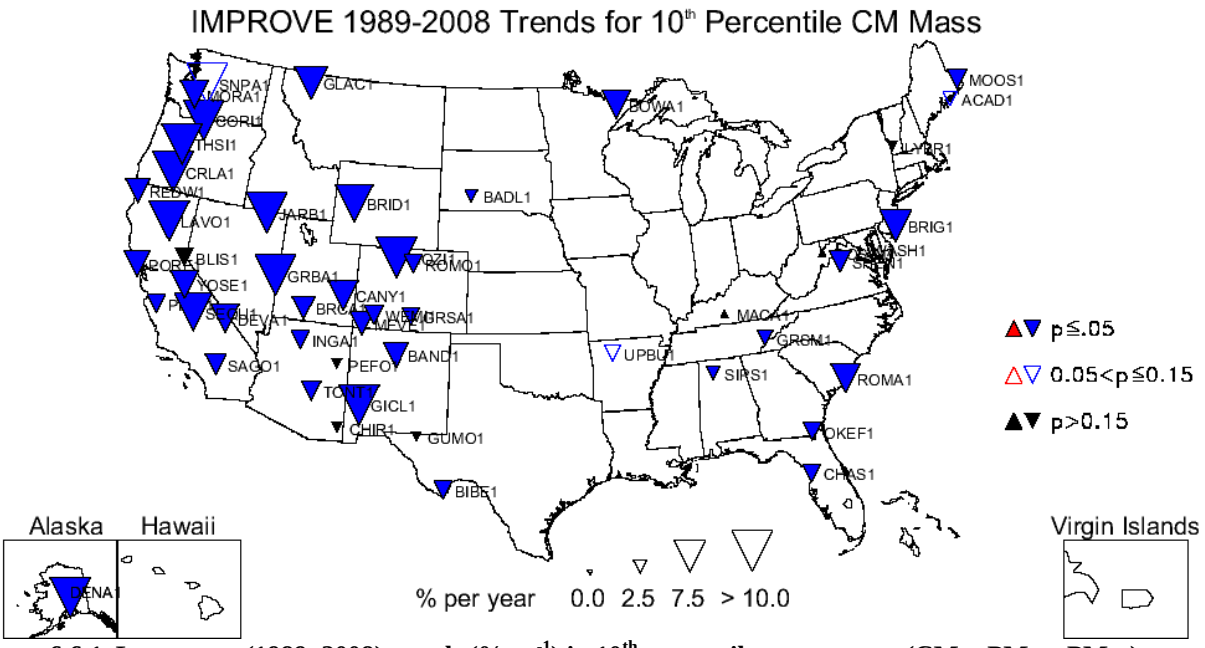

Figure 6.6.1. Long-term (1989–2008) trends (% yr^{-1}) in 10th percentile coarse mass (CM = PM_{10} - $PM_{2.5}$) concentrations.

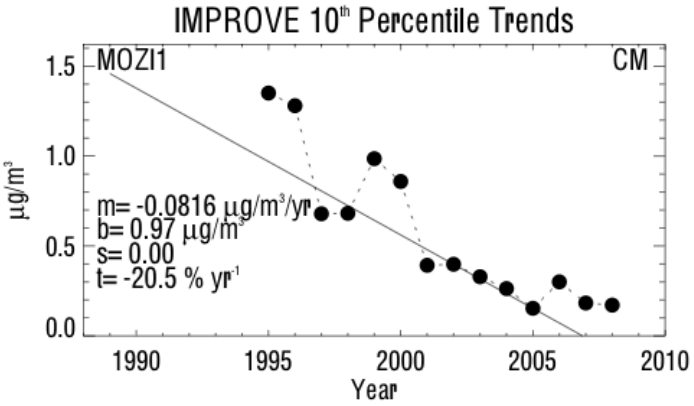

Figure 6.6.2. 10th percentile coarse mass (CM = PM_{10} - $PM_{2.5}$) concentrations (µg m^{-3}) for Mount Zirkel, Colorado (MOZI1). Regression results, including Theil slope (m, µg m^{-3} yr^{-1}), intercept (b, µg m^{-3}), significance (s), and trend (t, % yr^{-1}) are included. The trend line is plotted as a solid line. The intercept corresponds to the initial year of data.

The map of long-term winter trends in CM was very similar to the 10th percentile map (Figure 6.6.3). This similarity was not surprising given that the lowest CM concentration occurred during winter months for regions around the United States (Figure 4.8.1). The largest negative winter trend corresponded to the site at Snoqualmie Pass, Washington (SNPA1, -18.7% yr^{-1}), and Figure 6.6.4 shows the strong decrease in CM over time at that site. Winter CM concentrations decreased considerably in 2001 at SNPA and remained fairly steady through 2008. The least negative, winter, CM long-term trend occurred at Upper Buffalo, Arkansas (ULBU1, -1.8% yr^{-1}).

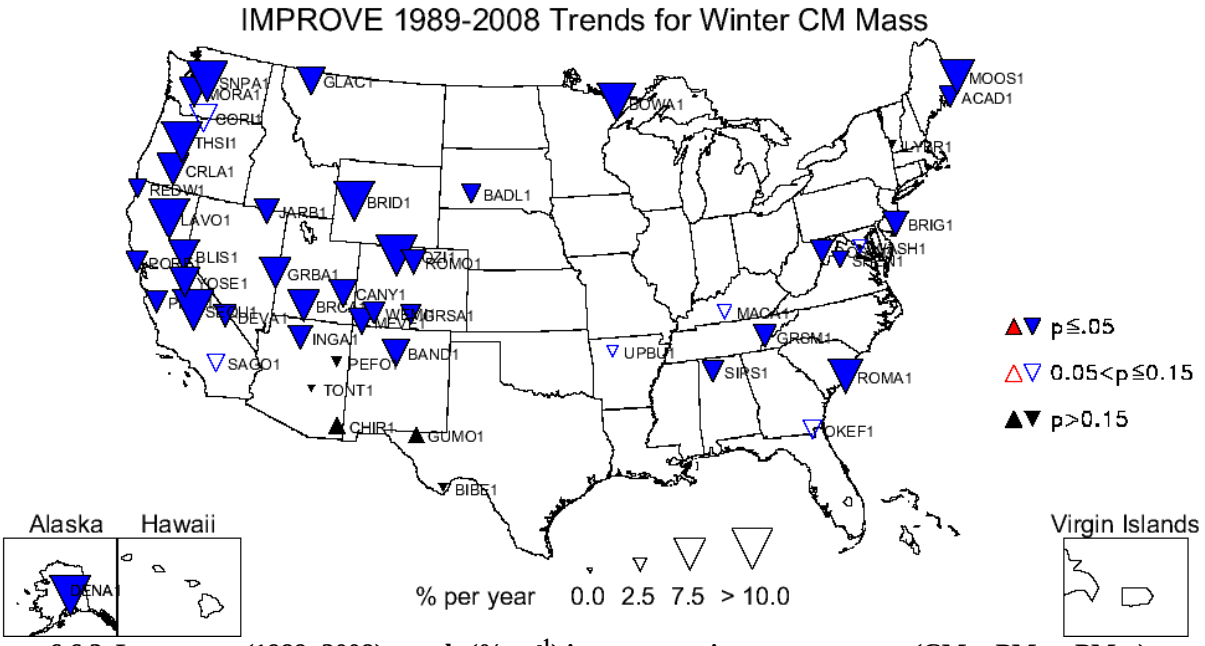

Figure 6.6.3. Long-term (1989–2008) trends (% yr^{-1}) in average winter coarse mass (CM = PM_{10} - $PM_{2.5}$) concentrations.

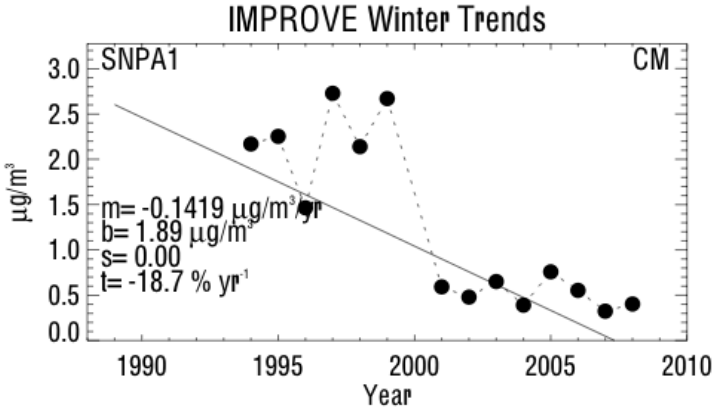

Figure 6.6.4. Average winter coarse mass (CM = PM_{10} - $PM_{2.5}$) concentrations (µg m^{-3}) for Snoqualmie Pass, Washington (SNPA1). Regression results, including Theil slope (m, µg m^{-3} yr^{-1}), intercept (b, µg m^{-3}), significance (s), and trend (t, % yr^{-1}) are included. The trend line is plotted as a solid line. The intercept corresponds to the initial year of data.

The 90th percentile, long-term CM trends corresponded to fewer statistically significant sites compared to the 10th percentile trends (34 versus 42, respectively), especially in the western United States (Figure 6.6.5). In addition, the magnitudes of 90th percentile trends were noticeably lower (less negative) than 10th percentile trends. No sites corresponded to positive 90th percentile CM trends. The largest negative 90th percentile, CM long-term trend occurred at Snoqualmie Pass, Washington (SNPA1, -8.2% yr^{-1}), and the least negative trend corresponded to Yosemite, California (YOSE1, -1.6% yr^{-1}). The timeline of the 90th percentile CM concentrations at YOSE1 is presented in Figure 6.6.6. Concentrations at YOSE1 were slowly decreasing, in contrast to the large decrease in CM concentrations at SNPA1 (see Figure 6.6.7). CM concentrations at SNPA1

were also significantly lower than those at YOSE1. Long-term summer trends in CM at individual sites are shown in Figure 6.6.8. Significant trends were negative at most sites, except at Badlands, South Dakota (BADL1, 2.2% yr^{-1}), and Columbia River Gorge, Washington (CORI1, 8.5% yr^{-1}). Like the previously discussed parameters, the largest negative summer long-term trend occurred at (SNPA1, -7.2% yr^{-1}).

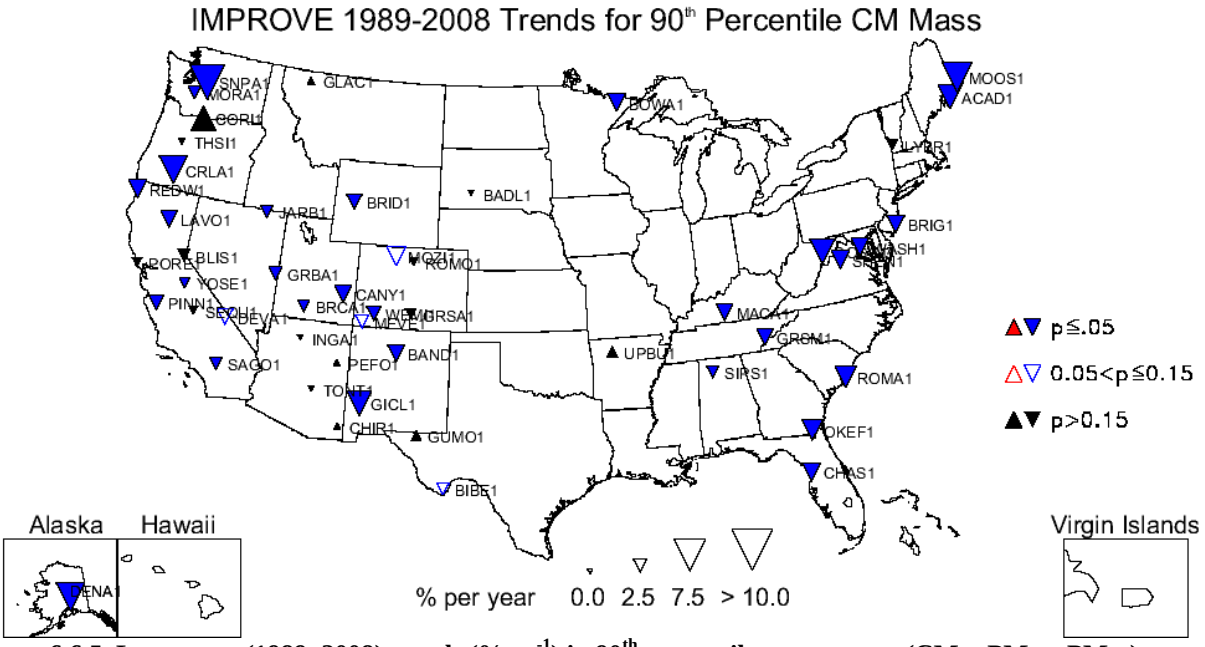

Figure 6.6.5. Long-term (1989–2008) trends (% yr^{-1}) in 90th percentile coarse mass (CM = PM_{10} - $PM_{2.5}$) concentrations.

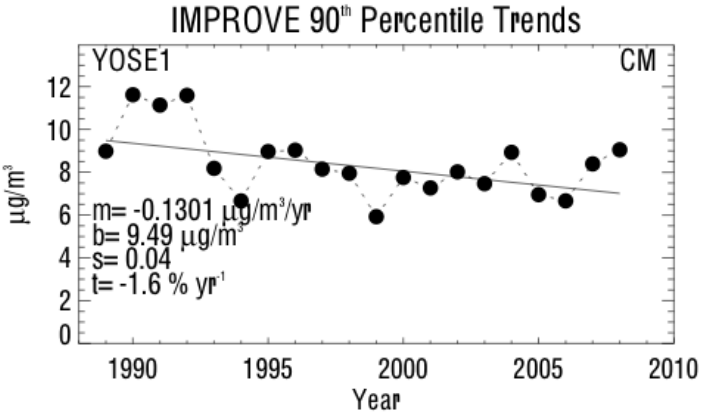

Figure 6.6.6. 90th percentile coarse mass (CM = PM_{10} - $PM_{2.5}$) concentrations (µg m^{-3}) for Yosemite, California (YOSE1). Regression results, including Theil slope (m, µg m^{-3} yr^{-1}), intercept (b, µg m^{-3}), significance (s), and trend (t, % yr^{-1}) are included. The trend line is plotted as a solid line. The intercept corresponds to the initial year of data.

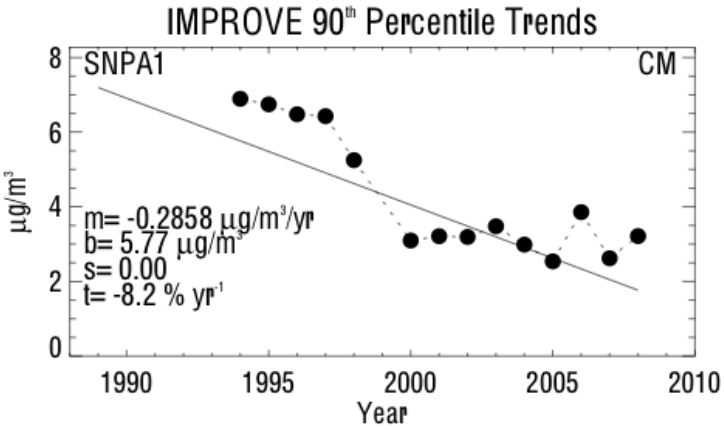

Figure 6.6.7. 90th percentile coarse mass (CM = PM_{10} - $PM_{2.5}$) concentrations (µg m^{-3}) for Snoqualmie Pass, Washington (SNPA1). Regression results, including Theil slope (m, µg m^{-3} yr^{-1}), intercept (b, µg m^{-3}), significance (s), and trend (t, % yr^{-1}) are included. The intercept corresponds to the initial year of data.

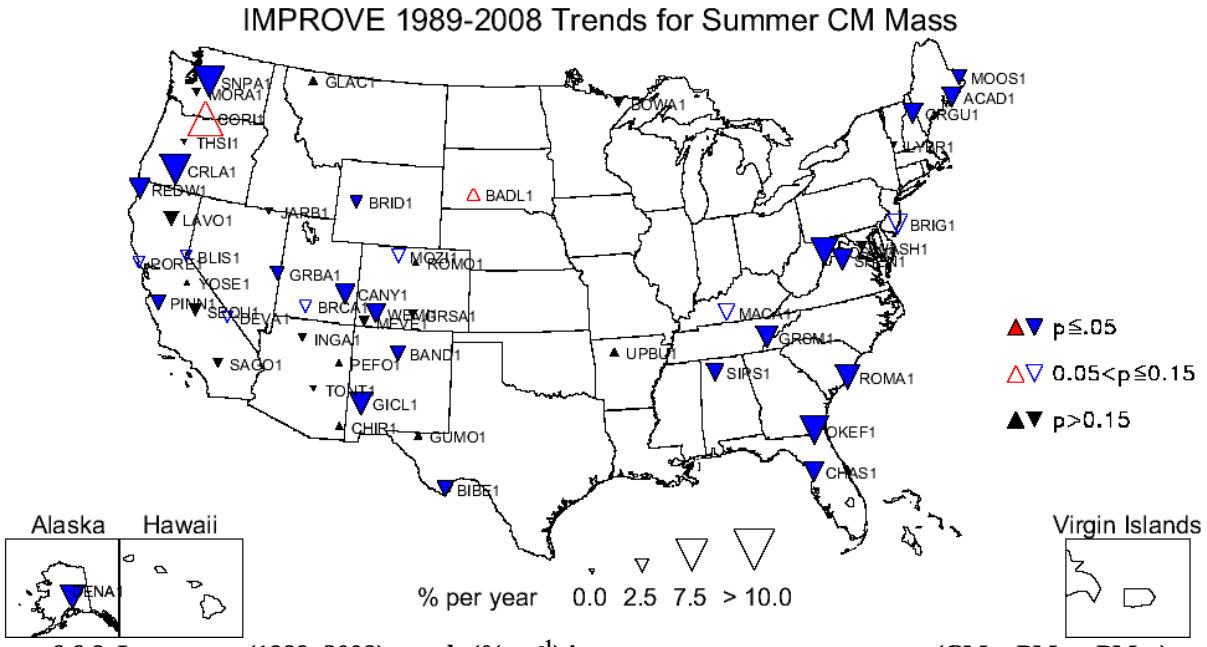

Figure 6.6.8. Long-term (1989–2008) trends (% yr^{-1}) in average summer coarse mass (CM = PM_{10} - $PM_{2.5}$) concentrations.

Of the ~153 sites used to investigate short-term CM trends, sites with significant trends ranged from 25 (fall) to 45 (50th percentile) (see Table 6.2). In addition, many more sites were associated with positive short-term trends compared to long-term CM trends. Short-term trends in the 90th percentile CM concentrations for individual sites are shown in Figure 6.6.9. Unlike the long-term, 90th percentile trends, short-term trends at several sites were positive (10 out of 34 statistically significant trends). The largest 90th percentile negative trend occurred at Monture, Montana (MONT1, -8.8% yr^{-1}), compared to the largest positive trend at Cohutta, Georgia (COHU1, 8.6% yr^{-1}). Decreasing 90th percentile CM concentrations at MONT1 are shown in Figure 6.6.10. High CM concentrations in 2000 decreased and remained steady through 2008. Relatively large negative short-term trends in winter CM concentrations are presented in Figure

6.6.11. Several southwestern sites corresponded to negative trends, compared to increasing trends in Idaho, Montana, Wyoming, and the northeastern United States. The largest negative winter CM trend corresponded to Hoover, California (HOOV1, -18.3% yr^{-1}), and the largest positive winter CM trend corresponded to Sula Peak, Montana (SULA1, 12.7% yr^{-1}). The winter CM concentrations at HOOV1 dropped considerably after 2002, from 4.8 µg m^{-3} to 0.5 µg m^{-3} from 2002 to 2008 (Figure 6.6.12).

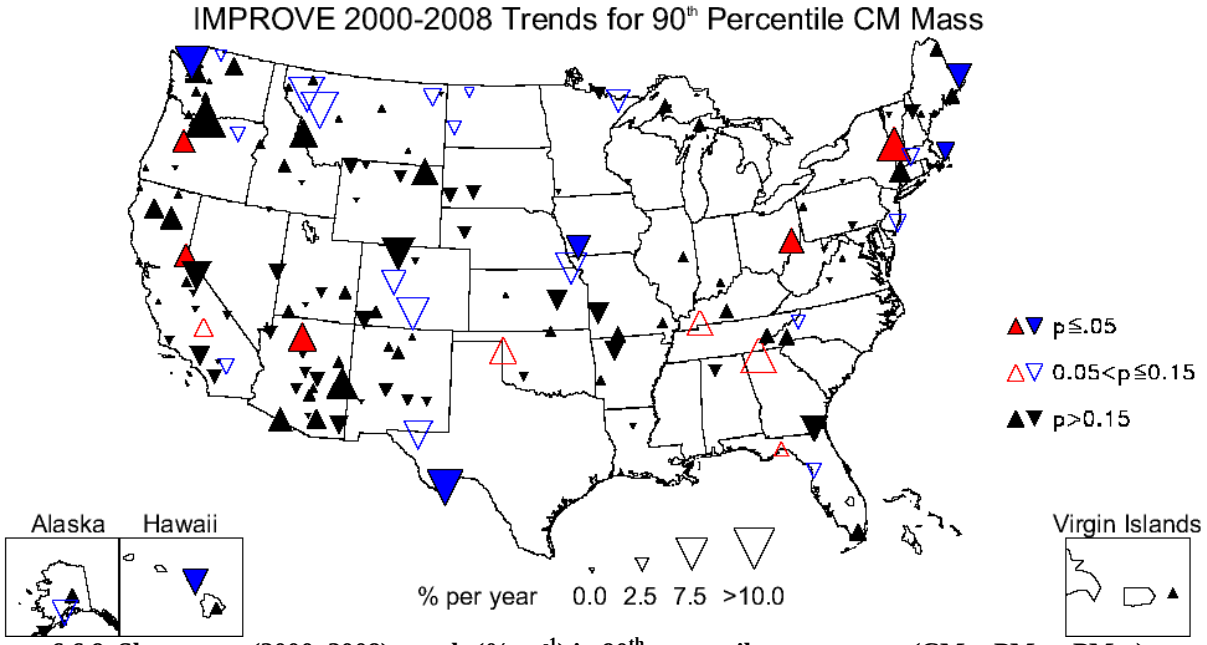

Figure 6.6.9. Short-term (2000–2008) trends (% yr^{-1}) in 90th percentile coarse mass (CM = PM_{10} - $PM_{2.5}$) concentrations.

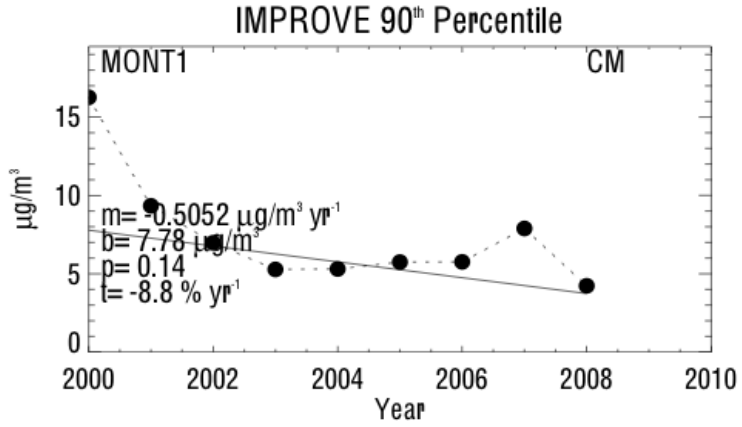

Figure 6.6.10. 90th percentile coarse mass (CM = PM_{10} - $PM_{2.5}$) concentrations (µg m^{-3}) for Monture, Montana (MONT1). Regression results, including Theil slope (m, µg m^{-3} yr^{-1}), intercept (b, µg m^{-3}), significance (p), and trend (t, % yr^{-1}) are included. The trend line is plotted as a solid line. The intercept corresponds to the initial year of data.

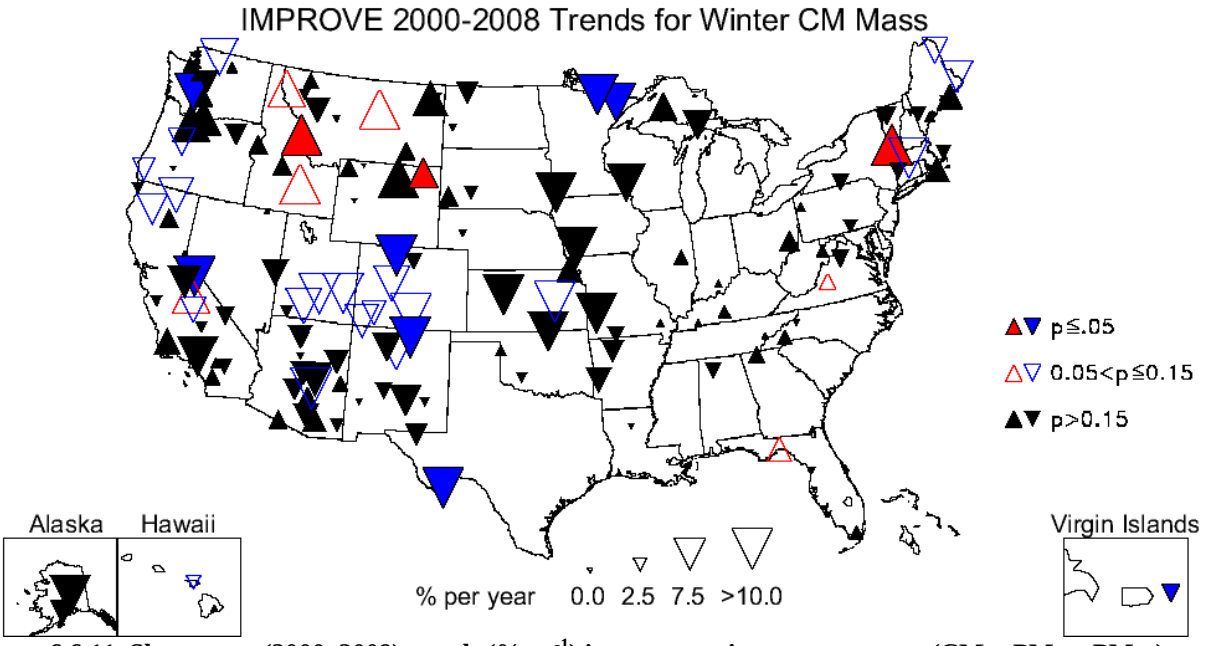

Figure 6.6.11. Short-term (2000–2008) trends (% yr^{-1}) in average winter coarse mass (CM = PM_{10} - $PM_{2.5}$) concentrations.

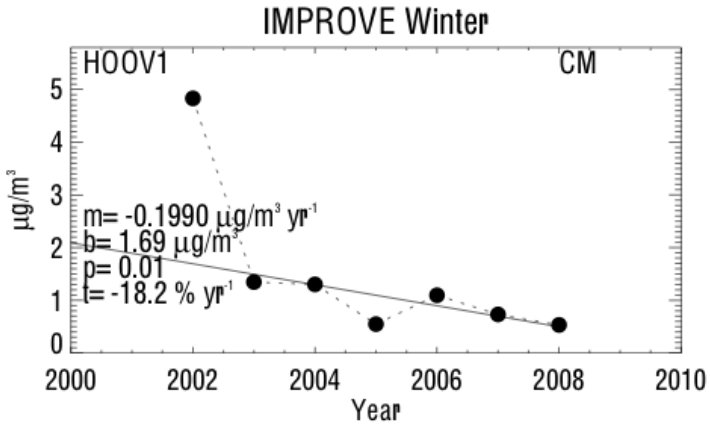

Figure 6.6.12. Average winter coarse mass (CM = PM_{10} - $PM_{2.5}$) concentrations (µg m^{-3}) for Hoover, California (HOOV1). Regression results, including Theil slope (m, µg m^{-3} yr^{-1}), intercept (b, µg m^{-3}), significance (p), and trend (t, % yr^{-1}) are included. The trend line is plotted as a solid line. The intercept corresponds to the initial year of data.

The 50th percentile and summer season were associated with the highest number of sites with significant short-term positive trends (Table 6.2). The 50th percentile trends included 19 sites with positive trends, several of which were in the eastern United States (Figure 6.6.13). The largest positive, 50th percentile trend occurred at Cohutta, Georgia (COHU1, 11.6% yr^{-1}), compared to the largest negative 50th percentile trend at Flathead, Montana (FLAT1, -16.3% yr^{-1}). Individual summer trends for CM are shown in Figure 6.1.14. Most eastern sites were associated with positive summer trends, as well as sites in the southwestern and northwestern United States. Of the 44 sites with significant summer trends, 27 were associated with positive trends. The largest positive short-term, summer trend occurred at Indian Gardens, Arizona

(INGA1, 12.9% yr^{-1}), and the largest negative trend occurred at Olympic, Washington (OLYM1, -9.6% yr^{-1}). Coarse mass summer concentrations at INGA1 (Figure 6.6.15) were much larger and increased steadily compared to the steadily decreasing low CM concentrations in summer at OLYM1 (Figure 6.1.16).

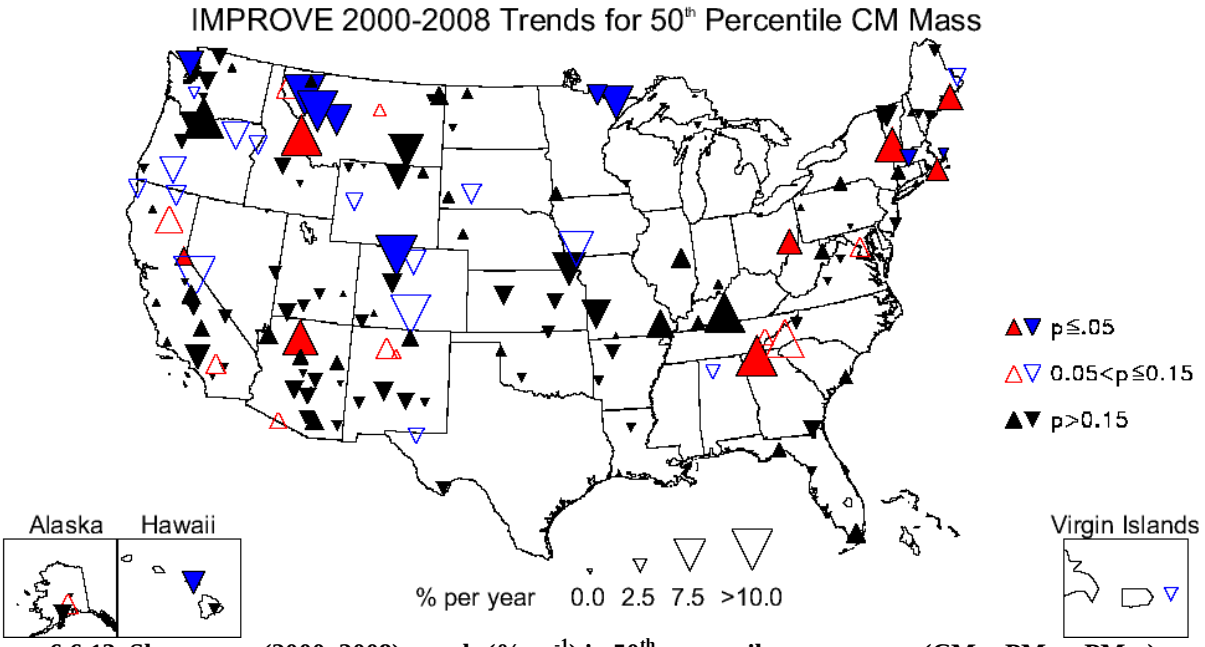

Figure 6.6.13. Short-term (2000–2008) trends (% yr^{-1}) in 50th percentile coarse mass (CM = PM_{10} - $PM_{2.5}$) concentrations.

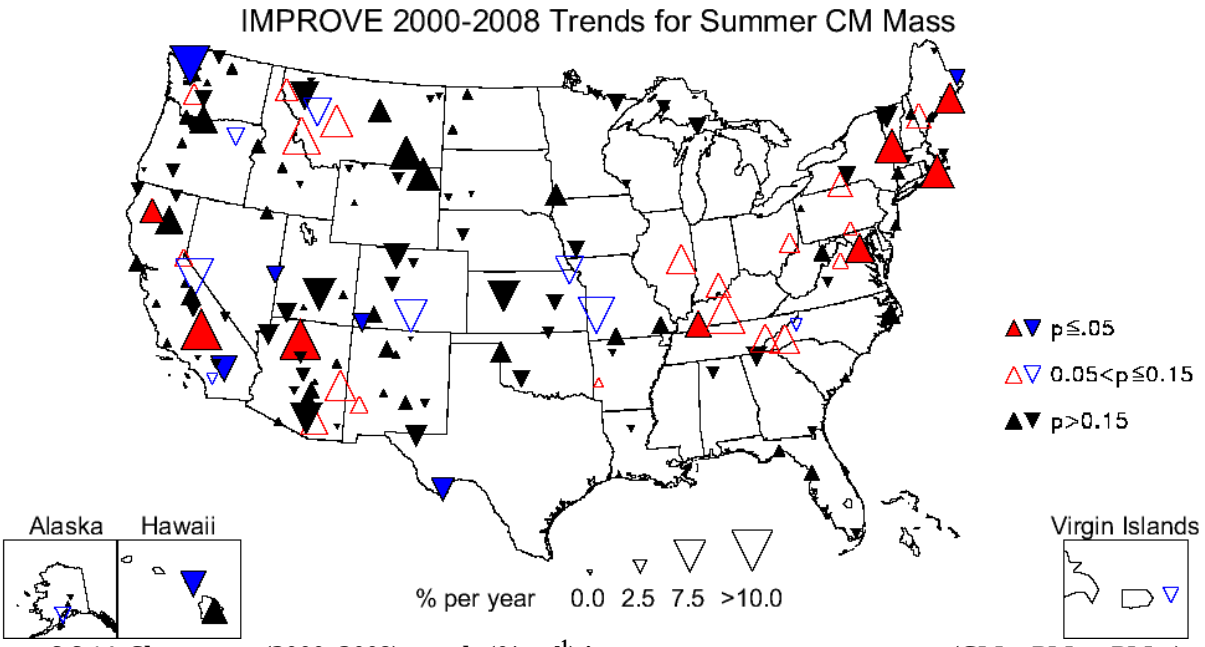

Figure 6.6.14. Short-term (2000–2008) trends (% yr^{-1}) in average summer coarse mass (CM = PM_{10} - $PM_{2.5}$) concentrations

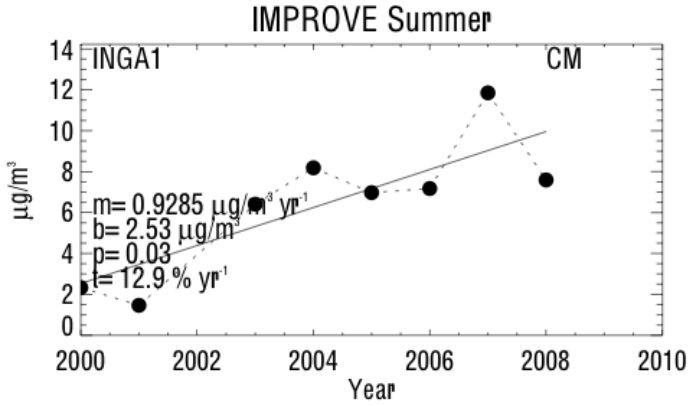

Figure 6.6.15. Average summer coarse mass (CM = PM_{10} - $PM_{2.5}$) concentrations (µg m^{-3}) for Indian Gardens, Arizona (INGA1). Regression results, including Theil slope (m, µg m^{-3} yr^{-1}), intercept (b, µg m^{-3}), significance (p), and trend (t, % yr^{-1}) are included. The trend line is plotted as a solid line. The intercept corresponds to the initial year of data.

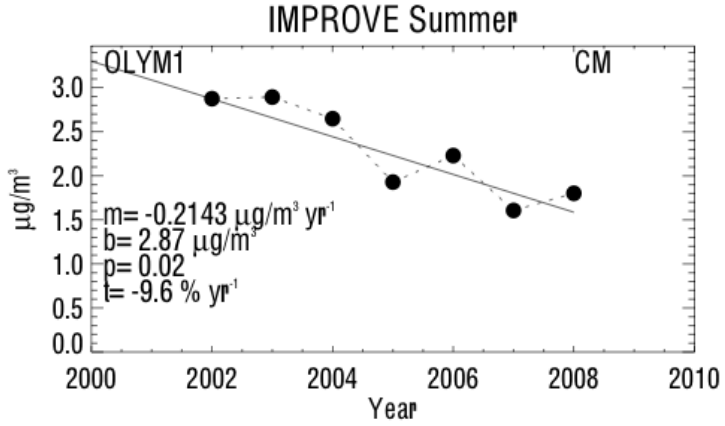

Figure 6.6.16. Average summer coarse mass (CM = PM_{10} - $PM_{2.5}$) concentrations (µg m^{-3}) for Olympic, Washington (OLYM1). Regression results, including Theil slope (m, µg m^{-3} yr^{-1}), intercept (b, µg m^{-3}), significance (p), and trend (t, % yr^{-1}) are included. The trend line is plotted as a solid line. The intercept corresponds to the initial year of data.

The interpretation of CM trends is complicated by the fact that the speciation of CM was unknown. For regions where CM concentrations were suspected to be dominated by soil (e.g., southwestern United States), we might expect the CM trends to be similar to the soil trends. Although some seasonal short-term trends suggest similarities, in general, comparisons of soil and CM trends between similar parameters were inconclusive. Reasons for discrepancies between soil and CM trends include the possibilities that soil trends may be more questionable than realized, CM trends were driven by species other than soil, or CM trends were questionable. Any changes in the cut points for the $PM_{2.5}$ and PM_{10} samplers over time could produce questionable trends in CM, although we have no specific evidence to support this possibility. Additionally, sites with statistically significant trends in soil may not have statistically significant trends in CM, further complicating comparisons between trends.

6.7 PM_{10} GRAVIMETRIC MASS TRENDS

PM_{10} concentrations are determined gravimetrically and correspond to particles with an aerodynamic diameter (D_{ae}) less than 10 μm. PM_{10} mass concentrations include all the species presented in the previous sections, and trends for PM_{10} concentrations represent the temporal behavior in the total (D_{ae} < 10 μm) aerosol mass concentration. Not surprisingly, the long-term trends were generally negative (see Figure 6.7.1), with the largest negative trends corresponding to the 10th percentile and winter season. The individual site trends for PM_{10}, 10th percentile concentrations are shown in Figure 6.7.1. All 50 sites with complete data corresponded to statistically significant 10th percentile trends, and the largest negative 10th percentile trend occurred at Mount Zirkel, Colorado (MOZI1, -9.9% yr^{-1}). The least negative 10th percentile trend corresponded to Mammoth Cave, Kentucky (MACA1, -1.2% yr^{-1}). Winter trends in PM_{10} concentrations are shown in Figure 6.7.2. Sites along the western United States were associated with relatively large negative winter trends, with the largest corresponding to Snoqualmie Pass, Washington (SNPA1, -9.0% yr^{-1}), similar to winter CM trends. The least negative winter trend occurred at Tonto, Arizona (TONT1, -1.7% yr^{-1}), and no sites were associated with positive winter trends. Winter PM_{10} concentrations at SNPA1 decreased after 2000 and remained fairly flat (Figure 6.7.3).

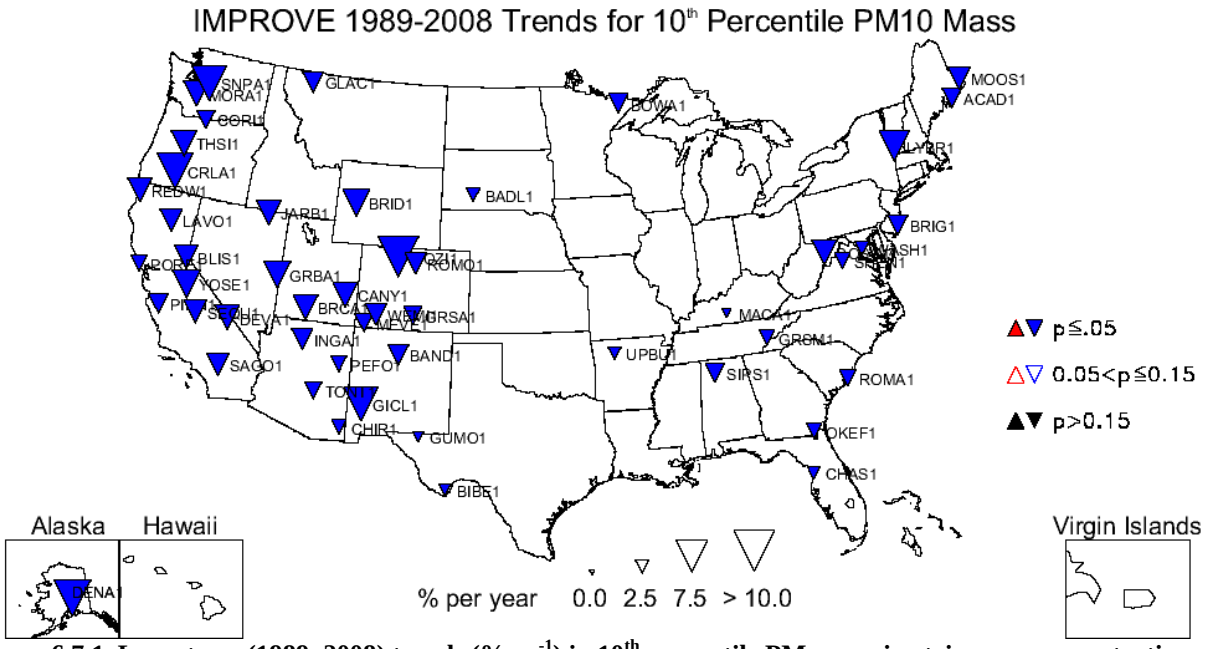

Figure 6.7.1. Long-term (1989–2008) trends (% yr^{-1}) in 10th percentile PM_{10} gravimetric mass concentrations.

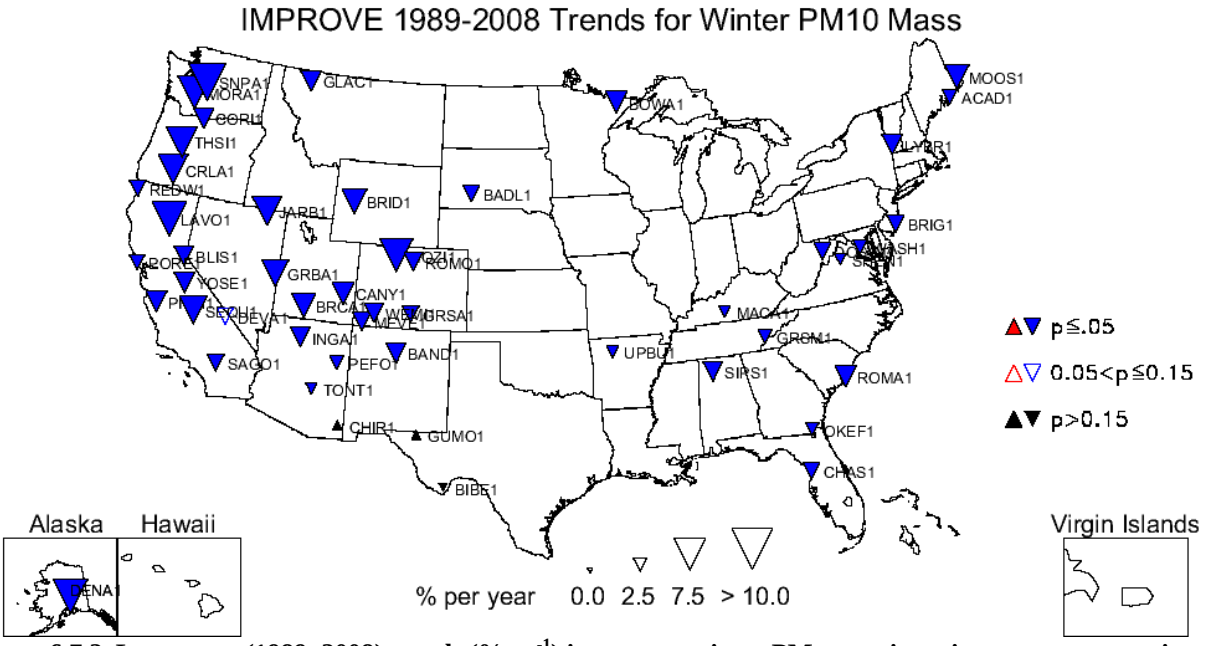

Figure 6.7.2. Long-term (1989–2008) trends (% yr^{-1}) in average winter PM_{10} gravimetric mass concentrations.

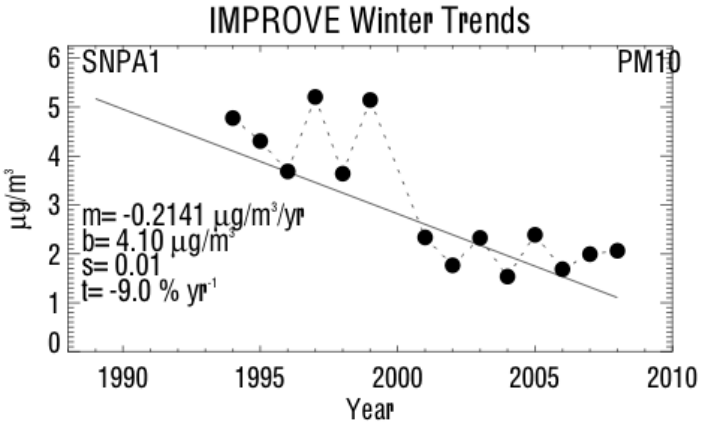

Figure 6.7.3. Average winter PM_{10} gravimetric mass concentrations (µg m^{-3}) for Snoqualmie Pass, Washington (SNPA1). Regression results, including Theil slope (m, µg m^{-3} yr^{-1}), intercept (b, µg m^{-3}), significance (s), and trend (t, % yr^{-1}) are included. The trend line is plotted as a solid line. The intercept corresponds to the initial year of data.

PM_{10} trends for the 90th percentile were considerably lower, or insignificant, compared to the 10th percentile trends (Figure 6.7.4). No sites corresponded to positive, 90th percentile, PM_{10} trends. Many eastern sites corresponded to negative summer PM_{10} trends, and many western sites were associated with insignificant summer trends (Figure 6.7.5). The largest negative summer trend occurred at Great Gulf, New Hampshire (GRGU1, -5.0% yr^{-1}), similar to FM summer trends. Only one significant positive trend occurred for long-term PM_{10} trends, and it was for summer concentrations at Columbia River Gorge, Washington (CORI1, 4.6% yr^{-1}). Recall that CORI1 was also associated with a large positive trend in soil in summer.

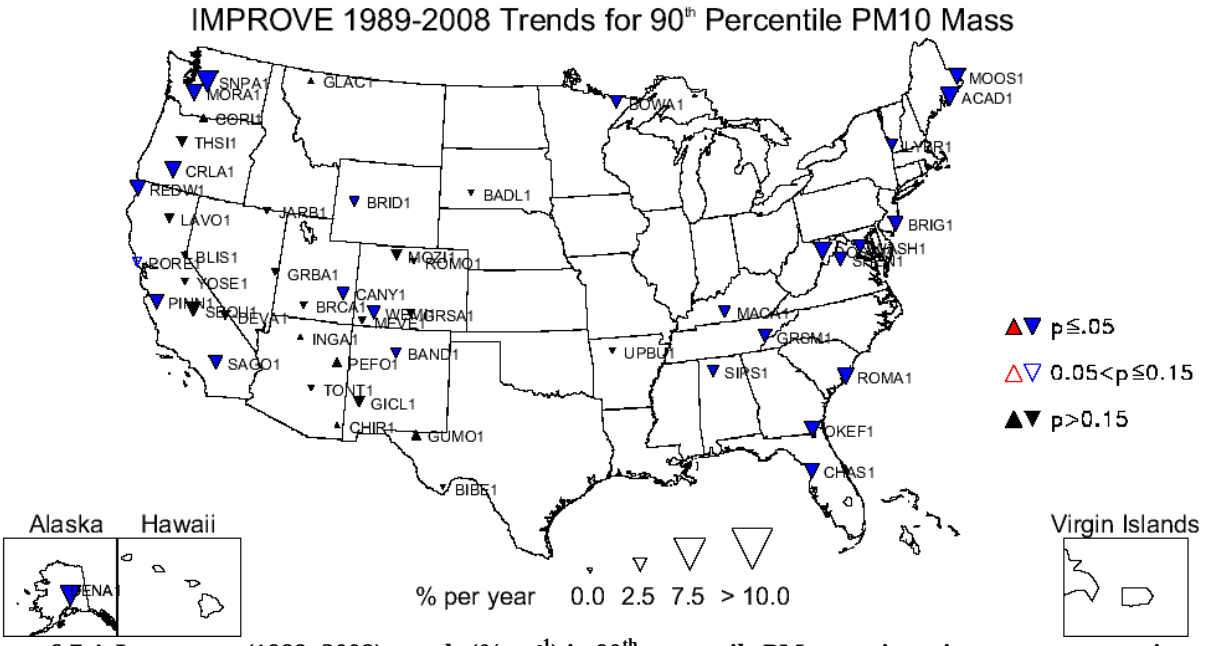

Figure 6.7.4. Long-term (1989–2008) trends (% yr^{-1}) in 90th percentile PM_{10} gravimetric mass concentrations.

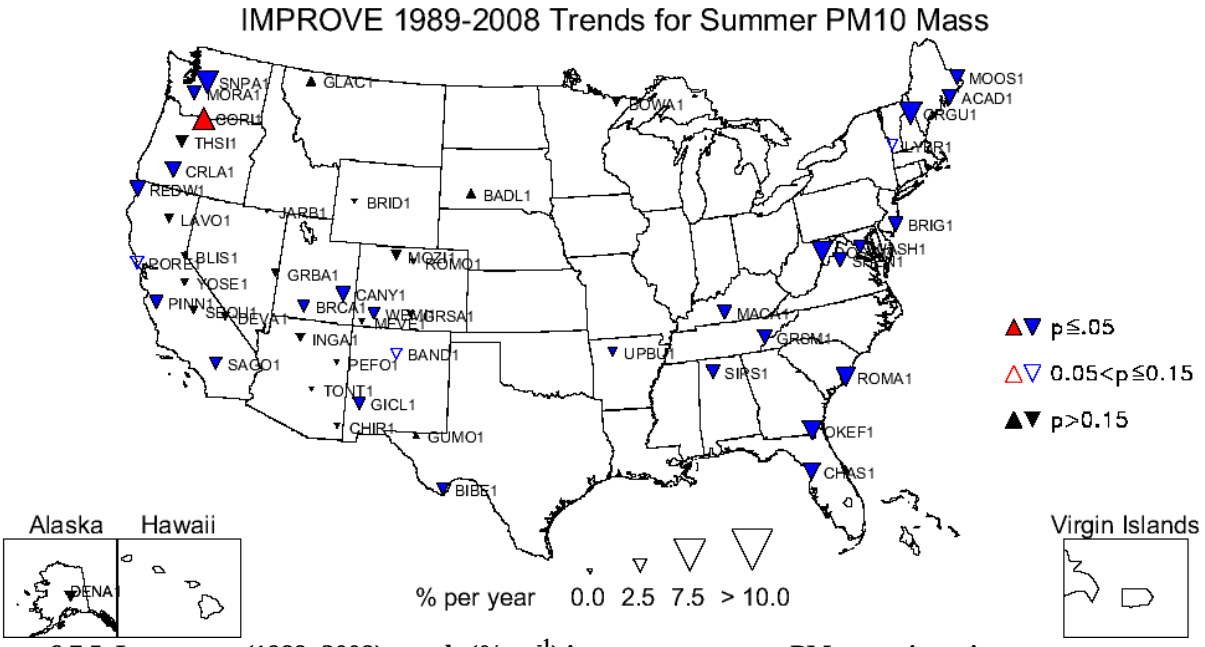

Figure 6.7.5. Long-term (1989–2008) trends (% yr^{-1}) in average summer PM_{10} gravimetric mass concentrations.

Although short-term PM_{10} trends were associated with more sites with positive significant trends compared to long-term PM_{10} trends, they still were dominated by sites with negative trends (see Table 6.2). The map of sites for short-term 10th percentile PM_{10} trends suggested that statistically significant trends were more negative in the central, western, and northwestern United States (Figure 6.7.6). The largest negative 10th percentile, short-term PM_{10} trend was associated with Starkey, Oregon (STAR1, -15.10% yr^{-1}), similar to FM trends. The

largest positive 10th percentile, short-term, PM_{10} trend corresponded to Trapper Creek, Alaska (TRCR1, 12.10% yr^{-1}), also similar to FM trends. In addition to the TRCR1 site, two sites were associated with positive trends: Nebraska NF, Nebraska (NEBR1, 3.8% yr^{-1}), and Denali, Alaska (DENA1, 8.7% yr^{-1}). Winter PM_{10} short-term trends were most negative in the western United States (Figure 6.7.7). The largest negative winter, PM_{10} trend occurred at Starkey, Oregon (STAR1, -12.9% yr^{-1}), similar to FM trends. The largest positive winter trend occurred at Bondville, Illinois (BOND1, 1.7% yr^{-1}). Figure 6.7.8 shows a slow but steady increase in the winter PM_{10} concentrations at BOND1.

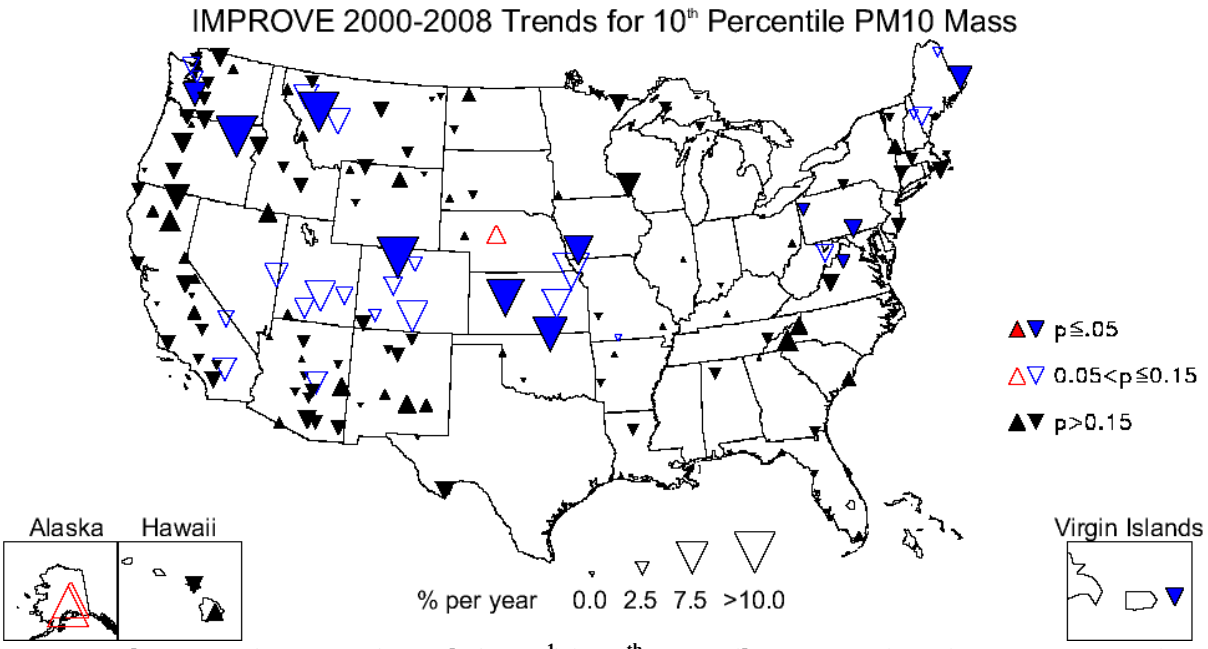

Figure 6.7.6. Short-term (2000–2008) trends (% yr^{-1}) in 10th percentile PM_{10} gravimetric mass concentrations.

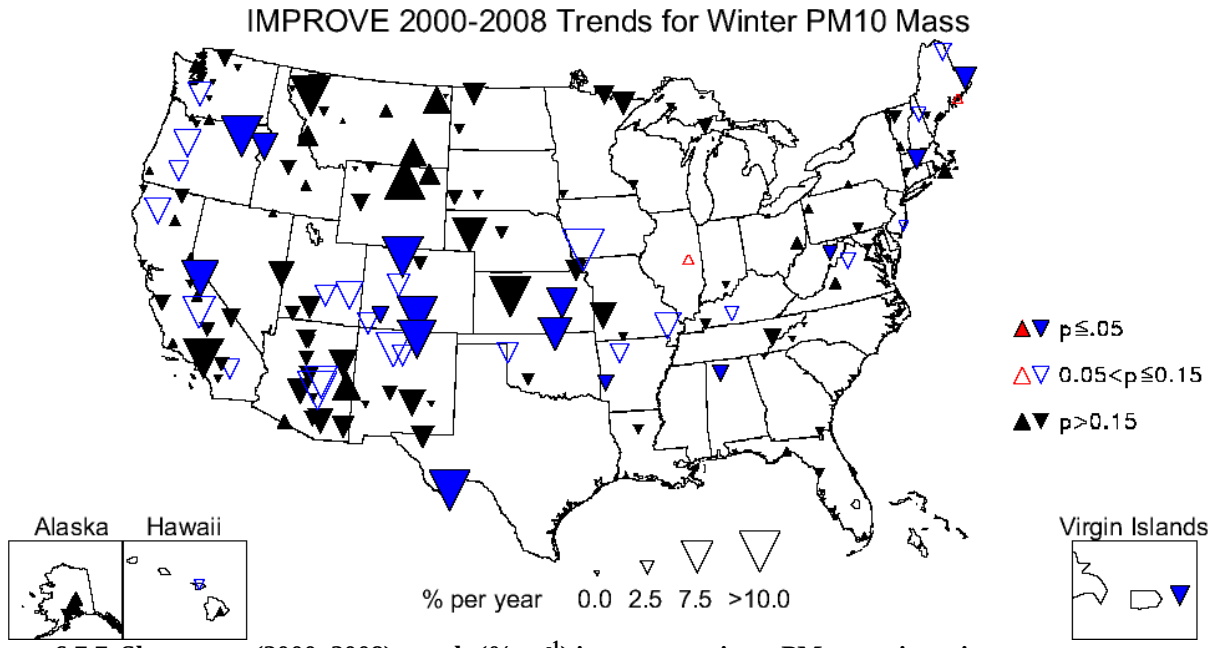

Figure 6.7.7. Short-term (2000–2008) trends (% yr^{-1}) in average winter PM_{10} gravimetric mass concentrations.

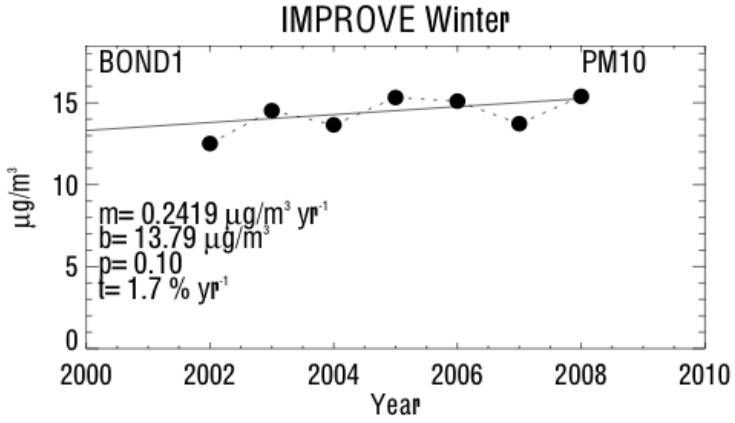

Figure 6.7.8. Average winter PM_{10} gravimetric mass concentrations (µg m^{-3}) for Bondville, Illinois (BOND1). Regression results, including Theil slope (m, µg m^{-3} yr^{-1}), intercept (b, µg m^{-3}), significance (p), and trend (t, % yr^{-1}) are included. The trend line is plotted as a solid line. The intercept corresponds to the initial year of data.

The parameters associated with the largest number of positive trend sites were the 90th percentile and fall season. A map of 90th percentile, short-term PM_{10} trends is shown in Figure 6.7.9. Five sites were associated with positive 90th percentile trends, including the site at Hawaii Volcanoes (HAVO1) with the largest positive trend (12.5% yr^{-1}). The HAVO1 site was also associated with the largest FM and sulfate 90th percentile trends. The largest negative, short-term trend in 90th percentile PM_{10} concentrations corresponded to Tuxedni, Alaska (TUXE1, -8.10% yr^{-1}), which also corresponded to the largest negative, FM, 90th percentile trend. Fall PM_{10} trends were associated with eight positive trends, none of which were located in the eastern United States (Figure 6.7.10). The largest positive fall, PM_{10}, short-term trend corresponded to the Zion

Canyon, Utah, site (ZICA1, 10.0% yr^{-1}), similar to the fall FM and soil trends, and the largest negative fall, PM_{10} trend occurred at Gila, New Mexico (GICL1, -6.0% yr^{-1}). A timeline of fall PM_{10} concentrations at GICL1 is shown in Figure 6.7.11 and demonstrates a decrease in PM_{10} concentrations from 9.5 μg m^{-3} to 4.3 μg m^{-3} from 2000 to 2008. The fall PM_{10} concentration in 2000 was the largest concentration in 20 years, so the short-term fall trend at GICL1 was somewhat larger than the long-term trend (-4.5% yr^{-1}).

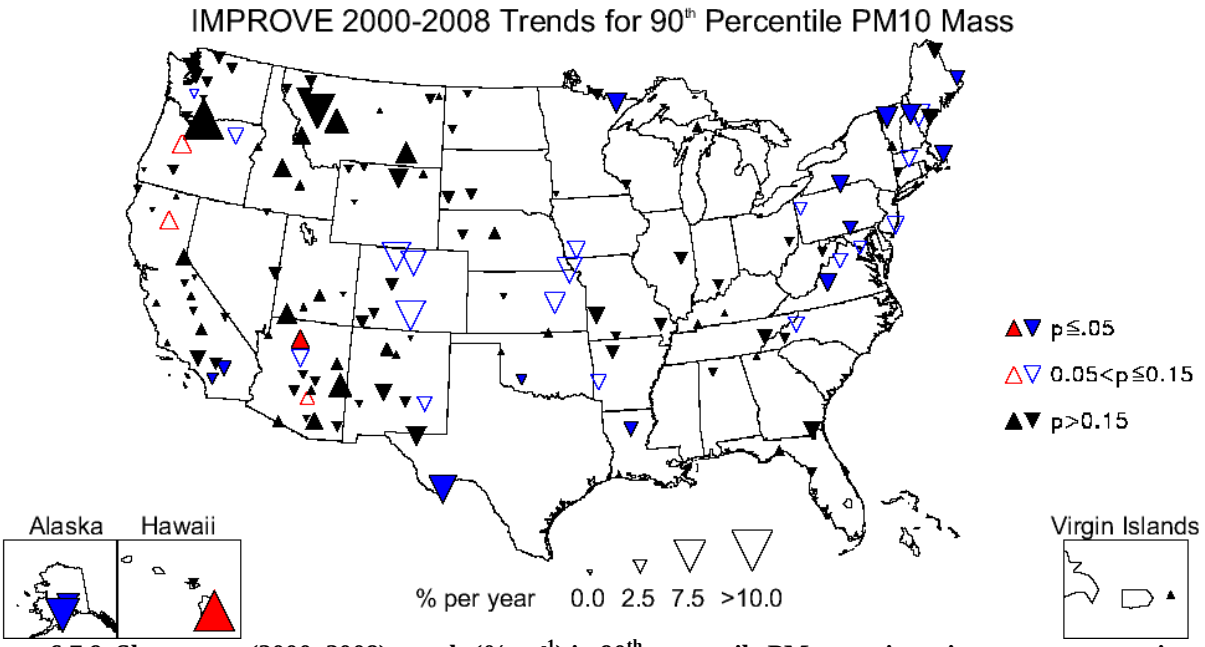

Figure 6.7.9. Short-term (2000–2008) trends (% yr^{-1}) in 90th percentile PM_{10} gravimetric mass concentrations.

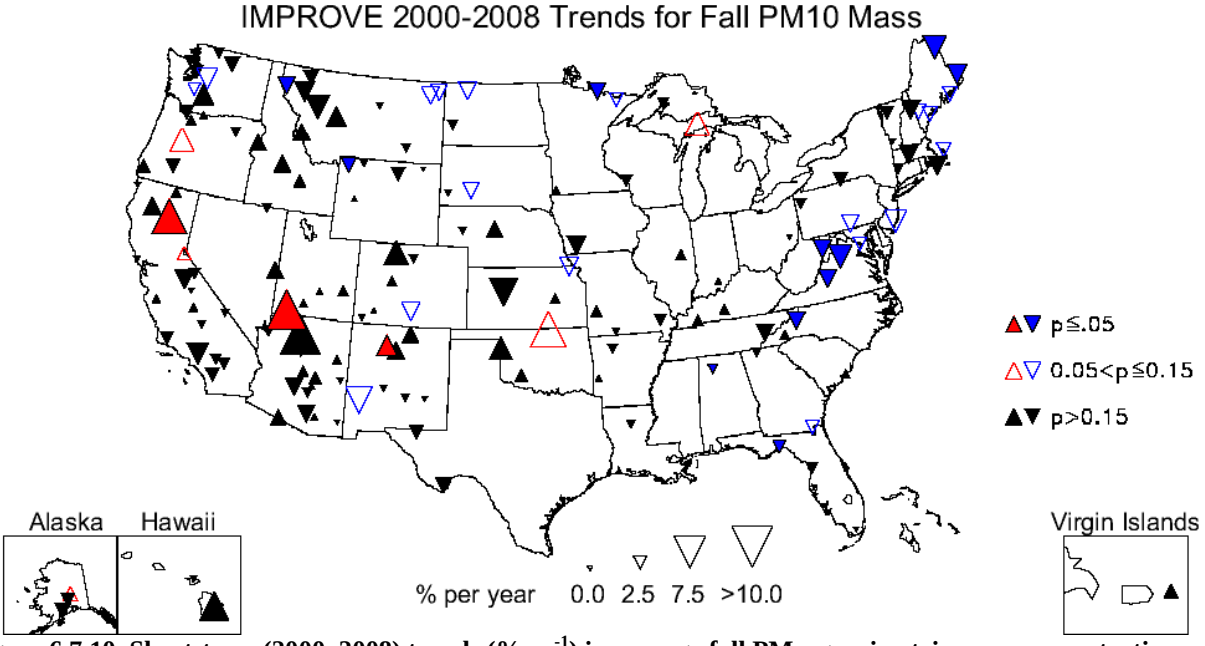

Figure 6.7.10. Short-term (2000–2008) trends (% yr^{-1}) in average fall PM_{10} gravimetric mass concentrations.

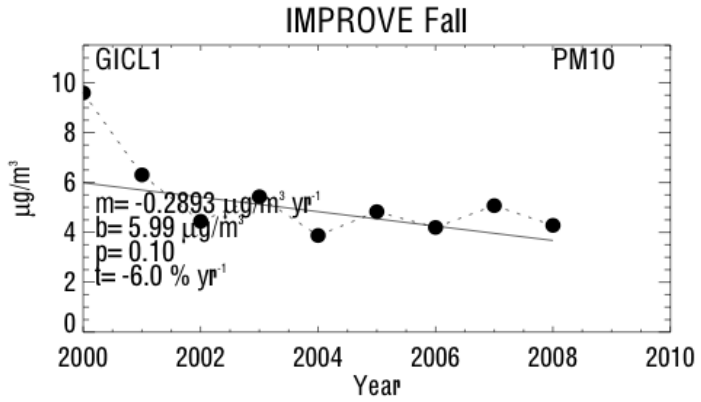

Figure 6.7.11. Average fall PM_{10} gravimetric mass concentrations (µg m^{-3}) for Gila, New Mexico (GICL1). Regression results, including Theil slope (m, µg m^{-3} yr^{-1}), intercept (b, µg m^{-3}), significance (p), and trend (t, % yr^{-1}) are included. The trend line is plotted as a solid line. The intercept corresponds to the initial year of data.

The trend results presented in this chapter were intended as a summary of the temporal changes in the mass concentrations of major aerosol species over short and long time periods. Results suggested that for most species, concentrations were decreasing at IMPROVE sites around the United States, and these decreasing trends were largest for the lowest concentrations and during winter seasons. Because we present normalized trends, it is not surprising that the 10th percentile trends were typically the largest in magnitude because they were normalized with the lowest concentrations. This general result may not hold for individual sites or for given species (e.g., soil), but overall this consistent pattern emerged. A similar pattern was presented in recent progress report for air quality in national parks (NPS, 2010) that demonstrated larger decreasing trends in deciview on the clearest days compared to the haziest days.

To demonstrate the visibility conditions associated with the trends in particle concentrations presented in this chapter, we used WinHaze 2.9.9 (Air Resource Specialists, 2011) to model the view of scenic areas with specified air quality levels. WinHaze is a computer software program that simulates visibility conditions from user-specified scenes and speciated aerosol concentrations or visibility levels. For our applications we chose scenes for parks and wilderness areas with speciated aerosol concentrations measured from the IMPROVE network. We specified 50th percentile aerosol concentrations for "beginning" and "end" periods corresponding to our trend analyses. We used default optical properties (i.e. "original" IMPROVE algorithm) and assumed an 80% relative humidity for all simulations. An example of results from WinHaze is shown in the split-image of a scene at Linville Gorge NC (LIVO) for aerosol levels in 2000 and 2008 (Figure 6.7.12). A noticeable improvement in visibility levels occurred due to the decrease in aerosol concentrations over the 9-year span. The cover of this report showing the scene in Acadia, ME is another example of split-images that represent the visibility conditions associated with the measured aerosol concentrations over the trend period. Winhaze is a powerful tool for visualizing the impact of aerosol trends on visibility conditions over time.

Figure 6.7.12. Split-image of visibility conditions in Linville Gorge, NC (LIVO) for 50th percentile speciated aerosol levels in 2000 (left-side) and 2008 (right-side). Images were generated using WinHaze 2.9.9.

Appendix F includes additional figures showing long-term and short-term trends for other percentiles and seasons that were not included in this discussion. The appendix also includes WinHaze images, like the one shown in Figure 6.7.12, for approximately fifty additional sites.

REFERENCES

Air Resource Specialists, Inc. (2011), WinHaze visual air quality modeler version 2.9.9, Fort Collins CO (http://www.air-resource.com/resources/downloads.html).

Bahadur, R., G. Habib, and L. M. Russell (2009), Climatology of PM2.5 organic carbon concentrations from a review of ground-based atmospheric measurements by evolved gas analysis, *Atmos. Environ, 43,* 1591-1602.

Chow, J. C., J. G. Watson, L.-W. A. Chen, M. C. O. Chang, N. F. Robinson, D. Trimble, and S. Kohl (2007), The IMPROVE_A temperature protocol for thermal/optical carbon analysis: Maintaining consistency with a long-term database, *J. Air & Waste Manage. Assoc., 57,* 1014-1023.

Gong, S. L., T. L. Zhao, S. Sharma, D. Toom-Sauntry, D. Lavoué, X. B. Zhang, W. R. Leaitch, and L. A. Barrie (2010), Identification of trends and interannual variability of sulfate and black carbon in the Canadian High Artic: 1981-2007, *J. Geophys. Res., 115,* D07305, doi:10.1029/2009JD012943.

Hirdman, D., J. F. Burkhart, H. Sodemann, S. Eckhardt, A. Jefferson, P. K. Quinn, S. Sharma, J. Ström, and A. Stohl (2010), *Atmos. Chem. Phys*., *10*, 9351–9368, doi:10.5194/acp-10-9351-2010.

Holland, D., C. Simmons, L. Smith, T. Cohn, G. Baier, J. Lynch, J. Grimm, G. Oehlert, and S. Lindberg (1995), Long-term trends in NADP/NTN precipitation chemistry data: Results of different statistical analyses, *Water Air Soil Pollut, 85,* 595-601.

Lehmann, C. M. B., V. C. Bowersox, R. S. Larson, and S. M. Larson (2007), Monitoring long-term trends in sulfate and ammonium in U.S. precipitation: Results from the National Atmospheric Deposition Program/National Trends Network, *Water Air Soil Pollut: Focus, 7,* 59-66, doi:10.1007/s11267-006-9100-z.

Lloyd, P. J., (2010), Changes in the wet precipitation of sodium an chloride over the continental United States, 1984-2006, *Atmos. Environ., 44,* 3196-3206.

Lynch, J. A., J. W. Grimm, and V. C. Bowersox (1995), Trends in precipitation chemistry in the United States: A national perspective, 1980-1992, *Atmos. Environ., 29,*11, 1231-1246.

Malm, W. C., B. A. Schichtel, R. B. Ames, and K. A. Gebhart (2002), A 10-year spatial and temporal trend of sulfate across the United States, *J. Geophys. Res*., 107(D22), 4627, doi:10.1029/2002JD002107.

Malm, W. C., B. A. Schichtel, and M. L. Pitchford (2011), Uncertainties in PM2.5 gravimetric and speciation measurements and what we can learn from them, *J. Air Waste Manage,* In press.

McDade, C. E. (2007), Diminished wintertime nitrate concentrations in late 1990s, Doc. # da0002, http://vista.cira.colostate.edu/improve/Data/QA_QC/Advisory/da0002/da0002_WinterNO3.pdf.

Mishchenko, M. I., I. V. Geogdzhayev, W. B. Rossow, B. Cairns, B. E. Carlson, A. A. Lacis, L. Liu, and L. D. Travis (2007), Long-term satellite record reveals likely recent aerosol trend, *Science*, *315*, 1543.

Mishchenko, M. I., and I. V. Geogdzhayev (2007), Satellite remote sensing reveals regional tropospheric aerosol trends, *Optics Express, 15,* 12, 7423-7438.

Nilles, M. A., and B. E. Conley (2001), Changes in the chemistry of precipitation in the United States, 1981-1998, *Water, Air and Soil Pollut., 130,* 409-414.

NPS (2010), Air quality in National Parks, 2009 Annual Performance and Progress Report, Natural Resource Report NPS/NRPC/ARD/NRR-2010/266.

Polissar, A. V., P. K. Hopke, P. Paatero, Y. J. Kaufmann, D. K. Hall, B. A. Bodhaine, E. G. Dutton, and J. M. Harris (1999), The aerosol at Barrow, Alaska: long term trends and source locations, *Atmos. Environ., 33,* 2441-2458.

Quinn, P. K., G. Shaw, E. Andrews, E. G. Dutton, T. Ruoho-Airola, and S. L. Gong (2007), Artic haze: current trends and knowledge gaps, *Tellus, 59B*, 99-114.

Sirois, A., and L. A. Barrie (1999), Artic lower tropospheric aerosol trends and composition at Alert, Canada: 1980-1995, *J. Geophys. Res., 104*, D9, 11599-11618.

Streets, D. G., F. Yan, M. Chin, T. Diehl, N. Mahowald, M. Schultz, M. Wild, Y. Wu, and C. Yu (2009), Anthropogenic and natural contributions to regional trends in aerosol optical depth, 1980–2006, *J. Geophys. Res*., *114*, D00D18, doi:10.1029/2008JD011624.

Theil, H. (1950), A rank-invariant method of linear and polynomial regression analysis, *Proc. Kon. Ned. Akad. V. Wetensch. A., 53*, 386-392, 521-525, 1397-1412.

U.S. EPA (1999), Regional Haze Regulations; Final Rule, 40 CFR 51, Federal Register, 64, 35714-35774.

Wild, M., H. Gilgen, A. Roesch, A. Ohmura, C. N. Long, E. G. Dutton, B. Forgan, A. Kallis, V. Russak, and A. Tsvetkov (2005), From dimming to brightening: decadal changes in solar radiation at the Earth's surface, *Science, 308*, 847-850.

White, W. H. (2007), Shift in EC/OC split with 1 January 2005 TOR hardware upgrade, Doc. # da0016, http://vista.cira.colostate.edu/improve/Data/QA_QC/Advisory/da0016/da0016_TOR2005.pdf.

White, W. H. (2008), Chemical markers for sea salt in IMPROVE aerosol data, *Atmos. Environ., 42*, 261-274.